European Union
European Social Fund

HAMK
HÄMEEN AMMATTIKORKEAKOULU
HÄME UNIVERSITY OF APPLIED SCIENCES

Proceedings of the METNET Seminar 2017 in Cottbus

Kuldeep Virdi and Lauri Tenhunen (Editors)

Proceedings of the METNET Seminar 2017 in Cottbus

Kuldeep Virdi and Lauri Tenhunen (Editors)

Häme University of Applied Sciences (HAMK)

Editors:
Kuldeep Virdi, City, University of London
Lauri Tenhunen, Häme University of Applied Sciences (HAMK)

Proceedings of the METNET Seminar 2017 in Cottbus

PRINTED
ISBN 978-951-784-794-0
ISSN 1795-4231
HAMKin julkaisuja 1/2018

ELECTRONIC
ISBN 978-951-784-793-3 (PDF)
ISSN 1795-424X
HAMKin e-julkaisuja 2/2018

© Häme University of Applied Sciences and writers

PUBLISHER
Häme University of Applied Sciences (HAMK)
PO Box 230
FI-13101 Hämeenlinna, FINLAND
tel. +358 3 6461
julkaisut@hamk.fi
www.hamk.fi/julkaisut

Hämeenlinna, February 2018

INDEX

PREFACE 4

Jakub Dolejš, Vikas Arora & Jiri Ilčík

UPDATING FINITE ELEMENT MODEL OF FAÇADE SCAFFOLDS ANCHOR CONSIDERING EXPERIMENTAL DATA 9

Maria Bronzova, Marsel Garifullin, Kristo Mela, Sami Pajunen & Markku Heinisuo

EFFECT OF AXIAL FORCE IN MAIN MEMBER ON INITIAL AXIAL STIFFNESS OF TUBULAR JOINTS ... 25

Lukáš Ledecký, Yvonne Ciupack, Hartmut Pasternak, Achim Geßler & Markus Feldmann

REDUCTION OF FATIGUE CRACK GROWTH RATE IN COMPACT TENSION SPECIMENS USING ADHESIVELY BONDED CFRP-STRIPS 30

Yvonne Ciupack, Hartmut Pasternak, Emre Yilmaz, Florian Sternsdorff & Ioannis Vayas

HYBRID REINFORCEMENT MEASURES AND INNOVATIVE MEASUREMENT METHODS IN STEEL CONSTRUCTION 43

Birgit Ragotzky, Benjamin Launert & Thomas Krausche

WELDING SIMULATION FOR THE CALCULATION OF THE WELDING RESIDUAL STRESSES IN WELDED I-GIRDERS 56

Viktor Karpilovsky, Eduard Kriksunov, Anatoly Perelmuter & Vitalina Yurchenko

SOFTWARE DEVELOPMENT EXPERIENCE IN DESIGNING OF STEEL STRUCTURAL JOINTS 69

Pichugin S. F. & Patenko Iu. E.

RELIABILITY OF STEEL FRAMEWORKS OF INDUSTRIAL BUILDINGS 83

Raimo Ruoppa, Raimo Vierelä, Marko Ylitolva, Rauno Toppila & Vili Kesti

BENDING TESTS OF VERY THICK PLATES WITH ADVANCED RESEARCH EQUIPMENT AND TECHNIQUES 94

L.I. Storozhenko & G.M. Gasii

NUMERICAL STUDIES OF BEHAVIOR OF A CURVED STEEL AND CONCRETE COMPOSITE CABLE SPACE FRAME 105

Igor Gavrilenko, Sergij Girenko, Anatoly Perelmuter, Michail Perelmuter & Vitalina Yurchenko

LOAD-BEARING CAPACITY AS AN INTERACTIVE ANALYSIS TOOL IN SCAD OFFICE 112

Kuldeep S Virdi

FIRE TEMPERATURE DISTRIBUTION IN TRAPEZOIDAL COMPOSITE FLOORS 128

Dr. Tarja Meristö & Jukka Laitinen

ALL ROADS LEAD TO ROME?
Vision-Based Scenario Evaluation concerning Sustainable Residential Areas. 140

Dr. Tarja Meristö & Jukka Laitinen

ROME WAS NOT BUILT IN ONE DAY
Future-oriented regional development towards energy-efficient residential areas 148

D. O. Kuzmenko, V. M. Fridkin & I. M. Kuzmenko

Technical Note
SELECTION OF FINITE ELEMENT FOR DESIGNING METAL BUILDING STRUCTURES 156

PREFACE

Kuldeep Virdi
City, University of London

Lauri Tenhunen
Häme University of Applied Sciences (HAMK)

Innovation activity is primarily systematic and interactive by nature. Several researchers have come to a definition similar to the following (Lundvall 1992, Lundvall & Borras 1997, Brazhyk et al. 1998, Kolehmainen 2001 and Ståhle et al. 2004):

> *"An innovation system is by nature a social system that emphasizes the significance of human interactions."*

An innovation environment (an innovative milieu) is a broader concept than an innovation system. An innovation system forms an institutional framework for the innovation environment and thus is like the skeleton of a living organism. The starting point for viewing innovation environments is that an organisation is not an actor separated or detached from its environment but is, in many ways, embedded into it (Kostiainen 2000).

Based on the results of earlier research it seems that active network collaboration is typical for successful innovation environments. The network is supplying deliberate connections between actors. In a networked activity, the channels of coordination and supervision are multidirectional and complex. In a network, information is flowing better vertically and horizontally than in any organisation that is functionally (horizontal) differentiated and hierarchically (vertically) lead.

METNET networking has existed since 2006. In this period, the METNET participants have organized twelve international conferences and seminars, as well as eleven separate workshops. These are listed on the METNET pages www.hamk.fi/metnet. Apart from helping research and development organisations in their scientific and applied research, during these years, METNET collaboration has expanded the innovation environment influencing profitability and employment potential of member companies.

Since the Århus seminar of 2011, articles presented i n the seminars have been published in the annual METNET Proceedings books. These books have presented scientific and development papers of high calibre and are available for downloading from the METNET pages. Today, the publication process of the METNET Proceedings books utilises blind peer review to assess the validity, quality and the originality of the articles for publication. The procedure fulfils the criteria of the Ministry of Education in Finland.

The following Figure is picked up from an article (Tenhunen & Ranta-Eskola 2013) in the METNET Luleå Proceedings book. Figure 1 is based on the theory of "Blue Box" analysis as well as the theory of "technological trajectories". The concept of technological trajectory means the companies' path dependence, telling how the selection of their strategies is restricted by their history and current situation, and by future opportunities (Kautonen & Tiainen 2000). Figure 1 shows which kind of university-business collaboration (UBC) options are typical for separate kinds of businesses. Emerging new businesses with many competing technological trajectories, for example, benefit especially from the basic scientific research. The nature of each competing trajectory is supposed to be deep and the stage of basic research and radical innovation possibilities covers a long period. In addition, companies, whose services are knowledge-based, look for strong partnerships fostering their activities.

On the other hand, all companies benefit from applied research as well as daily university-business collaboration with minor targets. The analysis forms a model to connect types of supplied university R&D services to typical cooperating companies.

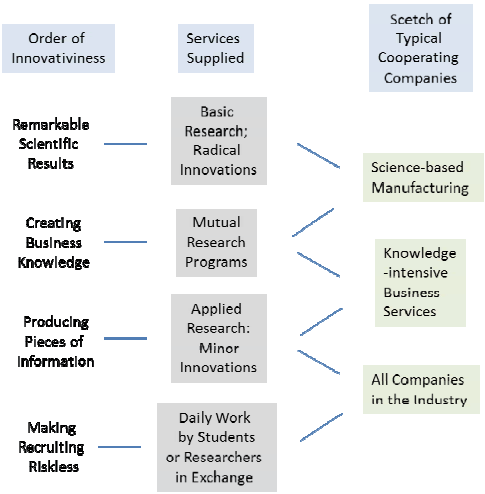

Figure 1. Supplied University R&D Services by Type of Industry (Tenhunen & Ranta-Eskola 2013).

METNET collaboration has been active on all the levels of University Research and Development Services described in Figure 1. For example, remarkable scientific results have been attained in international cooperation projects, financed by European Research Fund for Coal and Steel (RFCS). International businesses have been developed by development projects financed by the Nordic-Russian Cooperation Programme in Education and Research, which supports cooperation projects between higher education and research institutions in Russia and the Nordic Countries. Researchers and student exchanges between the collaboration partners, as well as students practicing periods have been organized bilaterally between many of the participating organisations.

The main target for METNET collaboration was set in 2006 as follows. “The purpose of METNET-network is to bring together European R&D and training organizations to develop new products and services to support innovative processes in companies working in the field of metallic construction and industry.” Today, after several years of collaboration, we find that the role of the collaboration stands today as it was originally stated. METNET network promotes transfer of knowledge and best practice between companies, research and training organizations at the European level.

Organisations participating in the METNET collaboration have arranged, among other things, yearly seminars and conferences, regular workshops and other types of flexible collaboration; to support, plan, prepare and manage extensive international ventures and share essential information and skills in the industry. The basic concepts are stated in the Figure 2 under. The METNET partners have regularly prepared large venture applications for EU authorities. Many of these applications have been successful.

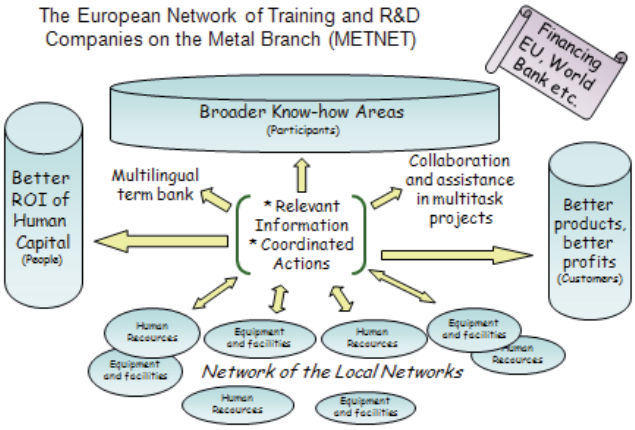

Figure 2. The basic concepts of Metnet (www.hamk.fi/metnet). R&D = Research and Development; ROI = Return on Investment.

Analyses of networks in general, seems to point out that the benefits gained by business operations from collaboration networks creating various innovation environments are significant and that it pays to maintain collaboration networks purposely.

Keeping the tradition of the annual seminars in preceding years, the 2017 Cottbus seminar received papers concerning experimental and numerical innovations relating to metal structures, as well as management topics focusing on planning projects for the future. A paper from the Czech Technical University described a new type of façade scaffold anchor, which overcomes some of the drawbacks of connectors currently used in practice. The paper from a team from Tampere University of Technology, focused on the effect of

axial stiffness on the behaviour of tubular frames. The authors propose a chord stress function, which gives the reduction of the axial stiffness with the value of the axial force. This should enable a more realistic analysis of structures adopting tubular members. Experiments on a novel approach towards repair of fatigue damaged steel structures using Carbon Fibre Reinforced Polymer strips were presented by a team from several German universities. Carefully selected test parameters and testing specimens allowed demonstration of the success of the technique.

A paper resulting from collaboration between Brandenburg University of Technology, Cottbus, and the National Technical University, Athens, describes an innovative application of thermal imaging for the purpose of strain measurement during experiments on structural elements reinforced with Carbon Fibre Reinforced Polymer strips. The paper, dedicated to Prof. Dr.-Ing.habil. Dieter Füg on his 80th birthday also shows that their collaboration covers not only the research topic described but also developing undergraduate and postgraduate dissertations in the two universities. Another paper from the host university presented experimental results on welded I-girders aimed at determining the residual stresses arising out of the welding process. The authors assess the performance of two software programs capable of simulating the welding process.

The team from Lapland University of Applied Science, working with SSAB, presented a paper describing the construction of a special machine for testing the bendability of plates of thickness up to 80mm. Based on their results; the paper concludes that equations used for bendability of thinner plates could be extended to plates up to 80 mm thick.

Researchers from Poltava National Technical Yuri Kondratyuk University described an interesting composite structure using concrete arch slabs interacting with cables in tension. Emanating from the same university another paper develops an approach for calculating the factor of safety of single storey steel frameworks under the specific loading related to travelling cranes. Also from Ukraine, two other paper described features of the SCAD/COMET software. One paper describes generation of parameters required for safe design of connections in steel structures. Another interesting paper explores the safety of the design of steel structural elements by exploring the entire regions, representing various combinations of design parameters. The paper points out that these regions are not always convex; pointing out that under certain combinations the element could be unsafe at lower applied loads when compared with some other combinations at the design loads.

A paper from City, University of London, described the use of the finite difference approach towards calculating the fire temperature distributions in trapezoidal composite floors. In particular, the paper shows how inclined boundaries, relative to the finite difference grid in two dimensions, could be handled to obtain results with this technique. The advantages of the finite difference solutions are that the data preparation is minimal, even for non-linear problems, resulting in efficient analysis by engineers.

Two papers from Laurea University of Applied Sciences, demonstrate a management approach towards making decisions regarding the future vision of a project. In one paper, the authors describe a systematic approach, which includes input from various 'actors' in the project. The other paper focuses on energy efficiency of buildings in residential areas. The background is climate change. The methodology adopted uses the "steps towards the vision" framework. Actions to be taken are discussed alongside consideration of persons with responsibility to achieve the objectives. The paper illustrates results from one of three areas where the methodology was applied. The paper concludes with general requirements for future-oriented regional development.

The proceedings include a technical note, from a team of Belorussian Universities, which compares efficacy of using solid, shell and beam elements when analysing structural frames.

Kuldeep Virdi
Lauri Tenhunen

SOURCES

Braczyk, H-J. & Cooke, P. & Heidenreich, M. (eds.) (1998). *Regional Innovation System: The Role of Governance in Globalized World*. London: UCL Press.

Kolehmainen, J. (2001). *Yritykset ja alueet tietointensiivisessä globaalitaloudessa*. Tampereen yliopisto, Alueellisen kehittämisen tutkimusyksikkö. Sentejulkaisuja 12/2001. (In Finnish.)

Kostiainen, J. (2000). Helsingin, Oulun ja Tampereen kaupunkiseudut innovatiivisina miljöinä. In J. Kostiainen, M. Sotarauta, & K. J. Kosonen (eds.). *Kaupunkiseudut innovatiivisina toimintaympäristöinä*. Helsinki: Tekniikan akateemisten liitto. (In Finnish.)

Lundvall, B.-Å. (1992). User-Producer Relationships, National Systems of Innovation and Internationalization. In B.-Å. Lundvall (ed.). *National system of innovation and interactive learning*. New York: Printer.

Lundvall, B. & Borras, S. (1997). *The Globalising Learning Economy: Implications for Innovation Policy*. Commission of the European Union, DG XII.

Ståhle, P., Sotarauta, M. & Pöyhönen, A. (2004). *Innovatiivisten ympäristöjen ja organisaatioiden johtaminen*. Eduskunnan kanslian julkaisu 6/2004. Tulevaisuusvaliokunta, Teknologian arviointeja 19.

Tenhunen, L. & Ranta-Eskola, A. (2013). The Blue Box and the Technological Trajectories in context of University-Business Cooperation (UBC). In K. Virdi & L. Tenhunen (eds). Proceedings of the METNET seminar 2013 in Luleå. HAMKin julkaisuja 1/2014.

UPDATING FINITE ELEMENT MODEL OF FAÇADE SCAFFOLDS ANCHOR CONSIDERING EXPERIMENTAL DATA

Jakub Dolejš
Faculty of Civil Engineering – Department of Steel and Timber Structures, Czech Technical University in Prague, Thakurova 7, 166 29 Praha 6, Czech Republic

Vikas Arora
Department of Technology and Innovation, University of Southern Denmark, Campusvej 55, Odense 5230, Denmark

Jiri Ilčík
J2L CONSULT, s.r.o., Brandlova 2536/36, 69501, Hodonin, Czech Republic

ABSTRACT

Considering the stability of the façade scaffolds, their anchoring is one of the most important phenomena. The anchors secure scaffolding against overturning and also help transfer the horizontal forces from the scaffold to the façade. There are many different types of anchors in the construction field, but the principle used to join these anchors to the thermal insulated façade is basically the same. A new type of façade scaffold anchor was developed and is described in this paper. Main problems associated with the existing anchors are: damage of façade thermal insulation layers, insufficient supporting of the scaffold standards and decreasing the stability of the scaffold construction. The newly developed anchor overcomes these problems associated with existing anchoring. An experiment on the developed anchor has been carried out and it has been observed that the experimental results (force–displacement curve) do not match with the finite element predictions. Subsequently the finite element model (FEM) of the developed anchor has been updated in the light of experimental results. The finite element model of the anchor was corrected using the parameter-based finite element model updating method. The results have shown that now there is a good correlation between the updated finite element model and the experimental data. The accuracy of updated finite element model is demonstrated by plotting the predictions made by finite element model with experimental results. The overlay of finite element model predictions and experimental data has shown the success of the updating procedure and thus it can accordingly be concluded that updated finite element model of the anchor represents the anchor behaviour with confidence.

Keywords: Parameter-based optimization; Stability-based anchor design; Experimentation of anchor, Finite element model of anchor, Façade scaffolds.

INTRODUCTION

Use of façade thermal insulation layers for new buildings as well as for the existing constructions is quite a common phenomenon. None of the existing fixing methods of scaffold structures consider these layers. For the best anchoring, a scaffold's tie member is pinned as near to a façade as possible (Dolejš 2013). In this way, the insulation layer has to be removed, which requires additional repairs. A more common option is to use a long scaffold screw, which connects tie member and façade as shown in Figure 1. Because of safety considerations, nowadays, scaffold systems are covered with nets or planks. However, the cladding increases horizontal force due to wind acting on anchors (Vlasák 2011), which is said to be crucial in most of the accident cases (Wang *et al.*, 2013; Wang et al. 2014). The long scaffold screw can transmit large forces from the scaffold construction into the façade, which results in a deformation of the screw as well as damage of the surrounding thermal layers and the stiffness of the whole scaffold system is considerably decreased (Dolejš 2013). It should also be noted that due to loosened connections of components (Chandrangsu & Rasmussen 2009), the scaffold system becomes weak which brings difficulties in stabilizing the construction and in anchoring (Beale 2014). The stability of the frame scaffoldings has been observed in many papers, see (Liu et al. 2010, Peng et al. 2013). The insufficient stability of the tube scaffoldings is described by Dolejš (2013). The scaffolding has been modeled as netted cladding and the load combinations have been based on European standards EN 12 811-1 (2003). The anchors have been modeled as a pinned supports. The scaffold´s tubes have been connected by semi-rigid joints respecting M – φ relation obtained experimentally. Generally, the semi-rigid connections as well as initial imperfections have a significant effect on the results (Prabhakaran et al. 2011, Chandrangsu & Rasmussen 2011). Critical load coefficients for each combination were computed. The values vary in the range from 1.68 to 2.74 only. If the same model is supported by a rigid fixing, then the critical coefficient values became higher even if the number of the anchors decreased.

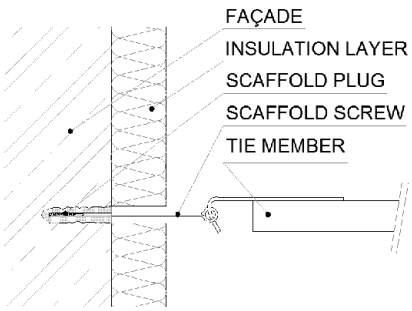

Figure 1. Vertical section of the plugged anchor with a long screw connecting the insulation layer.

Based on these analyses, it was determined that any newly developed anchor should provide a rigid-torsion support in a horizontal plane. It is obvious

that final behavior of a real anchor will be semi-rigid, but even a semi-rigid support could have a large effect on the complex stability (Peng et al. 2009, Beale & Godley 2009).

For further analyses and development, the tubular scaffold systems has been mainly considered. The reasons are that a tubular scaffold is generally a weaker system then a frame scaffold (Dolejš et al. 2011, Chandrangsu & Rasmussen 2011) and because of that, the support forces in tubular scaffolding are greater.

PROPOSED ANCHOR DESIGN

In order to overcome the problems associated with the existing anchoring three shapes of the new anchor have been developed and officially registered. The original design of these anchors has been made in a simple empirical way. The three models have been termed as Type I (The Rigid Scaffold Anchor), Type II (The Oblique Scaffold Anchor) and Type III (The Oblique Sliding Scaffold Anchor). For the following study, only Type III has been used. Type III is represented by a main part, which is an oblique and adjustable arm. It can be observed from Figure 2, that at least two anchors in one horizontal plane must be used in a fixing system; these two anchors placed in the opposite orientation have to create a notional trapezoid with the surface of the façade.

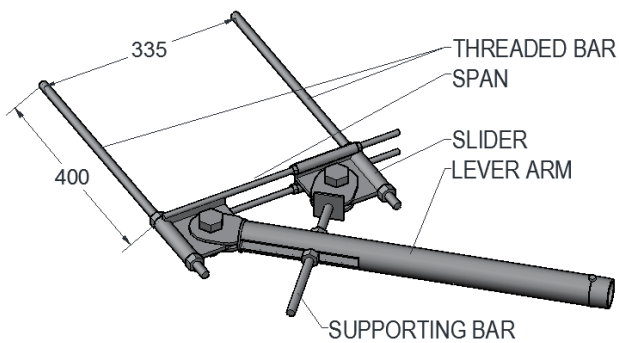

Figure 2. Type III Anchor.

If the outer plane seems to be stiff enough because of the vertical X-bracing, the inner plane can be moved only in a way parallel with the façade. By using Type III anchors, the displacement of the inner plane should be also restricted. Another advantage is that this anchor enables only a minimum displacement of the parallel threaded rods which are jointed into the façade and that ensures that the surrounding insulation layers are not damaged.

Details of particular parts are presented in Figure 3. The main part consists of two threaded bars with a circular cross section M16/8.8. Bars are plugged into the façade while the thermal insulation layers surround these two bars. The members “Span” and “Slider” are put on “Threaded bars”. “Slider” is made of

steel plates with thickness 7 mm and of the steel tubes with dimension 48.3/3.2 class of steel S235J0. The “Slider” also provides a base for the “Supporting bar”. The “Span” member is basically of the same shape as the “Slider”, but there are two parallel threaded rods M10 /4.8 welded on it. Because of the length of the rods, the “Threaded bars” could be in any mutual distance up to 400 mm. Furthermore, the distance between the “Span” and the façade depends on a depth of insulation layers. The “Threaded bars”, “Slider” and “Span” create a rigid frame. The “Supporting bar” fixes the position of the “Lever arm”. The cross section of the bar is M16 /8.8. The “Lever arm” is made of the classic scaffold tube with dimensions 48.3/3.2 mm class of steel S235J0. The end of the “Lever arm” is connected with the scaffold´s standard. For the connections of the members to each other, there are two bolts M16 /8.8. Used parts connected by this way are naturally hinged with free rotations.

PERIMENT

The scheme diagram of the laboratory experiment is shown in Figure 3. The anchor was plugged into the fixed steel beam and loaded continually by tension force only in the vertical direction. The force was increased from 0 up to 3 kN and the displacement of the lever arm was recorded in real time. Output of the experiment was a force-displacement curve (Figure 4).

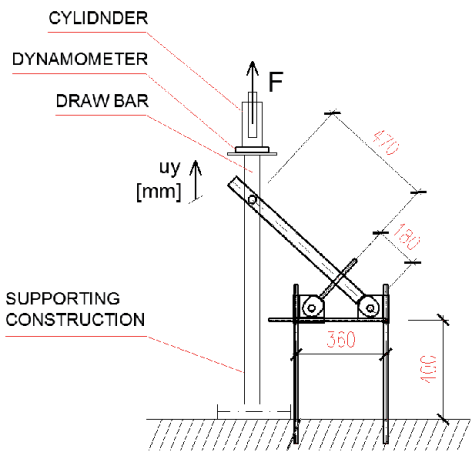

Figure 3. The vertical section of the laboratory experiment.

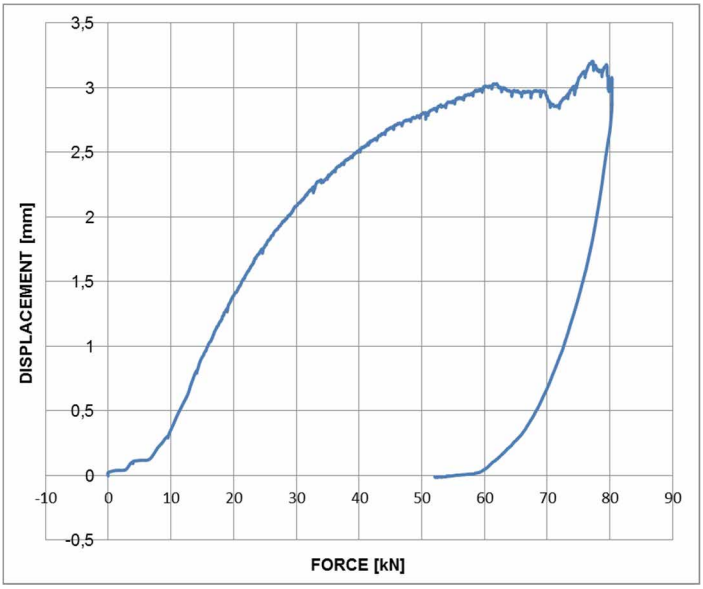

Figure 4. The final Force – Displacement curve of the experiment.

The force was provided by a single-acting hollow plunger cylinder ENERPAC RCH-123 with a one-handed pump ENERPAC P-392 (Enerpac data sheet 2010). The cylinder was situated on the top of the supporting steel construction made from two parallel columns with reversed T shape. This construction surrounded the Lever arm of the anchor. Between the cylinder and the upper surface of the construction was placed a pressure dynamometer (Tensiometric dynamometer S-35 data sheet 2011), which was connected with a computer to measure the actual loading force. The draw bar made of steel connected the hydraulic cylinder to the end of Lever arm. The output of this experiment was a vertical displacement of the Lever arm. This displacement was measured by a common absolute potentiometer sensor and real-time values were transferred to the computer. It seems that at the very beginning the "Span bar" reached the plastic behavior. After applying the force of approximately 3.0 kN the first small cracks on the span bars were detected. These cracks become larger at the end of the experiment. The weakest part of the anchor appeared to be the Span member.

THE ANCHOR ANALYSIS

For FE numerical analysis both beam and solid model have been developed. In these models, the applied force was increased from 0 up to 3.0 kN and the maximum deflection (u_y) at the end of the Lever arm should be 60 mm (according to the Figure 4). Because it was observed from the experiment that the anchor deformed permanently, beam and solid models with non-linear material for the anchor are developed.

In the numerical models, the cross sections of the all threaded rods are considered with the value of minor diameter. Also, it has to be mentioned that the real anchor consists of several single parts with the gaps between each other. Because of that, the initial displacement ($u_{y,initial}$) of the measured Lever arm was set up as 10 mm.

The Initial beam model

The beam model was created in ANSYS workbench. Geometry of the FE model corresponds to the geometry of the experimental anchor. The model consists of nine parts with 455 nodes and 226 elements; total weight is 4,91 kg (Figure 5). Parts 03 and 04 are not expected to deform, so they are simply modeled as rigidly connected beams with a circular cross section of diameter 13.0 mm. The member Lever arm consists of two parts, because of the different cross sections. The longer main part of Lever arm has a cross section of steel scaffold tube. The shorter part, which is closer to the Span bar, should have a cross section of weakened scaffold tube, but since there was no deformation observed during the experiment this part has been simply modeled as the scaffold tube also. Cross sections of other members have been described in the text above.

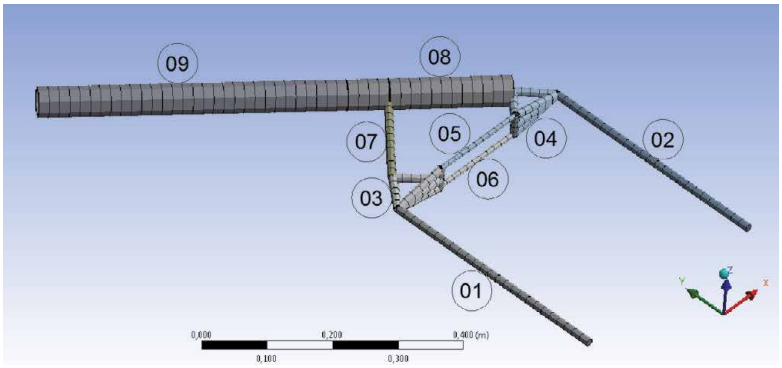

Figure 5. The beam model, Parts: 01-Left Threaded Bar, 02-Right Threaded Bar, 03-Slider, 04-Span Bar (base), 05-Span Bar (Upper rod), 06-Span Bar (Bottom rod), 07-Support Rod, 08 and 09-Lever Arm.

Three materials were used for the models. The structural steel S235 has yield strength of 200 MPa. Steel grades used for rods 4.8 and 8.8 have yield strengths of 300 MPa and 580 MPa, respectively. Plastic behavior of these materials was expected, so the stress-strain diagrams are considered as bilinear with isotropic hardening. Young's modulus of all materials is 210 GPa.

Single members of the anchor were connected together with both of the longitudinal (along X and Y-axes) and also with torsional stiffness (along the Z-axis). Table 1 summarizes degrees of freedom of each joint. The bolted

joints (3-7 and 4-8 according to Table 1) are considered as hinged connections. The initial values of longitudinal stiffness were computed using empirical equations. However, the real values of stiffness of the joints are unknown. This may be considered to be a source of error in the finite element model.

Table 1. Degrees of freedom in joints.

Table 1 - Degrees of freedom in joints

PARTS	JOINT NAME	X	Y	Z	ROT X	ROT Y	ROT Z
		[MN/m]			[MNm/rad]		
1 - 3	L	1470	406,9	free	free	free	0,1
2 - 4	R	1470	406,9	free	free	free	0,1
3 - 5	LN-U	351,9	9000	free	free	free	0,01
3 - 6	LN-D	351,9	9000	free	free	free	0,01
4 - 5	RN-U	387,9	21630	free	free	free	0,1
4 - 6	RN-D	387,9	21630	free	free	free	0,1
3 - 7	/	rigid	rigid	rigid	free	free	free
4 - 8	/	rigid	rigid	rigid	free	free	free
7 - 8	/	rigid	rigid	rigid	free	free	free
8 - 9	/	rigid	rigid	rigid	rigid	rigid	rigid

The defection profile is calculated using the applied force and subsequently plotted along with the experimental results as shown in Figure 6. It can be observed that the finite element results do not match very well with the experimental results. This is discussed below.

The Initial solid model

The solid model has been also created in ANSYS workbench, as shown in Figure 7; indications of the parts are also given in this figure. The model consists of 11 parts. The mesh contains 30 415 nodes and 16 457 elements. As it was expected and according to the higher accuracy the total weight 7.57 kg is significantly more than the beam model weight (4.91 kg). All connections between FE were set up as joints. Cross sections and material properties have been used the same as for the beam model. Since the connections were entered as joints, in solid model the optimization parameters will be material properties only.

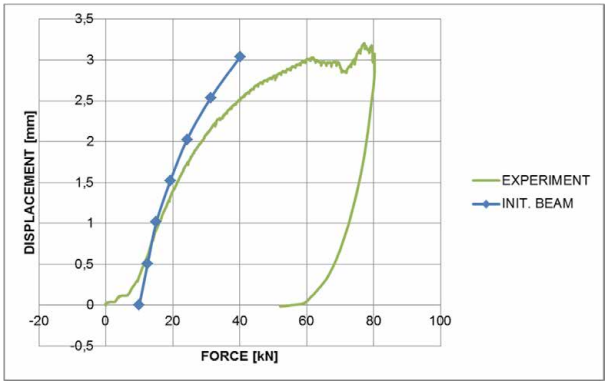

Figure 6. Force – Displacement curve of the Initial beam model.

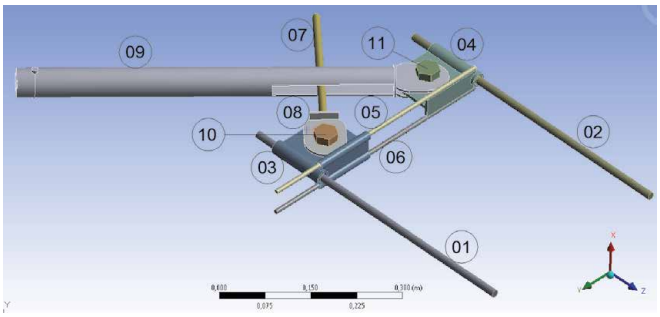

Figure 7. The solid model, 01-Left Threaded Bar, 02-Right Threaded Bar, 03-Slider, 04-Span Bar (base), 05-Span Bar (Upper rod), 06-Span Bar (Bottom rod), 07-Support Rod, 08-Support Rod (base), 09-Lever Arm, 10-Left Bolt, 11-Right Bolt.

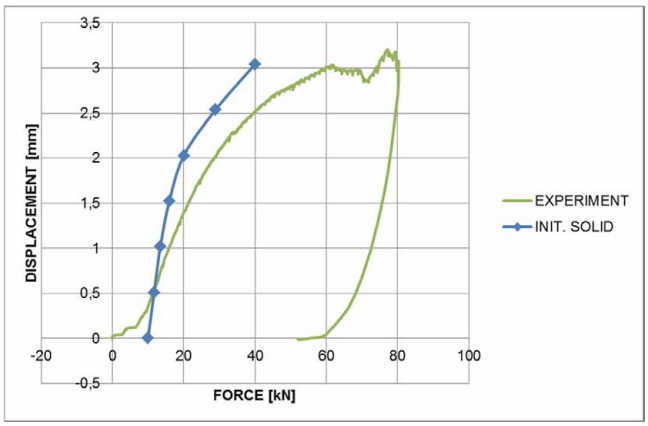

Figure 8. Force – Displacement curve of the initial solid model.

The output force-displacement curve is represented in Figure 8 and as expected, the curve also does not match with the experimental data perfectly.

OPTIMIZATION

Choice of updating parameters on the basis of engineering judgment about the possible locations of modelling errors in a structure is one of the strategies to ensure that only physically meaningful corrections are made. In case of an anchor, modelling of stiffness of the joints and the properties of the material is expected to be a dominant source of inaccuracy in the FE model, assuming that the geometric parameters are correctly known. The values of stiffness of joints and values of the material parameters are updated in the light of experimental results. Some work has been carried out to update the stiffness of joint in the light of experimental data. Arora et al. (2009) updated the joint stiffness of an F-shape structure using frequency response function data. The joints include both bolted and welded joints. Arora (2014) updated stiffness of the end of cantilever beam using resonance and anti-resonance frequencies. Gant et al. (2011) updated joint stiffness of large aeronautical structures. Okasha et al. (2012) updated the finite element models of bridges using strain data for lifetime reliability assessment of the bridges. All the above-mentioned methods of updating the finite element models are sensitivity based methods in which the sensitivities of parameters are used to reduce the error between the finite element predictions and experimental data.

Parameter-based finite element model

Updating method adopted here is an iterative and parameter-based model updating method and uses imperfections to update the finite element model. Following identities relating to stiffness (K) and deflection (Q) relating to analytical model as well as actual structure respectively can be written as:

$$k_A Q_A = F \tag{1}$$
$$k_X Q_X = F, \tag{2}$$

where subscript A and X denote an analytical (FE model) and experimental model respectively. As the right-hand sides of Equations. 1 and 2 are same, it follows that:

$$k_A Q_A = k_X Q_X \tag{3}$$

Considering experimental stiffness value is greater than analytical stiffness value, the experimental stiffness value can be written as:

$$k_X = k_A + \Delta k \tag{4}$$

Substituting Eq. 4 in Eq. 3 as:

$$k_A Q_A = (k_A + \Delta k) Q_X \tag{5}$$
$$k_A Q_A - k_A Q_X - \Delta k\, Q_X = 0 \tag{6}$$
$$k_A (Q_A - Q_X) - \Delta k\, Q_X = 0 \tag{7}$$
$$\frac{\Delta k\, Q_X}{k_A} = Q_A - Q_X \tag{8}$$
$$\Delta k = k_A \frac{Q_A - Q_X}{Q_X} \tag{9}$$

Eq. (9) is the basic equation for updating the stiffness matrix using imperfection. Analytical stiffness of structure consists of individual element stiffness as:

$$k_A = \sum_{i=1}^{n} k_i, \tag{10}$$

where n is number of elements. Linearizing with respect to the $\{p\}$, $\{p\}=\{p_1,p_2,\ldots,p_{nu}\}$, where nu is number of updating parameters, being the vector of updating variables associated with individual or group of finite elements, gives:

$$\Delta k = \sum_{j=1}^{nu} \left(\frac{\partial k_j}{\partial p_j} \Delta p_j \right) \tag{11}$$

Dividing and multiplying the above equation by p_j and then writing u_j in place of $\frac{\Delta p_j}{p_j}$, the equation becomes:

$$\Delta k = \sum_{j=1}^{nu} \left(\frac{\partial k_j}{\partial p_j} p_j \right) u_j \tag{12}$$

where is the correction factor and is the sensitivity of the stiffness matrix (S) with respect to the updating parameter:

$$S \,.\, u = k_A \frac{Q_A - Q_X}{Q_X} \tag{13}$$

In matrix term the Eq. (13) is written as:

$$[S]_{N\times N}\{u\}_{N\times 1} = [k_A]_{N\times N} \left\{ \frac{Q_A - Q_X}{Q_X} \right\}_{N\times 1}, \tag{14}$$

where N is the total degrees of freedom of the structure. The updating correction vector $\{u\}$, which consists of correction factor of stiffness parameters to update stiffness matrix of the structure. This process is repeated in an iterative way. The performance is judged on the basis of the accuracy with which the deflection predicted by updated FE model match the experimental values.

RESULTS

The results of optimization both of the models in contrast with the experimental measurement are plotted in the Figure 9.

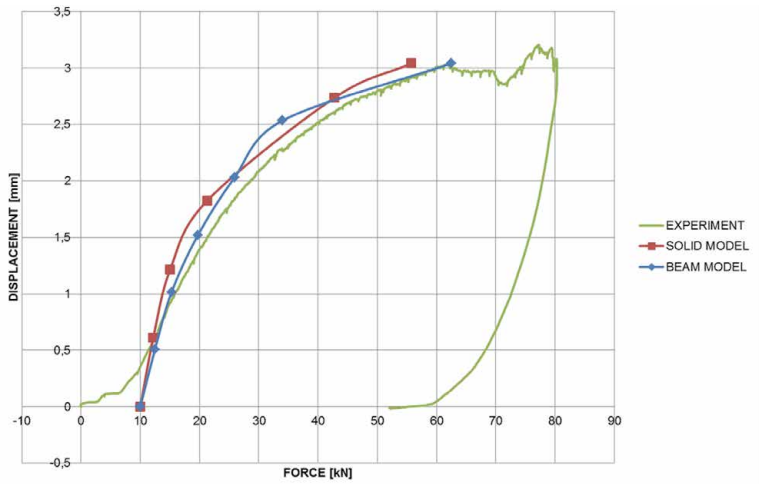

Figure 9. Force – Displacement curve and the deformed shape of optimized models.

Beam model optimization

In the ANSYS workbench a Goal Driven Optimization has been performed. The input parameters were both longitudinal and torsional stiffness as well as yield stress values of the non-linear materials. In the early stages of the optimization, it was observed that the most affecting parameters is the longitudinal stiffness. Unfortunately, the final total deformed shape of the FE model did not correspond with the deformed shape of the real anchor. Because of that, the input parameters of longitudinal stiffness were abandoned and left with the initial values and all optimization was focused only on the torsional stiffness and material properties. The values of the final optimized Beam model and the Initial beam model are shown in Table 2. Figure 10 demonstrates the final deformation. It can be observed from Figure 9, that the force – displacement curve predicted by the FE model now matches well with the experimental curve.

Table 2. The input values of the Initial beam model and optimized values of the Beam model.

INITIAL BEAM MODEL					BEAM MODEL
STIFNESS	NAMED			MN/m	MN/m
LONGITUNIDAL	R	Y		406,90	406,90
LONGITUNIDAL	L	Y		406,90	406,90
LONGITUNIDAL	L	X		1470,00	1470,00
LONGITUNIDAL	R	X		1470,00	1470,00
				MNm/rad	MNm/rad
TORSIONAL	L			0,10	2,41
TORSIONAL	R			0,10	2,41
				MN/m	MN/m
LONGITUNIDAL	RN	D	Y	21630,00	21630,00
LONGITUNIDAL	RN	D	X	387,90	387,90
LONGITUNIDAL	RN	U	Y	21630,00	21630,00
LONGITUNIDAL	RN	U	X	387,90	387,90
				MNm/rad	MNm/rad
TORSIONAL	RN	D		0,10	0,11
TORSIONAL	RN	U		0,10	0,11
				MN/m	MN/m
LONGITUNIDAL	UL	X		0,10	0,10
				MN/m	MN/m
LONGITUNIDAL	LN	D	Y	9000,00	9000,00
LONGITUNIDAL	LN	D	X	351,90	351,90
LONGITUNIDAL	LN	U	Y	9000,00	9000,00
LONGITUNIDAL	LN	U	X	351,90	351,90
				MNm/rad	MNm/rad
TORSIONAL	LN	D		0,01	0,34
TORSIONAL	LN	U		0,01	0,34
MATERIAL				MPa	MPa
STRUCTURAL STEEL NL S235				200	200
STRUCTURAL STEEL NL 4.8				300	275
STRUCTURAL STEEL NL 8.8				580	550

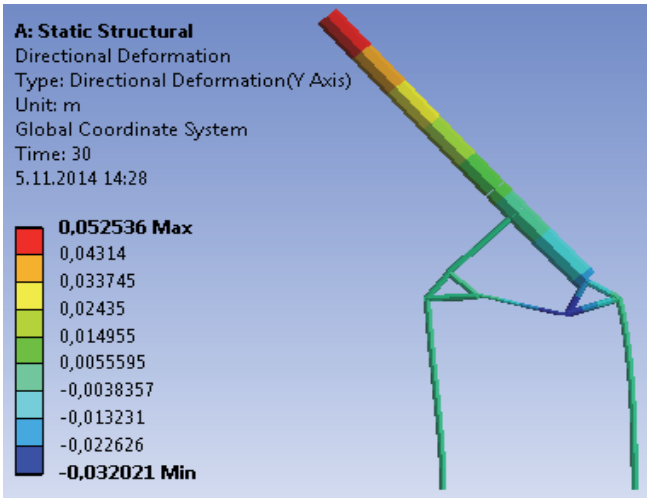

Figure 10. The deformed shape of the beam model.

Solid model optimization

Since contacts between all parts were modeled as joints, material properties represent the only possible input parameters. The Goal Driven Optimization has been carried out in the ANSYS workbench again. Optimized values are shown in Table 3 and the final deformed shape is shown in Figure 11. It can also be observed from the Figure 9 that the FE predicted force – displacement curve also matches well with the experimental curve.

Table 3. The input values of the Initial solid model and optimized values of the Solid model.

INITIAL SOLID MODEL		SOLID MODEL
	MPa	MPa
STRUCTURAL STEEL NL S235	200	200
STRUCTURAL STEEL NL 4.8	300	260
STRUCTURAL STEEL NL 8.8	580	500

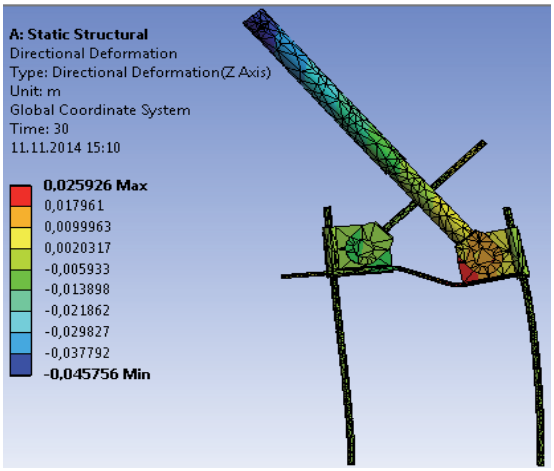

Figure 11. The deformed shape of the solid model.

CONCLUSIONS

In this paper a new Type III (The Oblique Sliding Scaffold Anchor) has been developed. Experiments have been conducted to evaluate the behavior of the anchor. The finite element models (beam and solid models) were developed. It was observed, that the finite element models did not match with the experimental results. A choice of updating parameters on the basis of engineering judgment considering the possible locations of modelling errors in a structure was the strategy adopted to ensure that only physically meaningful corrections are made. In case of an anchor, modelling of stiffness of the joints and values of the materials are expected to be dominant sources

of inaccuracy in the FE model, assuming that the geometric parameters are correctly known. After updating stiffness of the joints of the anchor, the finite element prediction matched with experimental results. The paper described the approach for optimising the parameters.

This paper is a part of the long-term development of a new fixing system for the façade scaffolding. Based on the FE models developed in this paper the anchor will be optimized to carry support forces adjusted in the new fixing system.

ACKNOWLEDGEMENTS

The authors are grateful to the financial support by the Czech Technical University (Project no. SGS17/124/OHK1/2T/11) and also to the program ERASMUS+ (CZ PRAHA10). The technical support and a supervision during experiments by Jonáš of HILTI is gratefully acknowledged as well as support from Experimental Centre of Faculty of the Civil Engineering, CTU in Prague, and Mr. Picek of PKL servis.

REFERENCES

Ansys Workbench, version 14.0.0 – Static Structural

Arora V., Singh S.P., & Kundra T.K. (2009). Damped FE model updating using complex updating parameters: its use for dynamic design. *Journal of Sound and Vibration*, 324(1–2), 350–364.

Arora V., Singh S.P., & Kundra T.K. (2009). Finite element model updating with damping identification. *Journal of Sound and Vibration*, 324(3–5), 1111–1123.

Arora V. (2014). Constrained antiresonance frequencies based model updating method for better matching of FRFs. *Inverse problems in Science and Engineering*, 22(6), 873–888.

Beale, R.G., & Godley, M.H.R. (2009). Numerical modeling of full-scale tube and fitting scaffold tests. In J. Ambrósio et al. (eds.) *7th Euromech solid mechanics conference*. Lisbon: Instituto Superior Técnico.

Beale, R.G. (2014). Scaffold research – A review. *Journal of Constructional Steel Research*, 98, 188–200.

CEN (2003). *EN 12811-1: Temporary works equipment – Part 1: Scaffolds – Performance requirements and general design*. European Committee for Standardization.

Chandrangsu, T., & Rasmussen, K.J.R. (2009). Geometric imperfection measurements and joint stiffness of support scaffold systems. Proc. 6th *International Conference on Advances Steel Structures*, Vol. 1, University of Lisbon, Portugal, 1075–82.

Chandrangsu, T. & Rasmussen, K. (2011). Investigation of geometric imperfections and joint stiffness of support scaffold systems. *Journal of Constructional Steel Research*, NSW, 67(4), 576–84.

Chandrangsu, T., & Rasmussen, K. (2011). Structural modelling of support scaffold systems. *Journal of Constructional Steel Research*, 67(5), 866–875.

Dolejš, J., Picek, Z., Škréta, K., Vlasák, M., & Vlasák, S. (2011). *Navrhování konstrukcí z lešení I*. Česká technika, CTU in Prague, 28–35. *(Czech text)*

Dolejš, J. (2013). Spatial coaction of facade scaffolds elements and components. *Habilitation thesis*, CTU in Prague, Prague, CZ. *(Czech text)*

Enerpac technical data sheet. (02/2010), Retrieved from https://www.enerpac.com/en/products

Gant F., Rouch Ph., Louf F., & Champaney L. (2011). Definition and updating of simplified models of joint stiffness. *International Journal of Solids and Structures,* 48(5), 775–784.

Ilčík, J. & Dolejš, J. (2013). The Oblique Sliding Scaffold Anchor. *Utility model* CZ26024, Prague, CZ.

Ilčík, J., & Dolejš, J. (2013). The Oblique Scaffold Anchor. *Utility model* CZ26023, Prague, CZ.

Ilčík, J., & Dolejš, J. (2013). The Rigid Scaffold Anchor. *Utility model* CZ26022, Prague, CZ.

Liu, H., Zhao, Q., Wang, X., Zhou, T., Wang, D., Liu, J., & Chen, Z. (2010). Experimental and analytical studies on the stability of structural steel tube and coupler scaffolds without X-bracing. *Engineering Structures*, 32(4), 1003–1015.

Okasha N.M., Frangopol D.M., & Orcesi A.D. (2012). Automated finite element updating using strain data for the lifetime reliability assessment of bridges. *Reliability Engineering and System Safety*, 99, 139–150.

Peng, J., Chen, K., Chan, S., & Chen, W. (2009). Experimental and analytical studies on steel scaffolds under eccentric loads. *Journal of Constructional Steel Research* 65(2), 422–435.

Peng, J., Wu, Ch., Chan, S., & Huang, Ch. (2013). Experimental and numerical studies of practical systems scaffolds. *Journal of Constructional Steel Research* 91, 64–75.

Prabhakaran, U., Beale, R., & Godley, M. (2011). Analysis of scaffolds with connections containing looseness. *Computers and Structures*, 89(21–22), 1944–55.

Vlasák, S. (2011). *Konstrukce z lešení podle evropských norem*. CTU in Prague, Faculty of Civil Engineering, Prague, CZ, 128–30. *(Czech text)*

Tensiometric dynamometer S-35 data sheet. (02/2011). Retrieved 12 January 2018 from http://www.lukas-tenzo.cz/?i=219/tenzometricky-silomer-s-35-s-35-a

Wang, F., Tamura, Y., & Yoshida, A. (2013). Wind loads on clad scaffolding with different geometries and building opening ratios. *Journal of Wind Engineering and Industrial Aerodynamics*, 120(37), 37–50.

Wang, F., Tamura, Y., & Yoshida, A. (2014). Interference effect of a neighboring building on wind loads on scaffolding. *Journal of Wind Engineering and Industrial Aerodynamics*, 125, 1–12.

EFFECT OF AXIAL FORCE IN MAIN MEMBER ON INITIAL AXIAL STIFFNESS OF TUBULAR JOINTS

Maria Bronzova
Peter the Great St.Petersburg Polytechnic University

Marsel Garifullin
Kristo Mela
Sami Pajunen
Markku Heinisuo
Tampere University of Technology

ABSTRACT

Initial stiffness of tubular joints plays considerable role in the global analysis of frames and trusses. Axial forces that occur in the chord can affect initial stiffness of joints, leading to noticeable redistribution of forces in members of structures. Generally, this effect is taken into account by chord stress functions. Currently many chord stress functions exist for resistance of joints; however, no function was determined for initial stiffness. Based on the comprehensive finite element analysis and the manual curve fitting approach, this paper develops a chord stress function for initial axial stiffness of square hollow section T joints.

INTRODUCTION

Rectangular hollow sections (RHS) joints combine high strength, simple end preparations and welding process (Wardenier 1982), leading to good appearance and high stiffness and resistance. Many researchers (Boel 2010, Snijder et al. 2011, Haakana 2014) have proved that the initial rotational stiffness plays a key role in buckling of tubular truss members. Affecting the distribution of forces between members, axial stiffness is also known to be essential in the global analysis of frames and trusses. Therefore, the neglect paid to the role of axial stiffness of joints in current design rules is considered to be unreasonable, leading to collapses of structural elements, particularly in shallow Virendeel girders such as the one shown in Figure 1.

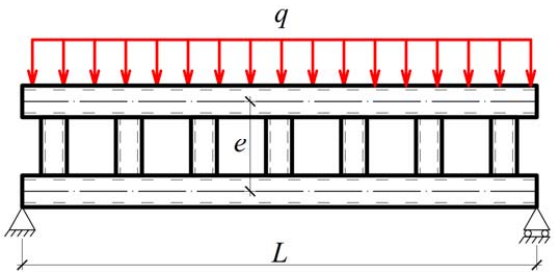

Figure 1. Shallow Virendeel girder.

Most of the publications and design guides for RHS T joints deal with the resistance of RHS joints (Yu 1997, Cao et al. 1998, Zhao & Hancock 1991, Packer et al. 2009, Zhao et al. 2010, Nizer et al. 2015). Initial stiffness of tubular joints was investigated by Mäkeläinen et al. (1988), Grotmann & Sedlacek (1998), de Matos et al., Neves (2004) and Weynand et al. (2015). However, none of these papers considers the effect of axial stresses in the chord on the initial axial stiffness of joints.

This paper, dealing with the axial stiffness of square hollow section T joints, develops the chord stress function, which defines the stiffness reduction produced by the axial forces in the main member. Investigation of the effect of the chord stresses is conducted using the FEM analysis. The final chord stress function is obtained via the approximation of the results using the linear and polynomial regressions. The chord stress function is determined by the following equation:

$$C = k_{sn,N} C_0 \,, \tag{1}$$

where C is the initial axial stiffness of the joints; C_0 is the initial stiffness of the joint with no axial force in the chord; $k_{sn,N}$ is the developed chord stress function.

RESULTS

The conducted FE simulation shows that axial forces in the chord significantly affect the initial axial stiffness of joints. Compressive loads lead to a maximum of 65% reduction of the stiffness, while tensile loads increase it by a maximum of 30%. The observed influence is found to depend on chord width-to-thickness ratio $\gamma = b_0/2t_0$ (Figure 2a), brace-to-chord width ratio $\beta = b_1/b_0$ (Figure 2b) and the steel grade f_{y0} (Figure 2c).

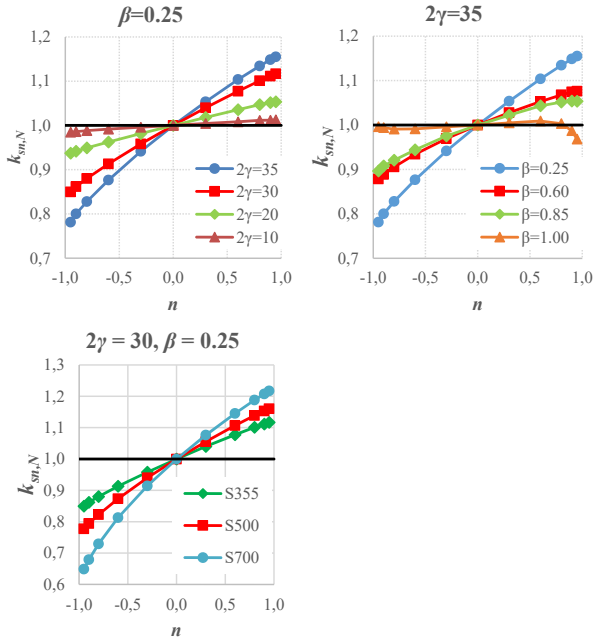

Figure 2. Dependence of the observed effect on γ (a), β (b) and steel grade (c).

Based on these observations, the following equation is proposed as a chord stress function:

$$k_{sn,N} = 1 + 10^{-5} \cdot f(\beta) \cdot f(\gamma) \cdot f(f_{y0}) \cdot n \tag{2}$$

where

$$f(\beta) = -2\beta^2 + 1.6\beta + 0.3$$
$$f(\gamma) = 1.3\gamma^2 - 38$$
$$f(f_{y0}) = 0.02 f_{y0}^{1.4} \tag{3}$$

Validation with an independent series of FE results shows that the proposed chord stress function provides good correlation with numerical results.

CONCLUSIONS

The conducted FE research has shown that axial forces in the main member significantly affect the initial axial stiffness of tubular joints. Based on the numerical results, a chord stress function is developed for initial axial stiffness of square hollow section T joints. When compared to numerical results, the proposed equation provides accurate results within the considered range.

However, it should be noted that this study was performed for square hollow section joints and further investigations are required to extend the proposed chord stress function to rectangular hollow section joints.

REFERENCES

Boel, H. (2010). *Buckling Length Factors of Hollow Section Members in Lattice Girders. Ms Sci thesis*. Eindhoven: Eindhoven University of Technology.

Cao, J.J., Packer, J.A., & Yang, G.J. (1998). Yield line analysis of RHS connections with axial loads. *Journal of Constructional Steel Research*, 48(1), 1–25.

Grotmann, D. & Sedlacek, G. (1998). *Rotational stiffness of welded RHS beam-to-column joints. Cidect 5BB-8/98*. Aachen: RWTH-Aachen.

Haakana, Ä. (2014). *In-Plane Buckling and Semi-Rigid Joints of Tubular High Strength Steel Trusses*. Master's thesis. Tampere: Tampere University of Technology.

Mäkeläinen, P., Puthli, R., & Bijlaard, F. (1988). Strength. stiffness and non-linear behaviour os simple tubular joints. IABSE congress report 13, 635–640.

Neves, L.F. d. C. (2004). *Monotonic and Cyclic Behaviour of Minor-axis and Hollow Section Joints in Steel and Composite Structures*. Doctoral Thesis, University of Coimbra.

Nizer, A., de Lima, L.R.O., Vellasco, P.C.G. da S., de Andrade, S.A.L., Goulart, E. da S., da Silva, A.T., & Neves, L.F. da C. (2015). Structural behaviour of T RHS joints subjected to chord axial force. *Proceedings of the 15th International Symposium on Tubular Structures, Rio de Janeiro, Brazil, 27-29 May 2015*, 371–378.

Packer, J.A., Wardenier, J., Zhao, X.-L., Vegte, A. van der, & Kurobane, Y. (2009). Design guide for rectangular hollow section (RHS) joints under predominantly static loading. *CIDECT Design Guide* No. 3, 2nd Edition, CIDECT, Geneva, Switzerland.

Snijder, H. H., Boel, H. D., Hoenderkamp, J. C. D., & Spoorenberg, R. C. (2011). Buckling length factors for welded lattice girders with hollow section braces and chords. *Proceedings of Eurosteel 2011*, 1881–1886.

Wardenier, J. (1982). *Hollow Section Joints*, Delft: Delft University of Technology.

Weynand, K., Jaspart, J. P., Demonceau, J.-F. & Zhang, L. (2015). *Component method for tubular joints*. CIDECT Report 16F – 3/15.

Yu, Y. (1997). *The static strength of uniplanar and multiplanar connections in rectangular hollow sections*. Doctoral Dissertation. Delft: Delft University of Technology.

Zhao, X.-L. & Hancock, G. J. (1991). T-joints in rectangular hollow sections subject to combined actions. *Journal of Structural Engineering*, 117(8), 2258–2277.

Zhao, X.-L., Wardenier, J., Packer, J. A., & Vegte, G. J. van der (2010). Current static design guidance for hollow-section joints. *Proceedings of the Institution of Civil Engineers - Structures and Buildings*, 163(6), 361–373.

REDUCTION OF FATIGUE CRACK GROWTH RATE IN COMPACT TENSION SPECIMENS USING ADHESIVE BONDED CFRP-STRIPS

Lukáš Ledecký
Yvonne Ciupack
Hartmut Pasternak
Brandenburg University of Technology (BTU), Chair of Steel and Timber Structures

Achim Geßler
Markus Feldmann
RWTH Aachen University, Institute for Steel Structures (STB RWTH Aachen)

ABSTRACT

Carbon fibre reinforced polymer strips (CFRP) are nowadays successfully used for structural concrete retrofitting. Some applications require pre-stressing of the CFRP-strips. The transfer of the pre-stressing force is usually achieved using mechanical anchorage systems. In the scope of a current research project, the usability of CFRP-strips for retrofitting fatigue damaged steel structures is being investigated. Thereby the adhesive bonding of the anchorage region is aspired. In this paper, criteria and testing procedures for the selection of adhesives are described, and the results of constant amplitude fatigue tests on compact tension (CT) specimens are given. In order to assess the long-term transfer of the pre-stressing force between the CFRP-strips and the steel component, in particular, the shear strength and creep behaviour of adhesives were determined. For both types of tests a modified specimen of the thick adherent shear test with an integrated CFRP-strip was used. Five epoxy adhesives and one acrylic-based adhesive were examined. The results of the modified shear tests showed a maximum shear strength of 28.2 MPa. The creep tests were conducted at room temperature under long-term load at a level of 40% of the shear strength of the respective adhesive. The acrylic-based adhesive showed as expected high creep sensitivity and therefore was eliminated from further investigation. In the first test phase of the fatigue testing of CT-specimens, a 20 mm long crack was induced and repaired in different ways in the second test phase: In this paper the fatigue behaviour of the CT-specimens repaired with non-pre-stressed CFRP-strips is compared to those being repaired using alternative methods for crack repairing (repair welding, drilling of the crack tip). The crack propagation during the fatigue tests was measured using RDS propagation gauges. Tests with pre-stressed CFRP-strips are being planned.

INTRODUCTION

There are many examples of retrofitting concrete structures applying adhesively bonded CFRP-strips. For this purpose systems of adhesives and CFRP-strips, for example (DIBt 2008), have been tested and approved. In Figure 1, applications of CFRP-strips for retrofitting bridge structures are shown. Pre-stressed CFRP-strips can be used to reduce bridge deformations caused by the traffic load (vom Berg 2007). To pre-stress the CFRP-strips systems with a fixed and a moveable anchorage connected by the CFRP-strip stress heads at both ends are used (Berset 2002). Because of the success in post-strengthening of concrete structures the usability of CFRP-strips for constructively strengthening steel structures is currently being investigated. In a previously completed research project (Pasternak et al. 2015) the potential of post-strengthening steel structures as well as the fatigue crack repairing using non-pre-stressed CFRP-strips were studied. Additionally, in (Pasternak *et al.* 2015) several FEM analyses of steel-CFRP connections were performed. Within the scope of this project, which has been conducted by the Chair of Steel and Timber Structures (BTU Cottbus-Senftenberg), Institute for Steel Structures (RWTH Aachen) as well as KIT Steel & Lightweight Structures, also a full-scale test of a crane runway, in the form of a 3-point bending test, was carried out.

That test proved the applicability of such CFRP-strips also in full scale, while the strain measurements on the CFRP-surface showed the full-load bearing capacity of the CFRP-strips together with the bonded steel. The test however had to be interrupted due to torsional buckling of the steel I-beam, but the CFRP-strips were not separated from the steel surface (Figure 2).

Figure 1. Two examples of the application of CFRP-strips to a bridge construction (HP-TL);
left: Retrofitting by adhesively bonded slack CFRP-strips;
right: Post-strengthening using a pre-stressing system.

The current research project (IGF-No. 19032 BG) is based on the experience from the previous project (Pasternak et al. 2015) and focuses on the reduction of fatigue crack growth rate using adhesively bonded pre-stressed CFRP-strips. It is being conducted by the above-mentioned research centres. Tests on small and full-scale specimens, as well as theoretical and numerical investigations, are being performed to get a deeper comprehension of the

behaviour and the usability of adhesively bonded CFRP-strips for reducing fatigue crack growth rates in steel structures. This paper presents the results of shear and creep tests of selected adhesives as well as the results of fatigue tests of CT-specimens with a pre-induced crack reinforced by adhesively bonded CFRP-strips.

Figure 2. Full-scale test of a crane runway beam (Pasternak et al. 2015).

SELECTION OF ADHESIVES

General Remarks

To repair fatigue cracks with adhesively bonded pre-stressed CFRP-strips the pre-stressing force in the CFRP-strip has to be transmitted to the steel component by the bond. Thus, the shear resistance of the used adhesive is of particular importance and furthermore, the adhesive bond must uphold the pre-stressing level during the intended service life of the fatigue crack repair measure. Therefore the shear strength and the creep behaviour of six different adhesive systems were investigated. Both types of tests were carried out on small-scale specimens with an integrated CFRP-strip (Figure 3), in accordance with (Meschut 2015). The CFRP was taken from 20 mm wide so-called slot-lamellas (with a tensile strength of 2350 MPa and a Young's modulus of 168000 MPa). Based on the test results and the other adhesive´s characteristics like glass transition temperature, handling and curing behaviour two epoxy systems were chosen for further investigation.

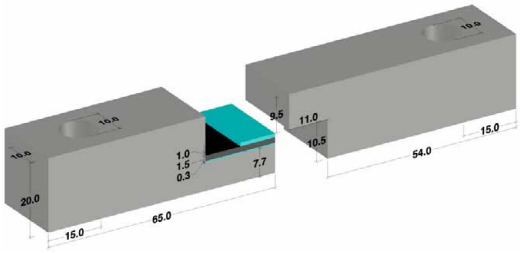

Figure 3. Geometry of the small-scale test specimen: modified thick adherent shear test with an integrated CFPR-strip, cf. (Meschut 2015).

Quasi-static tests

The quasi-static tests were conducted for six adhesive systems, among which were five different epoxy systems (from five different manufacturers) and one acrylate-based adhesive. In order to prepare the tests specimens, the CFRP-strip coupon was glued onto the longer leg with a 0.3 mm thick adhesive layer, before the second leg was bonded over a smaller area onto CFRPstrip with a 1.0 mm thick adhesive layer. The specimens were tested by subjecting them to a controlled tensile displacement (see Figure 4 left) until failure occurred at the thicker, but smaller, adhesive layer. For most specimens failure was cohesive near substrate, and mixed towards steel or CFRP. The diagram in Figure 4 right shows the shear stress-strain curves. The test results were averaged and smoothed for better evaluation for each adhesive system. Clearly, the lower load capacity of the acrylate system can be observed, while also for the epoxy adhesives differences with regard to stiffness and load capacity can be noted.

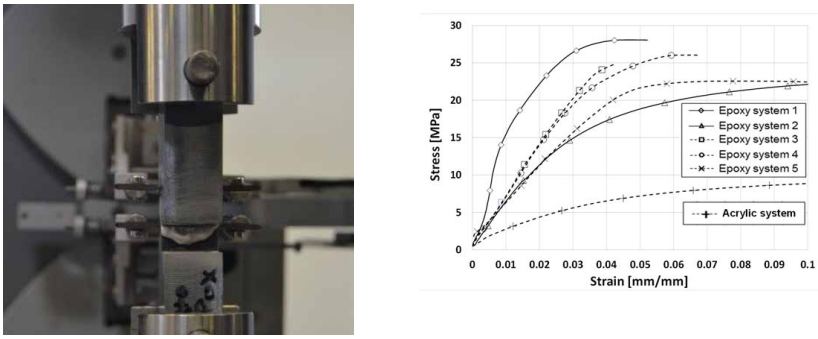

Figure 4. Quasi-static shear tension tests; left: test setup with extensometer measurements; right: test results shear stress-strain curves.

Creep tests

In order to determine the long-term behaviour of adhesives under predominant shear stress, two specimens for each of the six adhesive systems were exposed to a long-term shear loading at room temperature. The creep test stress level was chosen to be equal to 40% of the shear strength of the respective adhesive. This means that, for example, in the case of the two-epoxy systems that were subsequently selected for further investigation, the nominal shear stresses in the bond lines were 11.3 MPa (System 1) and 9.5 MPa (System 2). The extension in load direction of the test specimens has been measured between two fixed points on the two sides of the test specimens using a mechanical measuring device (Figure 5, left), over a total time of 1000 hours at regular intervals. At the beginning (first 8 hours) the measurements were made every 20 minutes and then in the longer intervals from 60 minutes up to 48 hours. The time-extension curves for the tested epoxy systems are given in Figure 5, middle. After 1000 hours, the measured extension of the specimens bonded with epoxy System 2 was 0.070 mm, while the epoxy System 1, despite the higher

absolute stress level, exhibited a lower extension of 0.054 mm. Both selected epoxy adhesives – as well as epoxy systems 3 and 4 – can be characterized as creep resistant. For comparison, the tested specimens bonded with acrylate system failed after 47 hours, whereby a maximum extension of 0.76 mm was measured before failure (Figure 5, right).

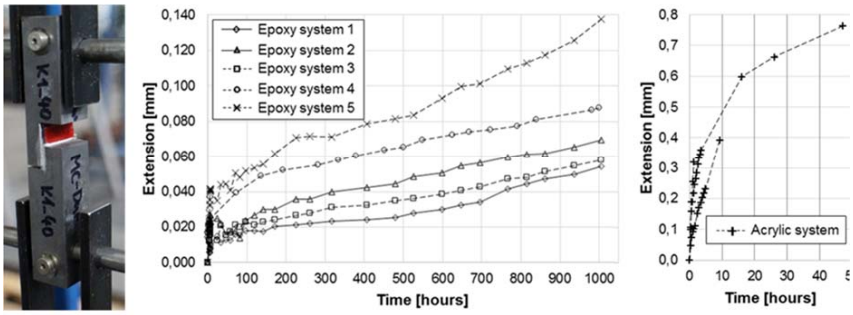

Figure 5. Creep tests; left: the specimen in the testing frame; middle: test results for epoxy systems; right: test results for acrylic system.

Selection of two adhesive systems

Based on the test results given above, the epoxy Systems 1 and 2 were chosen. While System 1 was rated top with regard to shear strength, high stiffness and low creep behaviour, the decision in favour of System 2 was based on the basis of using an adhesive system which offers some additional ductility before failure, while still maintaining high shear strength and low creep tendency.

EXPERIMENTAL INVESTIGATIONS ON COMPACT TENSION SPECIMENS

General Remarks

CT-specimens are commonly used for the determination of fracture mechanical characteristic values of steel (Heckel 1975) and its geometry is chosen following (ASTM E 399). Furthermore, in (ASTM E 399) standard geometry proportions of CT-specimens including different fatigue crack starter notches are defined. In order to determine the fatigue crack growth rate in steel, the fatigue tests were carried out on CT-specimens (Figure 8), similar to the ones used in (Ljustell 2013). After choosing these two adhesives, the fatigue tests were conducted on the CT-specimens with bonded CFRP-strips to reduce the crack growth rate in comparison with conventional methods used for crack repair.

Since the objective of these tests was not the determination of fatigue behaviour of steel, but the testing of crack repairs by means of CFRP-strips,

the thickness of the CT-specimens was reduced to 10 mm, following (Noack 2008). The obtained ratio between the dimension “w” (see Figure 10,left) and the thickness of CT-specimen is equal to 20. All specimens were produced from a S355 J2 steel. A starter notch is situated at mid-height of the CT-specimen. The starter notch has the form of a half circle with a diameter of 10 mm, which continues with a 5 mm long sharp edged cut (see the figures in Table 1 for detail). Under cyclic loading in plane of the CT-specimens surface, a fatigue crack is initiated perpendicular to the notch axis at the end of the starter notch.

Crack propagation measurement and the test phases

The crack initiation is followed by the crack propagation. In the first test phase, a 20 mm long fatigue crack was created in the specimens. Table 1 (test phase 1) illustrates the crack initiation at the end of the starter notch and the crack tip propagation almost parallel to the notch. The monitoring of the crack growth during this first test phase was carried out visually and by RDS propagation gauges. To verify the results given by the signals of the crack propagation gauges, the visual control was continuously carried out. It was observed that the visual measurement of the crack propagation can be used here with sufficient accuracy. At the end of the first test phase, for each CT-specimen, a dye penetrant inspection has been performed (Figure 6, left).

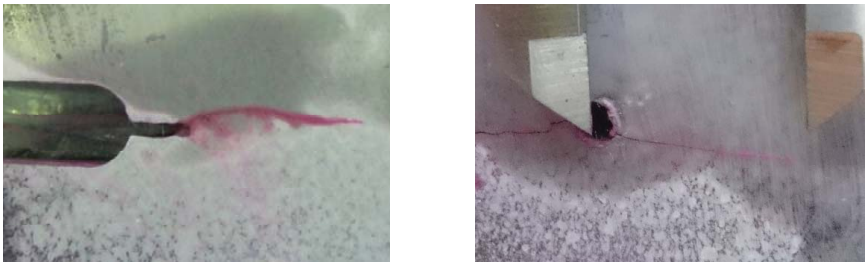

Figure 6. Dye penetrant inspection; left: After the first test phase (specimen “welding 01”); right: after Second test phase (specimen “welding 01”).

During the second test phase, the crack propagation was monitored for further 20 mm using RDS sensors, until the total crack length reached a length of 40 mm (see Table 1, test phase 2). After the test the dye penetrant inspection of the whole fatigue crack was performed again (Figure 6, right).

Between the first and second test phase, two commonly used crack repair methods were carried out:

- drilling of the crack tip or
- drilling of the crack tip combined with repair welding,

and compared to test specimens without crack repair.

The aim of these investigations was to obtain data for further comparison with the crack repairing method using CFRP-strips. If the drilling of the crack tip after the first test phase is applied, the observation of the crack growth velocity in phase two is only possible within a further length of 18 mm because of the position of the drilled hole. However the final crack length in all three cases is 40 mm. The crack propagation measurement procedure is shown in (Table 1).

Table 1. Crack propagation measurement procedure.

Test phase	No crack repair	Drilling of the crack tip and repair welding
1.	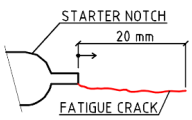	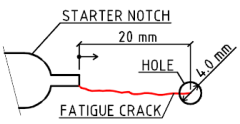
2	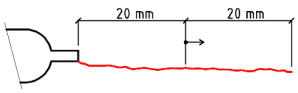	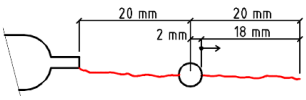

Figure 7 shows the preparation steps of the respective repair welded CT-specimen: After the drilling of the crack tip, steel in the region along the fatigue crack was removed for weld preparation. For that a “V” groove was ground to 2/3 of the depth of material thickness on both sides of the CT-specimen (step 3, Figure 7). In the next step, the region was X-welded using manual metal arc welding with basic coated electrode ISO 2560-A: E 46 4 B42 H5. It is important that during the welding procedure the hole with the diameter of 4.0 mm was not filled. Finally, the elevation of welding seam was ground to create an even steel surface (step 6 on Figure 7).

If only the drilling of the crack tip is carried out, the preparation of the CT-specimen for the second test phase ends at step 2 in Figure 7. For the specimens without any reparation the dye penetrant inspection was performed before the second test phase was started. In that case, the final crack is not interrupted by a hole (see Table 1).

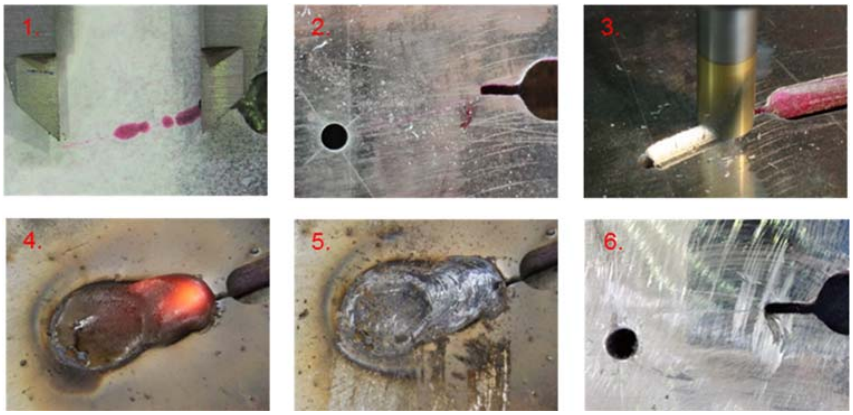

Figure 7. Preparation of the CT-specimen "welding 02" for the second test phase; 1. dye penetrant inspection; 2. drilling of the crack tip; 3. removal of the damaged metal; 4. repair welding; 5. removal of slag; 6. grind of welding seam elevation.

Test setup and results

Figure 8 shows the test setup of both test phases of the CT-specimens. In order to measure the crack growth rate an RDS propagation gauge was placed on one side of the CT-specimen (Figure 8, right above). The other side of the CT-specimen was painted white for a visual crack propagation control, and equipped with one extensometer (Figure 8, right below). The tests were performed on a hydraulic testing machine (maximum load up to 100kN). To reduce the moment transfer of the load two cylinders made of high-strength steel were placed in the two holes of the CT-specimen and clamped. The tests were conducted in a force controlled regime. In the first test phase (crack length smaller than 20 mm) cyclic loads with a load range of $\Delta F = 40$ kN and a mean load of 40 kN was applied. Therefore, the upper force was 60 kN and the stress ratio $R = 0.33$.

For the second test phase, the parameters of the cyclic load were changed to a load range of $\Delta F = 30$ kN and mean load of 25 kN ($R = 0.25$), because of the 20 mm increase of the load eccentricity, compared to the first test phase.

The test results of both test phases are given in Figure 9. For both applied crack repair methods, two tests were performed. Figure 9 shows six curves, as the results of two further tests without any crack repair were taken into comparison. The curves in both test phases are nearly bilinear, with a slower crack progression at the beginning. The curves define a relation between the crack length and corresponding number of cycles. The crack lengths limits are 20 mm for the first and 40 mm for the second test phase, respectively (Table 1). All tests were performed at a load frequency of 5 Hz. To create a 20 mm long fatigue crack between 12 to $18*10^3$ cycles were necessary (Figure 9, left).

Figure 8. Test setup; left: CT-specimen in the testing machine; upper right: Detail of the RDS propagation gauges; lower right: Extensometer and white painted area for visual crack control.

In the second test phase, the measurement was started at the end of the crack (which is the middle of the drilled hole). For this reason for the first two millimetres of crack length progress no cycles are needed (both specimens "drilling" and "welding", Figure 9, right). The diagram shows that both crack repair methods are effective at the beginning of the second test phase only. In the case of not repaired crack (for both specimens), approx. 2.0x10³ cycles were required for the first 1 mm of crack propagation. In the case of the specimens with the repaired cracks, 5.7x10³ and 7.2x10³ cycles were needed to achieve the same results for "drilling" and "welding" repairs, respectively. This means that the welding repair resulted in the highest resistance to repeated crack initiation. When the crack tip is situated behind the outer edge of the drilled hole, the fatigue crack propagation is no more influenced by the examined crack reparation methods.

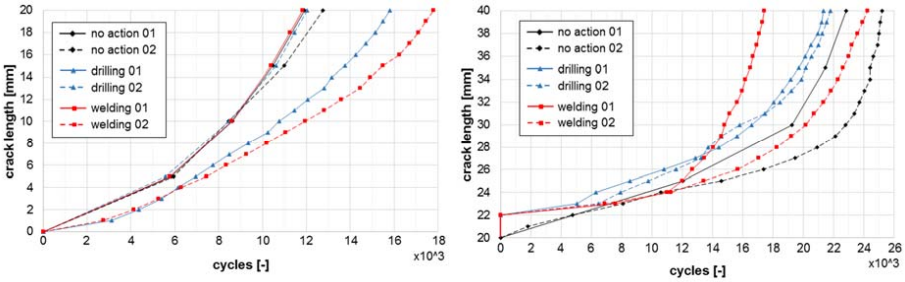

Figure 9. Fatigue crack growth rate; left: First test phase; right: Second test phase.

Compared to the other specimens, the CT-specimen repaired by welding marked “welding 01” showed a rapid increase of the crack growth velocity in the second part of the second test phase, i.e. for a crack length longer than 24 mm onwards. Up to that crack length, the two specimens “welding 01” and “welding 02” perform similarly. Thus, the reason for this effect cannot be directly related to the quality of the manual metal arc welding (human factor). The explanation for this may rather come from the metallurgical changes during the welding procedure, which can occur by the heat input (see Figure 7, step 4) in the heat affected zone. According to (Schulze 2010) the cooling rate influences the formation of martensite, which increases the susceptibility to cracking. The specimens “welding 01” and “welding 02” were welded at different times without measurement of the heat development and cooling rate.

To avoid these additional influencing effects coming from the welding process, the combination of the drilling of the crack tip and adhesively bonded CFRP-strips was chosen for further investigation. Also the drilling of the crack tip is with rather low expenditure and can be performed reproducible under in-situ conditions. Furthermore, these CT-specimens showed good results in comparison with the non-repaired specimens.

Fatigue crack repairing with CFRP-strips

The aim of the fatigue tests of CT-specimens is to compare the currently used methods for crack repair with the new method using adhesively bonded CFRP-strips. For the fatigue tests, adhesively bonded CFRP-strips were combined with the drilling of the crack tip, as described above. The following shows the results of the fatigue test of a CT-specimen prepared with a bonded non-pre-stressed CFRP-strip using epoxy system 1 (Figure 5).

The 20 mm-wide CFRP-strip with a thickness of 1.5 mm was placed at the end of the starter notch. The width of the CFRP-strip corresponds to the crack length (cf. Table 1, phase 1), which was completely covered by it. The thickness of the adhesive layer was 1.0 mm. Figure 10 shows the preparation of the CT-specimen for the second test phase. Cut wire blasting was applied for the preparation of the steel surface prior to bonding of the CFRP-strip, which was bonded on one side of the CT-specimen. The strain on the outer surface of the CFRP-strip was measured using strain gauges. At mid-height of the CT-specimen (at the starter notch) three strain gauges were spread over the CFRP-strip width. In addition to these three sensors, two more sensors were placed along the middle axis of the CFRP-strip, at a quarter of the height of the CT-specimen (Figure 10, right).

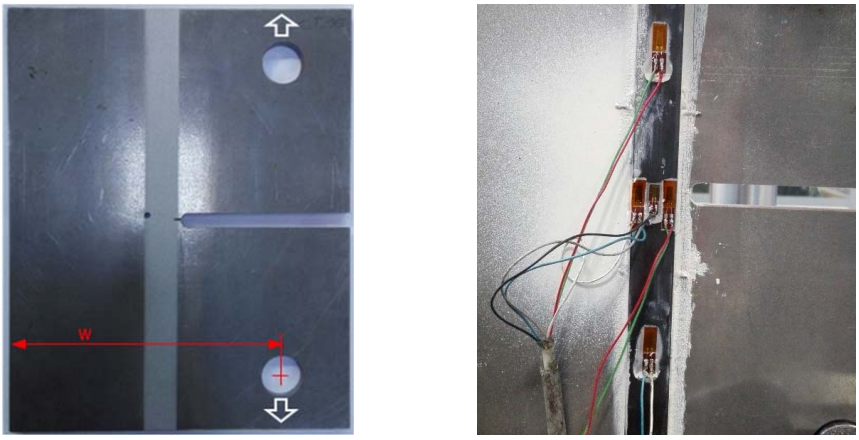

Figure 10. CT-specimen before the second test phase left: cut wire-blasted surface; right: bonded CFRP-strip with measuring equipment.

The test parameters remained the same as in the second test phase of the previous tests. A cycle load range of ΔF = 30 kN, a mean load of 25 kN and a test frequency of 5 Hz were used to determine the crack growth rate between a crack length of 20mm and 40 mm. For reasons of clarity, the obtained test result with non-pre-stressed CFRP-strip is compared only with the test results of the samples repaired by drilling the crack tip (Figure 11).

Figure 11 shows that the total number of cycles in the second test phase increased from approximately $22x10^3$ cycles (drilling) to $36x10^3$ cycles (CFRP). At the beginning of this test phase (until a crack length of 25 mm) no influence of the CFRP-strip could be seen. After this point, the specimen with CFRP-strip showed a significantly smaller crack growth rate compared to the specimens with a drilled crack tip. The tensile stress in the CFRP-strip, calculated from the measured strain of its outer surface, achieved a value of 370 MPa at the end of the test (at the upper force of 40 kN). This points out that the epoxy adhesive bond was capable of transmitting forces from the CT-specimen to the CFRP-strip. The high Young's modulus of the CFRP-strip contributed to smaller displacements at the end of the starter notch and, subsequently, a smaller crack growth rate compared to the drilled specimens.

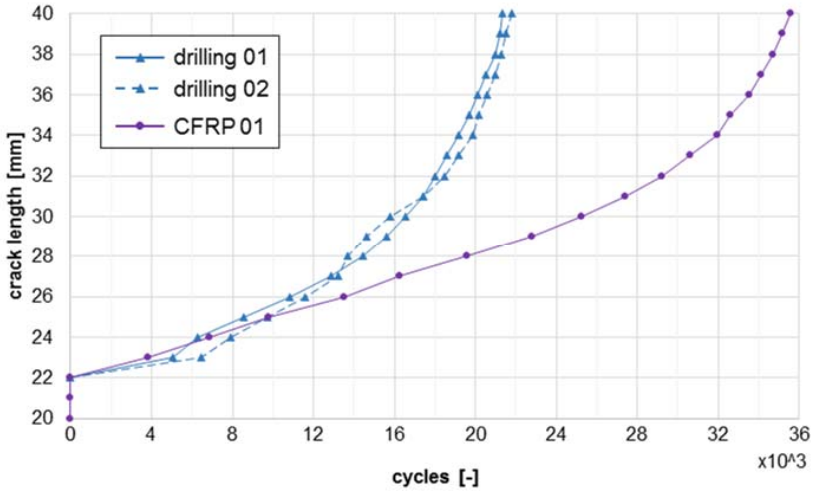

Figure 11. Comparison of the fatigue crack growth rates in the second test phase.

CONCLUSION

The fatigue test of a sample repaired by an adhesively bonded non-pre-stressed CFRP-strip showed a big potential for repairing fatigue cracks in steel. The test results showed a slower increase of the fatigue crack growth rate in the CT-specimen compared to the drilled specimens. This result gives good reason to further investigate the method of strengthening fatigue damaged steel structures using adhesively bonded CFRP-strips. Pre-stressing the CFRP-strip before the application might result in even slower crack growth rates and therefore is in the particular focus of the project investigations in the near future.

ACKNOWLEDGEMENT

The IGF research project (IGF-No. 19032 BG/ DVS-no. 09.072) of the Research Association "Research Association on Welding and Allied Processes of the DVS, Aachener Straße 172, 40223 Düsseldorf" has been funded by the AiF within the program for sponsorship by Industrial Joint Research (IGF) of the German Federal Ministry of Economic Affairs and Energy, based on an enactment of the German Parliament.

REFERENCES

ASTM E 399-90 (1997). Standard Test Method for Plane-Strain Fracture Toughness of Metallic Materials Designation: E 399-90. (Reapproved 1997).

Berset T., Schwegler G., & Trausch L. (2002). Post-strengthening of a motorway bridge with prestressed CFRP strips. tec21. Special print from issue 22/2002. Retrieved 23 January 2018 from http://www.stresshead.ch/assets/2002-fachbericht_sia_tec21_verstaerkung-einer-autobahnbruecke-mit-vorgespannten-cfk-lamellen.pdf

Deutsches Institut für Bautechnik (DIBt) (2008). Allgemeine bauaufsichtliche Zulassung Z-36.12-77: Verstärken von Stahlbetonbauteilen durch schubfest aufgeklebte MC-DUR CFK-Lamellen nach DIN 1045-1:2008-08 Berlin.

Heckel, K., & Wagner, R. (1975). The tensile fatigue behavior of CT-specimens with small notch root radius. International Journal of Fracture, 11(1).

HP-TL – Bauteilverstärkungen mit Carbon, http://www.hp-tl.com/de/field-app.html

Meschut, G., Teutenberg, D., & Wünsche M. (2015). Prüfkonzept für geklebte Stahl/CFK-Strukturen. Adhäsion KLEBEN & DICHTEN, 3.

Noack, M. (2008). Methodische Ansätze zum Rissmonitoring im Stahlbau durch automatisierte digitale Analysen an Modellversuchen. Master‘s thesis, BTU Cottbus-Senftenberg.

Ljustell, P. (2013). Fatigue crack growth experiments and analyses- from small scale to large scale yielding at constant and variable amplitude loading. Doctoral thesis. Royal Institute of Technology.

Pasternak, H., Ciupack, Y., Bartholomé, S., Feldmann, M., Richter, C., Geßler, A., Ummenhofer, T., Ruff, D., & Götz, F. (2015). Systematische Untersuchungen zur Verstärkung von Stahlkonstruktionen mit kohlefaserverstärkten Kunststoffen (CFK) – STAKOK. Schlussbericht zum IGF- Vorgaben 17700 BG.

Schulze, G. (2004). Die Metallurgie des Schweißens. Eisenwerkstoffe - Nichteisenmetallische Werkstoffe.

vom Berg, W. & Beecken, C. A. (2007). Geklebte Bewehrung aus Faserverbundwerkstoffen. Adhäsion KLEBEN & DICHTEN, 4.

HYBRID REINFORCEMENT MEASURES AND INNOVATIVE MEASUREMENT METHODS IN STEEL CONSTRUCTION

Yvonne Ciupack, Hartmut Pasternak, Emre Yilmaz, Florian Sternsdorff
Chair of Steel and Timber Structures, Brandenburg University of Technology, Cottbus, Germany

Ioannis Vayas
Institute for Steel Construction, National Technical University of Athens, Greece

Dedicated to Prof. Dr.-Ing.habil. Dieter Füg on his 80th birthday

ABSTRACT

The implementation of innovative ideas can be very efficient arising from an intensive collaboration of different research institutions. It is important to use the expertise of the research partners, to know precisely the possibilities and limitations and to create a future-oriented work schedule. In an ongoing DAAD project, this approach aims to strengthen the partnership between the authors' institutes. One objective of the project is to develop bonded reinforcement with CFRP laminates for steel construction. The focus is on fatigue-stressed constructions of steel bridges and structures exposed to seismic loading. A further research focus is the application of thermal vision for non-contact measurement of strains in steel components, bondlines and CFRP materials. The research is carried out within the scope of student theses, supervised by staff and doctoral students of the institutes. The sustainability of the measures used to deal with the project is essential for the success of the research project. In this way, the findings are integrated into university teaching, the knowledge gained is taught in summer schools, and young scientists are explicitly addressed. This paper presents the general approach in the project as well as the first findings on the thermostrain method.

INTRODUCTION

In order to ensure a lasting cooperation between research and teaching institutions, targeted cooperation is essential in specialist fields. Within the framework of the ongoing DAAD-project "hybrid reinforcement measures and innovative measurement methods in steel construction", the partnership between the Chair of Steel and Timber Structures (BTU) in Cottbus and the Institute for Steel Construction (NTU) in Athens is to be strengthened further. Specifically, the following objectives have been set:

- Strengthening of cooperation in teaching and research
- Improvement of employment opportunities for Greek graduates
- Internationalization of the research institutes

In order to achieve these objectives, a joint teaching concept for German and Greek students will be developed and the application for a research project is intended. In terms of content, the focus is on practical issues related to the upgrading of steel structures. Due to the increasing volume of traffic, the conversion of existing buildings and the prolongation of the service life, this subject presents a current problem in both Germany and Greece. The knowledge gained from the investigations is directly incorporated in the teaching at both institutes and thus contributes to a broad, future-oriented and problem-oriented education of civil engineering students. Through the exchange with the BTU, Greek students receive better professional opportunities in the European environment.

HYBRID REINFORCEMENT MEASURES

Renovation, restoration, expansion or upgrading of steel structures has played an increasingly important role in recent years. Reasons for this are growing requirements, for example by an increase in live loads, degradation of materials over time and usage and the occurrence of damage due to extraordinary events, e.g. strong earthquakes. Steel is one of the most suitable materials for such measures due to its homogeneous behaviour with a high intrinsic strength. However, using conventional reinforcement methods, as shown in Figure 1, is not always without problems.

Figure 1. Example for conventionally reinforcements of steel girders with screwed and b) welded steel plates.

If, for example, steel plates are used for reinforcement, specific problems arise depending on the type of connection. In the case of screw connections, the holes cause a reduction of the cross-section, which leads to stress concentrations and results in fatigue problems. On the other hand, due to the strong heat impact during the welding procedure, residual stresses and imperfections are introduced, which in particular reduce the carrying capacity of steel members. In recent years, innovative connection techniques and materials are increasingly being investigated, which permit a more user-friendly application and avoid the above-mentioned disadvantages. An innovative joining technique that offers these possibilities is adhesive bonding. In the case of adhesive joints, the individual elements are connected over the entire surface so that no stress concentrations or cross section weakening occur.

The application of adhesive bonds is carried out in the cold state without the development of residual stresses or restraints.

With regard to material selection, innovative developments can be used. Inspired by concrete technology, where plastics have been used for reinforcements for years, civil engineering is nowadays experimenting with fibre materials that are bonded to steel profiles (Figure 2). Carbon fibre reinforced polymer (CFRP) laminates are preferred, which have a high strength and increase in weight of the structure is insignificant. These are termed hybrid reinforcement measures, where two building materials - steel and plastic - are used.

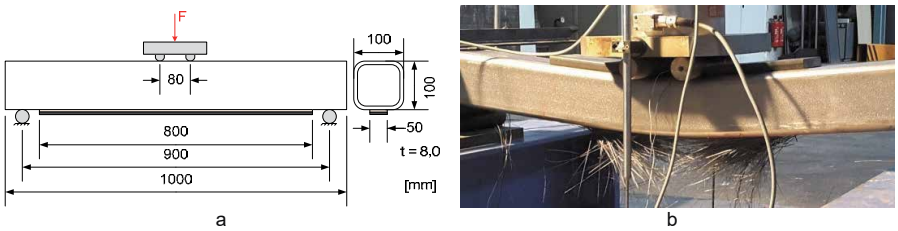

Figure 2. a) Test setup: hybrid reinforcement made of CFRP laminate; failure of CFRP laminate during testing.

The two institutes have a large number of investigations in this research area. At the Chair of Steel and Timber Structures (BTU), adhesive technology has been one of the research foci for many years. In this context, reinforcements of steel structures with bonded CFRP laminates were also investigated (Bartholomé et al. 2014, Pasternak et al. 2016). The NTU Institute of Steel Construction has also dealt with this topic in the context of renovations and upgrades of industrial and school buildings made of concrete structures (Vayas et al. 2014). In the latest investigations, reinforcements of steel angle profiles with CFRP laminates are studied experimentally (Moragiannis 2015). Both institutes can thus profit from the cooperation and exchange their knowledge, whereby a special synergy effect is to be expected, since the experience of the BTU is so far mainly based on quasi-statically and dynamically loaded steel structures, whereas the NTU has focused on seismic loaded concrete structures.

On the one hand, the application potential of bonded plastics for reinforcement and upgrading of steel structures is large. On the other hand, research in the field is rather sparse, especially compared to concrete construction. In the joint research project, existing gaps of knowledge will be filled by investigations on the load carrying behaviour of hybrid components made of steel and bonded CFRP laminates. From a wide range of possible applications, such objects are selected, which are based on the expertise of the institutes.

Reinforcement of Lightweight Steel Construction

Due to fatigue damage or problems, many steel structures, such as road and railway bridges, cranes or even large conveyor systems, have an enormous need for restoration. In particular, the average state of railway and road bridge structures has considerably deteriorated in recent years (Pasternak *et al.* 2016). Since, for economic and constructional reasons, existing structures cannot be easily replaced by new buildings, maintenance and retrofitting becomes necessary. The retrofitting by the application of fibre composite materials represents an optimally suitable option with high potential in order to increase the remaining service life of existing structures. The use of CFRP laminates for cracks in sheet metal (Figure 3a) and of so-called CFRP sheets in difficult-to-reach areas (Figure 3b) is possible.

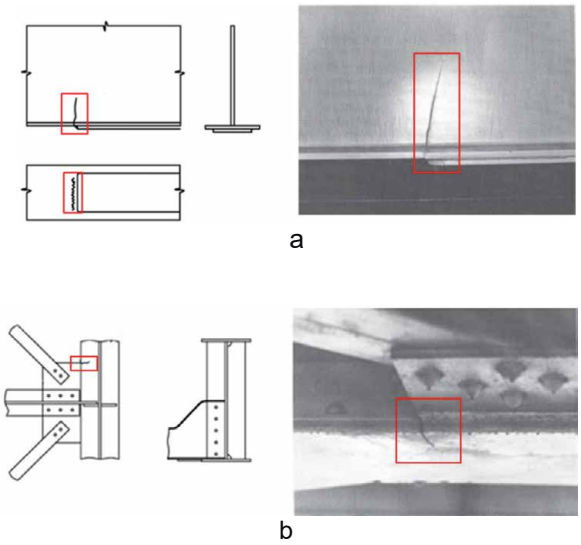

Figure 3. a) Fatigue crack at the end of a welded steel plate; b) crack in a difficult-to-reach area of a gusset.

Thus, these improvement methods allow the rehabilitation of cracked welds as well as the reduction and prevention of crack propagation in the material of existing structures.

Reinforcement for Seismic Loading

Beam-to-column connections are the most sensitive parts of rigid frame structures in earthquake areas and the most important to ensure stability and usability. To increase the load-carrying capacity, gussets are commonly reinforced by the use of stiffeners. These stiffeners can be replaced by CFRP laminates in a crossed configuration, as shown in Figure 4. A crossed arrangement is necessary, since the direction of the earthquake effects is reversible.

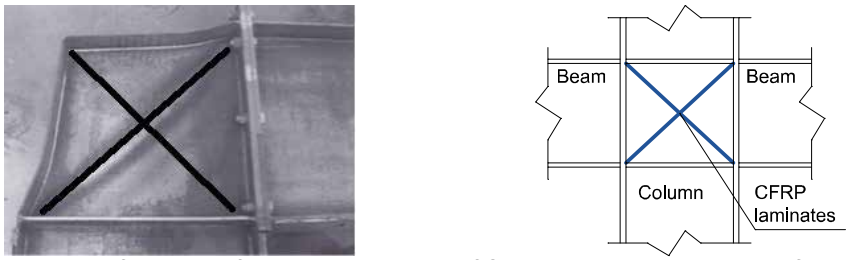

Figure 4. Reinforcement of gussets with the help of CFRP laminates in crossed configuration.

Rigid steel frame structures in earthquake areas are designed in such a way that seismic energy is consumed by the development of plastic hinges. The concept of “weak beam - strong column” is used, meaning the formation of the plastic hinge takes place in the beams and not in the columns or the nodes. In the usual practice, this is ensured as shown in Figure 5, either by reinforcing the connection or weakening the beam ends. As an alternative, the reinforcement of the beam chords can be provided by CFRP laminates at the beam ends. The plastic deformations thus form directly at the end of the cross-section reinforcement.

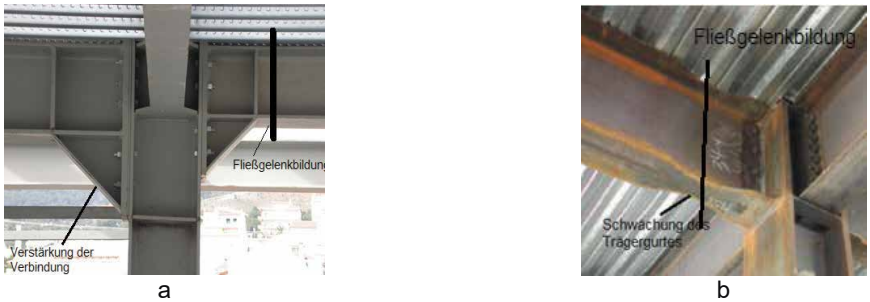

Figure 5. Constructive measures for the development of plastic hinges at the beam end.

THERMOSTRAIN

The second research focus of the project is the application of innovative measuring techniques. The motivation for this research lies in the disadvantages and limitations of classical measurement using strain gauges. In experimental investigation of components, stresses cannot be measured directly. Instead, the strains are recorded by strain gauges and the stresses are calculated according to a material law. Disadvantages of the method include the limited local determination of the strain, the necessity of contact with the object under measurement and, as a consequence, the disturbance

of the strain field. An alternative to the strain gauge measurement is infrared thermography, which exploits the fact that during expansion the temperature of the steel changes due to energy conversion. The method known as thermostrain has been fundamentally investigated at the Chair of Steel and Timber Structures and offers the advantage of a non-contact measurement. The emitted infrared radiation of the specimen is recorded by a thermograhpic camera during the experiment so that the mentioned disadvantages of the strain gauge measurement can be avoided. The deduction of the existing stresses is drawn by means of energy conversion laws.

Both institutes are leading in Europe with regard to the application of thermography in the measurement technology of metal construction. The first developments started at BTU about fifteen years ago (Horvath 2003, Müller 2005). The temperature development of various materials under static and dynamic loads was experimentally determined and FEM-based calculations were used to deduce strains (Figure 6).

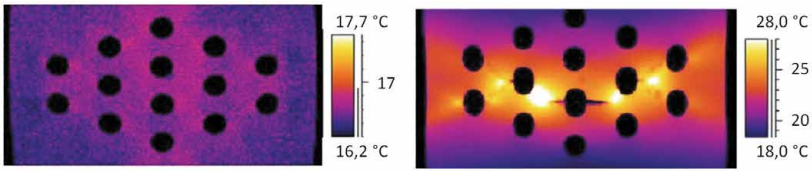

Figure 6. Temperature development of a tensile loaded specimen with holes at test beginning (left) and ending (right) (Müller 2005).

Similarly, at NTU, surveys with a thermographic camera at tests under seismic loading are carried out in order to detect the dissipative zones of earthquake-resistant constructions (Kouniaki 2015). Therefore, a complementary synergy effect can be developed in the field of measurement technology, so that both institutes can benefit from the knowledge and experience of the partners.

Principle of Thermostrain Method

The thermostrain method is an innovative measuring technique in which the material stress on flat structural components under varying loads can be measured visually and without contact. In contrast with common techniques, e.g. strain gauges, this method measures the heat radiation of the stressed component instead of the deformation. The heat radiation is scanned with a high-resolution infrared camera and converted into a corresponding false colour image as shown in Figure 7. From the registered temperature changes a deformation state of the specimen can be deduced. This is done with the help of a specific thermo-mechanical correlation of the material taking into account thermodynamic laws.

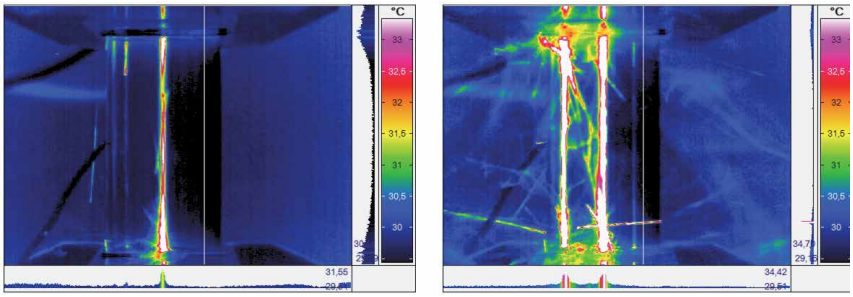

Figure 7. False colour images of tensile-stressed carbon fibre reinforced polymer lamella during failure.

Experimental Investigation on CFRP Laminates

In the framework of a bachelor thesis at BTU the application of the thermostrain method for fibre reinforced polymer laminates is being investigated. Eight identical specimens with the dimensions 250 mm x 80 mm x 1.2 mm (length x width x thickness) were prepared and tested under tension.

Figure 8. Specimen (left) and prepared specimens (right).

The specimens were clamped in a 500 kN tensile testing machine and a 'VarioCAM® high resolution' thermal imaging camera was placed at a distance of about 50 cm in front of the specimen. To measure the displacement of the specimen a tensometer was fixed on the side facing away from the camera to avoid disturbance of the thermal image. Additionally a film camera was placed to the side of the thermal imaging camera to record the whole process. A felt mat was positioned behind the specimen to increase the contrast and to enable the camera to focus on the specimen.

The loading rate under displacement control was varied for the test series. The objective was to determine the influence of the loading rate on the mechanical and / or thermal behaviour of the CFRP laminate. Due to the polymer specific properties of the CFRP matrix, a dependency of the temperature development on the loading rate could be registered. For the first three specimens a loading

rate of 5 mm/min was used, as recommended in DIN EN ISO 527-4 for the quality control of CFRP laminates. Specimens 04-06 and 07-08 were tested with a loading rate of 2.5 mm/min and 10 mm/min respectively (see Table 1). The tests were conducted under approximately constant climate conditions, with an air temperature 28° C and a relative humidity of 70 %.

Table 1. Loading rate under displacement control and recording frequency of data.

Specimen	Test velocity [mm/min]	Recording frequency of data [Hz]
01-03	5,0	25
04-06	2,5	25
07-09	10,0	50

The results of the experiments are summarized in a stress-strain-diagram shown in Figure 9. It can be seen that the CFRP material shows linear-elastic behaviour. During the test the elastic deformation leads to a slight temperature reduction, which is known as the thermo-elastic effect. The thermo-elastic effect is followed by a noticeable warming (0.5–0.6 K) at the clamping jaws (Figure 10). An enormous thermal energy release can be observed when the specimen fails (see Figure 7 right).

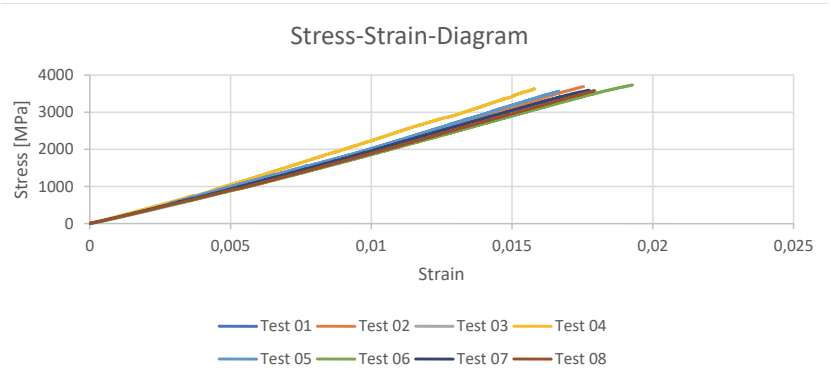

Figure 9. Stress-strain-diagram of the test series.

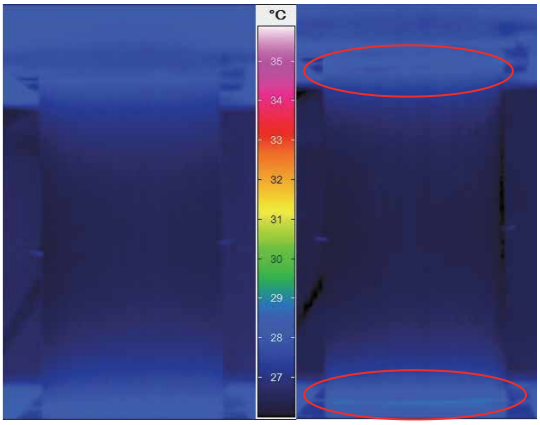

Figure 10. Comparison of thermographic images: during the test (left) and just before failure (right).

The characteristic heating of the CFRP laminate surface near the clamping jaws (Figure 10 right) could be an indicator for the failure of the specimen. Thus the thermostrain method could be used to predict the failure of CFRP elements due to stress concentrations. It is assumed that the observed behaviour results from transverse contraction effects at the clamping jaws.

Future investigation will show whether the registered energy conversion results from starting of fibre failure or other phenomena. Thus, future research in this field will focus on the influence of the test setup for the application of the thermostrain method. On the one hand the geometry of the clamping jaws should be investigated more deeply. As shown in Figure 11 the clamping area of the machine consists of jaws and an inclined plane. This mentioned geometry (angle of the plane) leads to an increasing horizontal pressure while increasing the vertical force. Thus stress concentrations at the claiming support are introduced. Further, friction effects at this critical point should be evaluated in more detail.

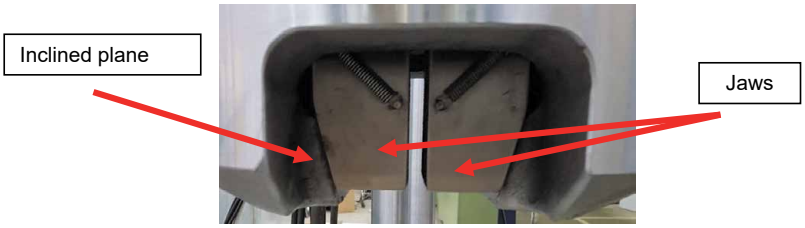

Figure 11. Grip-setup.

In order to deduce a relation between the measured mechanical and thermal properties a numerical simulation using the general-purpose-software ABAQUS/CAE was carried out. The created model was simplified without

considering plastic effects or stress redistribution due to the failure of single fibres, so as to be manageable as a student project. The results in Figure 12 for the stresses in longitudinal and transversal direction indicate a stress concentration at the supports. This distribution is in accordance with the observed behaviour in the experiments, more specifically in the thermal images. In the longitudinal direction, the stresses are concentrated at the specimen corners.

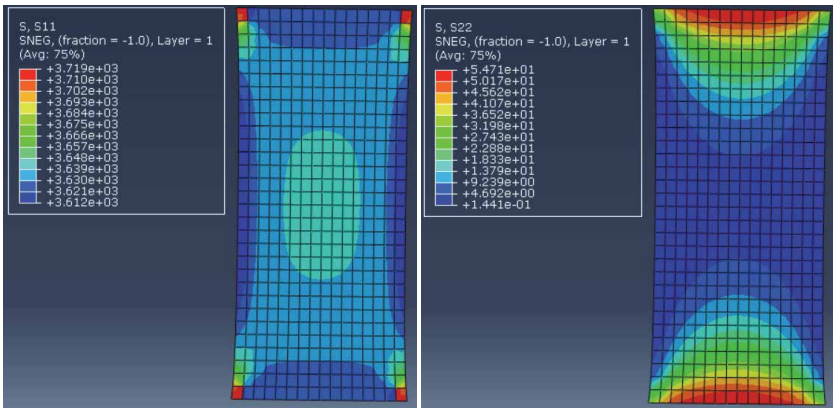

Figure 12. Stresses in longitudinal (left) and transverse direction (right).

The presented investigation should be understood as preliminary work to indicate the applicability of the thermostrain method for CFRP materials. Following conclusion can be drawn from the experimental and numerical findings:

- During testing a slight surface temperature variation was observed. Thus, it is of major importance to guarantee constant environmental conditions (temperature, humidity). The failure occurs with a high-energy release, which can be registered as a significant temperature change with the help of a thermal imaging camera.

- Stress concentration at the clamping jaws result from transverse contraction effects and leads to an energy release.

- To avoid a failure due to stress peaks, weakening of the specimen cross section in the middle of the longitudinal direction is recommended.

- A suitable numerical model should include the classical laminate theory as well as redistribution effects between single fibres due to the matrix compound.

IMPROVEMENT OF ACADEMIC COOPERATION

In addition to the specialist knowledge, the DAAD project aims above all at an improvement in the academic partnership between Greek and German universities. The project is designed in such a way that the common creation of teaching events and the supervision of master or bachelor theses as well as diploma theses is done in cooperation. Within the framework of student theses, numerical investigations are carried out at the BTU for quasi-static and at the NTU for seismic loading. One or two master's or diploma theses per year, supervised by scientific staff or doctoral students, are visualised to at each institute.

At each institute, experimental investigations on component specimens are carried out for selected reinforcement measures. The strain measurement is realised by thermostrain due to the above-mentioned reasons. The aim of the tests is to calibrate the numerical models as well as the combination of temperatures and strains/stresses of the materials used and thus the expansion of the existing knowledge on CFRP-reinforced steel components. These studies are implemented as part of student work and are supervised by Greek and German staff. Joint teaching sessions are held at the BTU and the NTU. This requires the specific definition of the contents of teaching in close cooperation, which also strengthens the partnership at academic staff level. Such coordinated teaching program can also be transferred across the project to other content or used for future lectures and adopted in general academic courses.

The findings of the examinations will be presented to students and interested employees within two summer schools in the years 2018 and 2019, thereby enabling the participants to plan, evaluate and design reinforcement measures for steel structures. The know-how gained can be regarded as a unique feature, since the adhesive technology as well as the thermostrain method is not part of general university courses in civil engineering. The graduates of the Summer School thus receive a broader education compared to international standards, which means a benefit for future employment opportunities, especially for Greek university graduates. In addition to the international contacts, students receive an additional scientific and technical qualification by exchanging with the partner institution, since the contents are experimental-oriented. Thus, a link between teaching and research takes place, which increases the career opportunities of the graduates in research facilities.

SUSTAINABILITY OF MEASURES

The approach in the project is designed so that sustainable results are to be expected. Professional subjects of the theses and summer schools are oriented towards future problems of civil engineering. As a result of the increase in loads and increasing service life of steel structures, reinforcement measures and, in the future, rehabilitation and retrofitting measures are required

(Bartholomé et al. 2014). The design of such methods has been the aim of the investigations.

Further, young scientists and students are explicitly associated with the project. In this way network relations with a thematic focus will be created, which can be actively used for future tasks. It is also planned to continue the cooperation on content in the field of research on follow-up projects.

CONCLUSIONS AND FUTURE WORK

The bonding technology has the potential to efficiently design reinforcement of existing buildings in steel construction. The bondlines can be designed in such a way that a quasi-rigid compound is realized and thus the load bearing capacities as well as the stiffness of components are increased. Various applications, for example, for the rehabilitation of steel bridges, are analysed and evaluated within the framework of the presented project. A further possibility consists of utilizing the energy dissipation capacity of elastic bondlines for the earthquake-resistant design of steel structures. Initial research on this methodology will be pursued for student theses in 2018. The applicability of the time-temperature superposition principle of selected adhesives will be considered. By means of experimental investigations, the frequency-dependent carrier behaviour of bondlines will be determined. In final master's or diploma theses in 2019, large-scale test specimens are to be experimentally studied and numerically modelled. The objective is to develop a suitable design for steel reinforcements in bridge construction as well as the earthquake-proof design of reinforcements in structural engineering. The knowledge gained will be disseminated to all interested students and engineers in two multi-day summer schools 2018 in Athens and 2019 in Cottbus.

In addition to the scientific advance, the students and employees involved in the project benefit from the intensive exchange and the improvement of linguistic and cultural skills. In particular, Greek graduates will be given the opportunity to make contacts in Germany and thus have a better employment perspective in the profession of civil engineering. This aimed at alleviating the negative impact of the current economic crisis in the construction sector in Greece.

ACKNOWLEDGEMENT

The project "hybrid reinforcement measures and innovative measurement methods in steel construction" is funded by the German Academic Exchange Service (DAAD) through the Ministry of Foreign Affairs (AA) within the framework of the funding program "university partnerships with Greece 2016".

REFERENCES

Bartholomé, S., Götz, F., Ummenhofer, T., Geßler, A., & Feldmann, M. (2014). Zum Kleben von CFK Lamellen im Stahlbau. Schriftenreihe Stahlbau 8, BTU Stahlbau-Symposium 2014, 83–90, May 2014.

Bartholomé S., Pasternak H., Ummenhofer, T., Götz, F., Feldmann, M., & Geßler, A. (2016). Verstärkung von Stahlkonstruktionen durch geklebte CFK Lamellen. 20. DASt-Forschungskolloquium, 89–94, Essen, Germany, March 2016.

Pasternak, H., Bartholomé, S., Feldmann, M., Geßler, A., Ummenhofer, T., & Ruff, D. (2016). Alternative Verstärkungsmaßnahme im Stahlbau mit aufgeklebten unidirektionalen CFK-Lamellen. Schweißen und Schneiden 68 (2016) 8, 490–499.

Ummenhofer, T., Pasternak, H., & Feldmann, M. (2016). IGF Project No. 19032 BG, Einsatz von geklebten Kohlestoff-Faserverbundwerkstoffen zur Sanierung ermüdungsgeschädigter Stahlkonstruktionen (FASS), ongoing research project, Germany, 01.02.2016–31.07.2018.

Vayas, I., Spiliopoulos, A., Dasiou, M. E., Dougka, G., & Dimakogianni, D. (2014). Instandsetzung von Bauten des Kraftwerks Meliti, Griechenland, nach einem Brand. *Stahlbau* 83. 47–56.

Vayas, I., Dougka, G., & Dimakogianni, D. (2014). Umbau und Erweiterung des Kindergartens der Deutschen Schule Athen. *Bauingenieur* 89.

Moragiannis, P. I. (2015). *Experimental study of steel equal-leg angles strengthened with CFRP subjected to compression and to bending*. Diploma Thesis. Institute of Steel Structures, NTUA.

Horvath, L. (2003). *Experimentelle Untersuchungen der im Stahlbau typischen Bauteile mit Thermovision*. Dissertation. BTU Cottbus.

Müller, L. (2005). *Entwicklung eines neuen Verfahrens zur Dehnungsanalyse beanspruchter Stahlbauteile*. Dissertation. BTU Cottbus.

Kouniaki, M. (2015). *Investigation of the structural behaviour of metallic elements with the thermovision method*. Diploma Thesis. Institute of Steel Structures, NTUA.

WELDING SIMULATION FOR THE CALCULATION OF THE WELDING RESIDUAL STRESSES IN WELDED I-GIRDERS

Birgit Ragotzky
Brandenburg University of Technology (BTU), Chair of Steel and Timber Structures

Benjamin Launert
Brandenburg University of Technology (BTU), Chair of Steel and Timber Structures

Thomas Krausche
Brandenburg University of Technology (BTU), Chair of Steel and Timber Structures

INTRODUCTION

Welding is one of the most important and widely used joining processes in steel construction. It offers the advantage of building cross section dimensions freely based on individual design requirements. On the other hand, welding also results in residual stresses and deformations that need to be taken into account in the design process. These develop due to the restrained expansion and shrinkage of the weld zone as a result of non-uniform heating of the component. Thereby, thin sheets are expected to show higher distortion while thick sheets are more characterized by higher residual stresses. Both phenomena influence directly as well as indirectly the internal stresses and hence also affect the loadbearing behaviour.

Residual stresses represent the primary focus of the following contribution. They are generally dependent on the welding parameters, the material as well as on the geometrical dimensions. A modern numerical welding simulation can provide a realistic assessment of these values compared to available simplified assumptions. These can then be incorporated into the design at an early stage or also support an optimization of the welding process. Nevertheless, the welding simulation also contains several restrictions such as complicated modelling and large calculation times. Even smallscale specimens can easily take several days to solve, depending on component size, meshing and number of welds.

In the following, results of numerical welding simulations obtained by two different calculation programs are presented and compared against each other. In particular, the specialized software Simufact.Welding and a freely available add-on to the commercial software code Abaqus, the Abaqus Welding Interface (AWI), are used. The basis for a model calibration and evaluation of the results is provided by experiments carried out on four I-girders welded by conventional metal active gas (MAG) welding.

ORIGIN OF RESIDUAL STRESSES

Residual stresses are often considered as a superposition of so-called *shrinkage stresses* and *transformation stresses* (Fahrenwaldt et al. 2014).

Shrinkage stresses are produced by a restraint of shrinkage of the so-called plasticity zone. In this, the plasticity zone is the zone that experiences plastic deformation during welding. Shrinkage stresses are produced in longitudinal and transverse direction of the weld seam and with increasing thickness also through the thickness. In longitudinal direction, tensile residual stresses often reach the yield stress of the material. Self-equilibrating compressive residual stresses are found away from the weld (Figure 1a).

Additionally, *transformation stresses* result due to phase transformation in the fusion zone (FZ) and the heat-affected zone (HAZ) (Figure 1b). Depending on the cooling behaviour, different microstructures with different crystalline structures develop that show different characteristics in strength and ductility. The transformation from austenite into different phase fractions also involves thermal expansion that is restricted by nontransforming areas causing more or less significant local compressive residual stresses. These superpose with shrinkage stresses. The resulting positive effect of a local stress reduction is accompanied by specific microstructure properties such as high hardness and increased susceptibility to cracks.

The generation of residual stresses cannot be suppressed. “Local” residual stresses are always created by expansion and shrinkage as a function of the given material thicknesses and strengths of the material. For typical structures in steel construction, it is not possible to stress relieve the components because of their, in general, large sizes. Hence, their calculation and adequate consideration in the design is of particular interest.

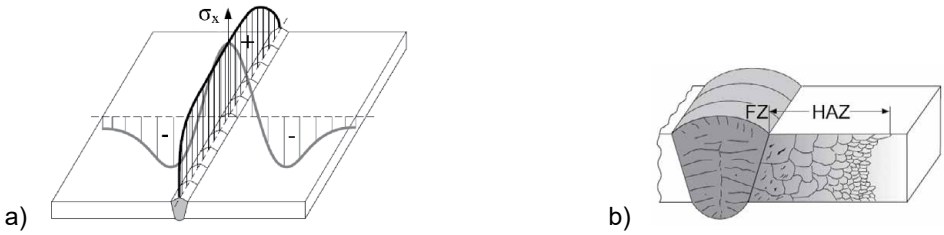

Figure 1. a) Typical pattern of longitudinal residual stress,
b) microstructure due to welding (Wohlfahrt and Schmidt 2001).

EXPERIMENTAL RESULTS

Experimental investigations allow the validation of hand calculations as well as numerical calculations. Besides, in academic research, they are also

used for calibration of input data such as material properties or heat source parameters. Measurements on four reference-welded I-girders are used for comparison in this paper.

All experiments and evaluations were carried out as part of the national research project "Erhöhung der Tragfähigkeit geschweißter I-Träger aus hochfestem Baustahl durch verbesserte Ansätze zur Berücksichtigung von Eigenspannungen" (IGF-Vorhaben-Nr. 18104 BG) (Pasternak et al. 2018).

Prior to welding of the sheets, tensile coupons were cut out and tensile coupon tests were performed for the determination of relevant material properties. The results are given in Table 1. These are more or less in accordance with the supplied acceptance test certificates. Most importantly, it can be seen that the investigated materials showed significantly higher strengths than the nominal values. To take into account this in the welding simulation, the material data sheets from the software library Simufact.material (v. 2016) had to be adjusted. A uniform upscaling was performed for the entire temperature range, because experimental information has only been available at room temperature.

Table 1. Material data from tensile coupons (acceptance tests certificates in brackets).

Steel grade	S355J2+N		S690QL	
Plate thickness [mm]	15	25	15	25
Yield Stress [MPa]	480 (451)	464 (470)	780 (803)	840 (825)
Tensile strength [MPa	538 (576)	571 (581)	830 (850)	865 (859)
Young's modulus [GPa]	221.8 (-)	226.7 (-)	209.8 (-)	221.1 (-)

Following the material tests, the I-girders were welded. The web height was 220 mm (h) with a thickness of 15 mm (t_w) and the flange width was 150 mm (b) showing a thickness of 25 mm (t_f) in all specimens. All plates were water-jet cut in order to avoid additional thermal cutting effects. Conventional MAG welding process was used. All welds were singlelayer fillet welds. Corresponding welding parameters are listed in Table 2.

Table 2. Welding parameters for girders 1–4.

Girder-No.	S1	S2	W1	W2
Steel grade	S355J2+N		S690QL	
Current [A]	338	327	324	329
Voltage [V]	33	33	34	34
Welding speed [cm/min]	49	31	49	31

During the welding process, six thermocouples measured the temperature profiles in the flange at different distances from the weld. Three thermocouples were placed on the other side of the web for the measurement of the global temperature development. This is used for the calibration of the total heat input in the later numerical models.

Measurements were performed separately for each weld. Figure 2a shows results of the measurements on Girder S1 during welding and cooling of the first weld. The numbers and positions of the thermocouples are shown in Figure 2b.

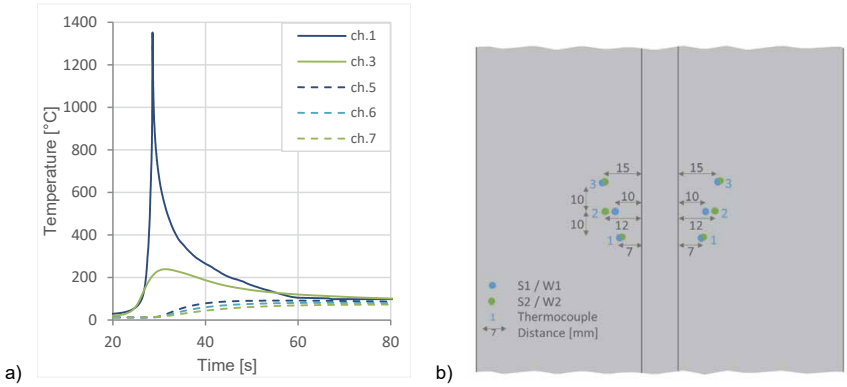

Figure 2. Measured temperature cycles, exemplary a) S1 – weld 1, b) Numbers and positions of thermocouples.

The local calibration of the heat source model requires additional knowledge on the weld dimensions. These were obtained from macrosections that were cut out and prepared for each welded specimen.

Subsequently, longitudinal stresses were determined by the sectioning method. This method is known to be “robust” in its application to large sections. Strain gauges are applied in longitudinal and transverse direction of the weld assuming a two-dimensional stress state for the calculation of longitudinal residual stresses. In particular, the strain gauges were applied to only a quarter of the section to each side of the flange and the web respectively. The specimen is then sequentially sliced by vertical cuts using a conventional band saw. Figure 3 shows the cutting process and the positioning of strain gauges.

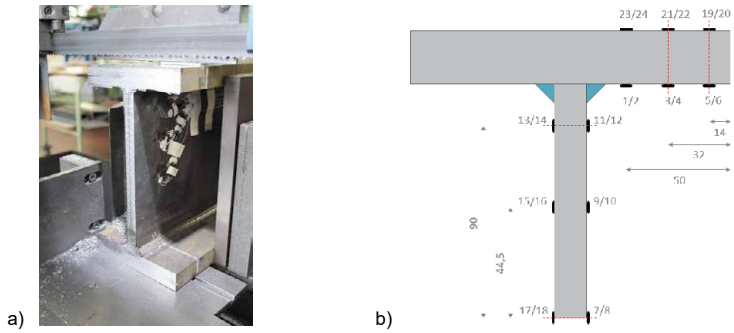

Figure 3. Sectioning method: a) Vertical slicing of the specimen, b) Strain gauge application scheme.

The applied sectioning scheme is idealized in Figure 4 starting with larger cuts at the beginning and then smaller intervals towards the measured section in the middle of the specimens. The sectioning was then repeated from the other side. Based on the results of the first specimen, the sectioning sequence then was simplified.

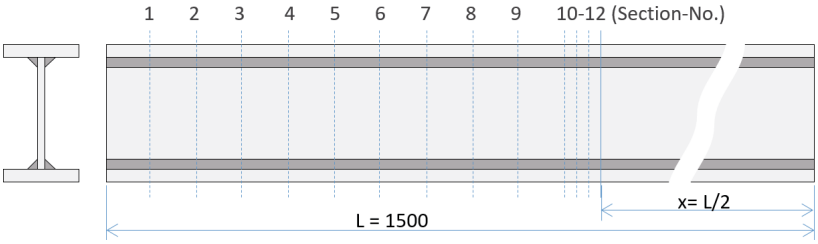

Figure 4. Vertical sectioning scheme of welded I-girders.

After evaluation of the results, the following longitudinal residual stresses were calculated for the flanges (Figure 5).

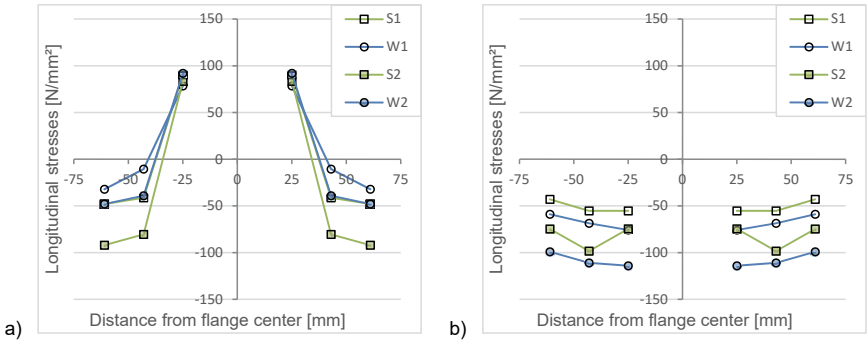

Figure 5. Longitudinal residual stresses in the flange: a) Inner side, b) Outer side.

Tensile residual stresses are seen close to the weld on position “1/2”. Apart from that, stresses turn into equilibrating compression. Due to the relation of the heat input and comparatively thick flanges, the outer surface of the flanges is under, more or less, uniform compression. The compression magnitudes seem to be almost independent of the material grade. The energy input has some additional but only small effect in this study. The maximum tensile stresses however remain unknown due to the rather large distance of strain gauges from the weld that was restricted by the strain gauge dimensions as well as the application in two directions. The tensile residual stresses may however be calculated from equilibrium in longitudinal direction using the compressive residual stresses, or later from the simulation.

NUMERICAL WELDING SIMULATION

A numerical simulation allows performing a virtual weld under realistic boundary conditions as a computer model. By this, information on the weld-induced imperfections such as the distortions or the residual stresses can be obtained and also information on the material behaviour and the microstructure during and after welding.

In the following, the results of such numerical welding simulation from two different software tools will be presented. Two identical geometries have been previously built and meshed using Abaqus. One is with a very fine mesh with a minimum element edge length of 1 mm; the other is with an optimized reduced meshing density and a minimum element edge length of 2 mm. These models have been set as a basis for both approaches. Additionally, the supporting conditions were kept constant in all models providing a free support of the specimen in order not to induce external (“global” or reaction) stresses.

Simufact Welding (v. 2016)

Simufact Welding is a program that has been specially developed to perform welding simulations and hence reduces many input steps and settings for the user. Main goals of the software are in the prediction of temperature fields, microstructure, welding distortion as well as welding residual stresses. It covers the branch of the socalled “structural” welding simulation that includes the modelling of elasto-plastic material behaviour under an idealized local heat input using the finite element method.

With Simufact Welding different welding sequences, breaks or pause times, different materials, influence of clampings and fixings or additional heat treatments such as preheating can be implemented, calculated and visualized with a comparatively small effort.

The calculation is usually composed of two steps; that is initially the temperature field calculation aiming at the calibration of the temperature results, locally as well as globally, and then the performance of a coupled

thermomechanical analysis. Figure 6 shows the first step and a comparison with the experimental results of the previous section.

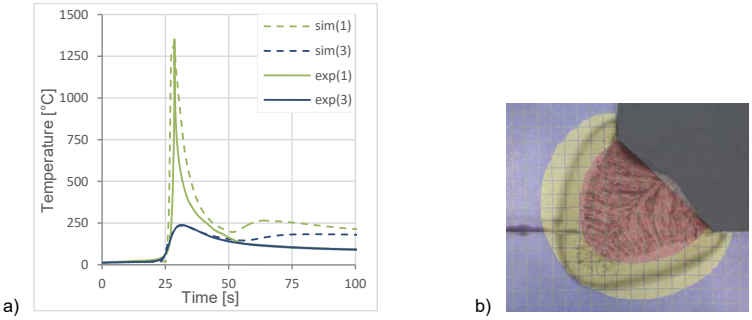

Figure 6. a) Comparison of simulated and measured temperature cycles (exemplary S1), b) Numerically calculated maximum temperature isotherms vs. macrosection (exemplary W1).

The results of the thermomechanical calculation are shown in Figure 7. Results are given with respect to the material grade and the weld heat input for the flanges of the 1 mm model. Due to subsequent welding of the seams, the calculated residual stress distribution is only approximately symmetrical.

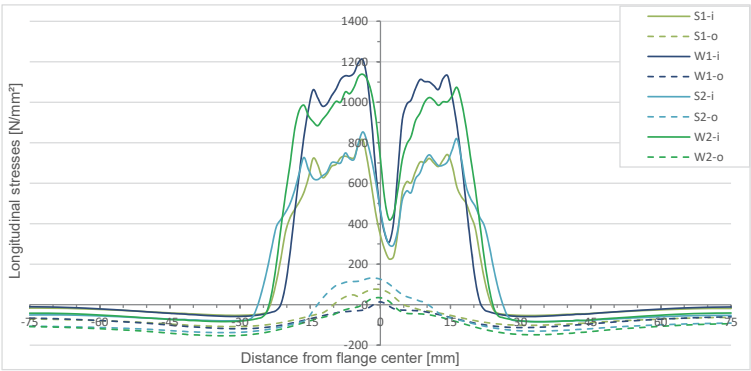

Figure 7. Longitudinal residual stresses for S1-2, W1-W2 (i-inside, o-outside).

Figure 7 generally shows higher local tensile residual stresses for the S690 but at a comparatively reduced tensile width and more or less similar compressive residual stresses irrespective of the steel grade. With respect to the weld heat input, only small differences are noticed in both materials. Higher heat input led to wider tensile widths and by this also slightly increased the compressive residual stresses.

Figure 8 shows an additional magnification of the compressive residual stresses that were of particular interest in this study. In addition, results have been normalized using the particular yield stress.

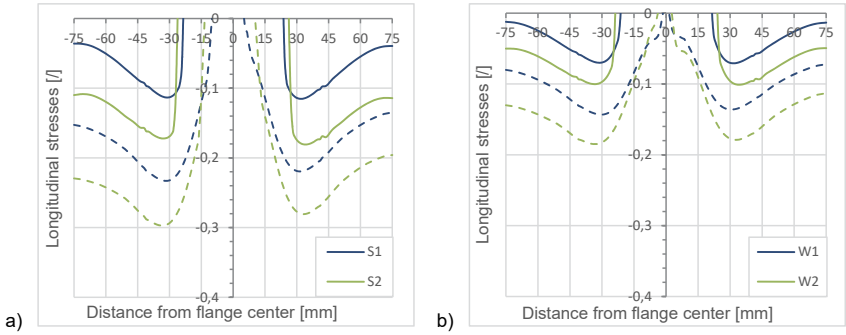

Figure 8. Compressive residual stresses (from Figure 7, normalized values).

It can be seen that these relative residual stress values are lower for the S690 in comparison to S355. This difference is largely ignored in the Eurocode 3. The Eurocode 3 assumes a direct proportionality of compressive residual stresses to the yield stress. This assumption is for example, meaningful for the buckling curve assignment of welded sections having different structural steel grades (EN 1993-1-1). Currently, no distinction is made here, which limits the advantages in the application of high strength steel grades to some degree. Specifically, the relative compressive stress values of the S690 are at approximately half of the values of the S355. However, some dependency on the weld heat input also appears to exist, because this difference is more visible for the steels with higher weld heat input.

So far, the phase transformation (PT) in the material has been neglected. This additional transformation effect, that becomes even more visible for high strength steel grades, can considerably influence the local residual stress distribution and by equilibrium, also the global residual stresses to some smaller extent. The influence of this phenomenon is shown in Figure 9, where stresses are again normalised with respect to the yield stress.

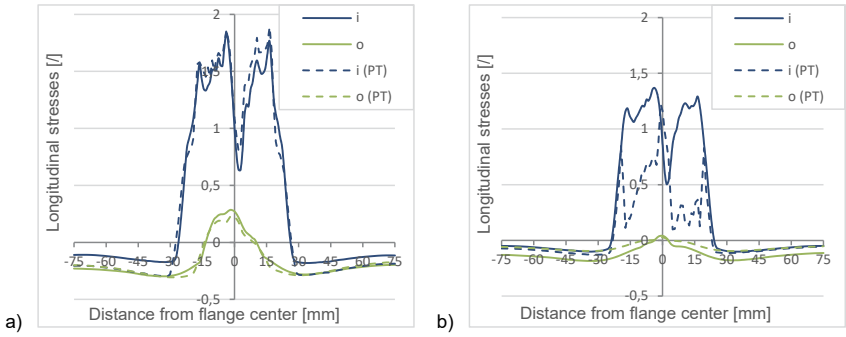

Figure 9. Normalized longitudinal residual stresses taking into account phase transformation effects: a) S2, b) W2.

The results indicate that a larger phase transformation effect on the residual stresses is only present for the high strength steel grade. Besides, this effect is particularly a local effect that leads to comparatively more moderate tensile residual stress magnitudes for the S690.

The influence of a more coarse mesh on the results was studied by a second model with a minimum element edge length of 2 mm. The comparison with previous results of the 1 mm model is shown in Figure 10. Both models agree reasonably well. Figure 10a for S2 shows an almost perfect match while for Figure 10b and W2 some local difference is noticed in the tensile areas.

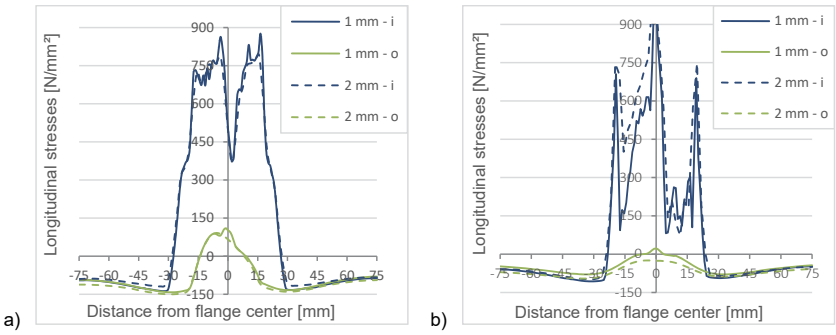

Figure 10. Influence of minimum element edge length, exemplary S2 (a) and W2 (b).

The reduction in meshing density considerably reduced the calculation effort. The corresponding calculation times are summarized in Table 4. A careful consideration is hence always recommended.

Table 4. Calculation times [h:min] in Simufact welding.

	S1		**S2**		**W1**		**W2**	
Mesh	1 mm	2 mm	1 mm	2 mm	1 mm	2 mm	1 mm	2 mm
without PT	112:09	9:28	69:52	6:13	154:00	8:52	86:35	7:06
with PT	127:31	10:29	85:58	6:38	219:24	11:24	133:50	7:35

Figure 11 shows the comparison of the numerical (1 mm, with PT) and experimental results.

Figure 11. Comparison of experiment and simulation: a) S1, b) S2, c) W1, d) W2.

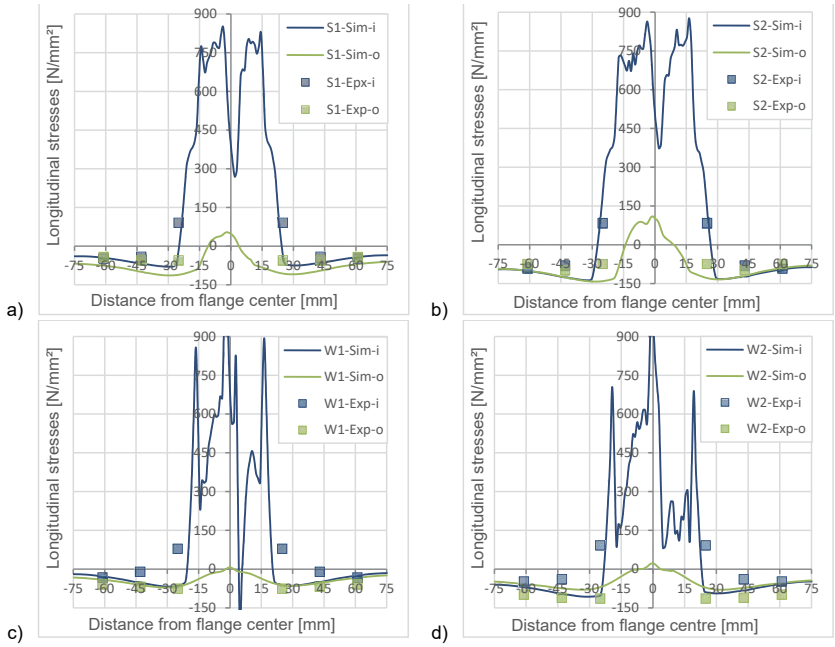

For steel grade S355, results generally agree well. The tensile width seems to be in good agreement. While the compressive residual stresses are slightly lower and on the safe side in the numerical models. Some influence of a change in the weld heat input is seen but is comparatively small in the experiments as well in the numerical models. On the other hand, the results in S690 seem to be slightly different. The tensile width in the experiments are wider. This could be due to neglecting the initial girder temperature due to preheating. The compressive residual stresses are matched on average but are not always on the safe side. Nevertheless, these values are broadly similar for S355 and S690.

Differences between experiments and numerical models can be due to various reasons but are probably mainly due to the implemented material models and the introduced simplifications of the welding process.

Abaqus (Abaqus Welding Interface)

In addition to Simufact welding, a specialized plug-in for Abaqus was used, the Abaqus Welding Interface (AWI). This is freely available for Abaqus users and provides some useful simplified temperaturebased approach. A more general approach in Abaqus is possible by user subroutines but this was not investigated.

The advantage in AWI is particularly in the automation of steps that are very time consuming for the user. In this particular approach, user-defined temperatures are directly applied via the weld-attached faces instead of the more "traditional" way by using distributed heat based on certain mathematical functions. The temperature loading is realized by so-called chunks that are subsequently applied. The user defines the number of chunks that each bead is split-up into. This enables also simplified and fast solutions by considering the weld consisting of only very few chunks. On the other hand, the more the number of chunks, the more the simulation aims to the fully transient approach. A general disadvantage is however still that the user is not able to define welding parameters or the weld heat input directly.

In this paper, the chunks were chosen in approximate accordance with the expected weld pool lengths and activation rates were adapted to meet the given welding speed. The torch heatup temperature was taken by default as 1500 °C as a first approach.

The thermal and the mechanical models are automatically generated after the user is guided through a few input masks and are calculated sequentially. In contrast to Simufact Welding, it is not possible to include a back-coupling of the mechanics to the temperature field. The effect of a phase transformation is also not included in the AWI.

Due to the mentioned simplifications in the temperature application, large differences are noticed in the evaluated thermal cycles in Figure 12a. The temperature peaks are generally lower in Abaqus. The points for evaluation of the results are the same as in Figure 6 or Figure 2 respectively.

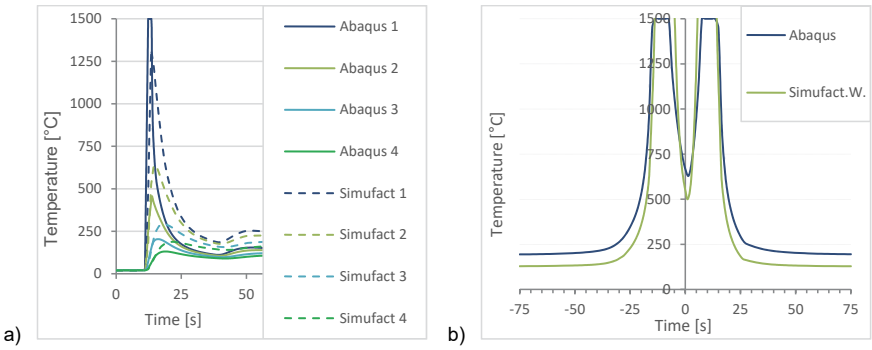

Figure 12. Comparison of calculated temperature cycles and maximum temperature distribution (b) in Abaqus and Simufact (2 mm, S1).

Less difference is however noticed in the comparison of the callculated maximum temperature isotherms in Figure 12b that represent a major factor in the evaluation of the longitudinal residual welding stresses.

The results of the subsequent mechanical calculation of S1 and S2 are evaluated in Figure 13.

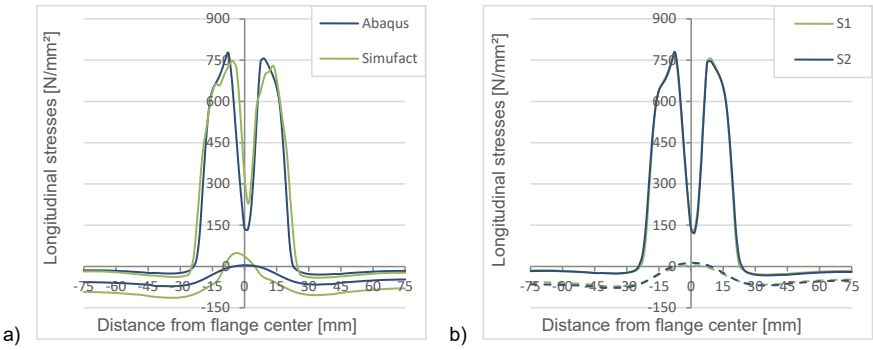

Figure 13. Comparison of longitudinal residual stresses: a) Abaqus and Simufact (S1), b) S1 und S2 in Abaqus.

At first sight, the match in Figure 13a is surprisingly good. Tensile peaks match relatively well while the tensile width is slightly smaller in Abaqus. In compression, values are on the unsafe side on the lower flange. More importantly, in Figure 13b it can be seen that the cases S1 and S2 show virtually identical results. It was not possible to capture the effects of a different weld heat input correctly. Accordingly, the previous match seems to be also coincidental to some extent. Thus, the results from AWI should only be used as a coarse approximation but not for quantitative evaluation. Nevertheless, there is definitely potential to develop the method further.

CONCLUSIONS

The numerical welding simulation has reached a level of practical application in some branches. However, accompanying experiments are still necessary to some extent. Special programmes such as Simufact Welding have dramatically eased the performance of such simulations and also include a large library of material data. The simulations using Simufact Welding have proven to be able to realistically describe residual stresses. The results helped to clarify the influence of the material grade as well as the welding parameters in addition to the available experiments. It was for example shown that the S690 shows a relatively favourable residual stress state in comparison to a conventional S355.

A second simplified approach that is available as a plugin for the general purpose FEcode Abaqus has been additionally investigated for comparison. The results in terms of temperature and residual stresses have shown some deviations. Besides, it was not able to reproduce the influence of the weld heat input realistically. Besides, the influence of phase transformation, if required, is not available in this specific approach. This method is however simpler and might be applicable to larger components if the number of chunks is reduced

accordingly. For such case, further modifications in the heat input are then needed to ensure results of acceptable quality.

In summary, the modern welding simulation can provide a future alternative for the calculation of the weld-induced imperfections, e.g. the residual stresses. However, the effort in the classical approaches is still very high and not at a practical level with respect to the civil engineering sector. Different solutions are available, from which two have been presented here. The choice of a specific modelling approach, sophisticated or simplified, eventually depends on the further use of results to a very large extent and should be carefully evaluated by the user. For the research sector on the other hand, it will be important to further contribute to sufficiently simplified approaches in order to ensure an earlier practical application of these methods.

REFERENCES

Fahrenwaldt, H., Schuler, V., & Twrdek, J. (2014). *Praxiswissen Schweißtechnik*. Wiesbaden: Springer Fachmedien.

Wohlfahrt, H., & Schmidt, J. (2001). *Simulation der Vorgänge im Schmelzbad beim Laserstrahlschweißen zur Voraussage von Nahtbildung, Gefüge, Verzug und Schweißeigenspannungen*. TU Braunschweig, Institut für Schweißtechnik, Institut für Strömungstechnik und Thermodynamik.

Pasternak, H., Kannengiesser, T., Launert, B. & Rhode, M. (2018). *Erhöhung der Tragfähigkeit geschweißter I-Träger aus hochfestem Baustahl durch verbesserte Ansätze zur Berücksichtigung von Eigenspannungen*. Düsseldorf: Verlag und Vertriebsgesellschaft mbH (in print).

SOFTWARE DEVELOPMENT EXPERIENCE IN DESIGNING OF STEEL STRUCTURAL JOINTS

Viktor Karpilovsky, Eduard Kriksunov, Anatoly Perelmuter
SCAD Soft Ltd., Kyiv, Ukraine

Vitalina Yurchenko
Kyiv National University of Civil Engineering and Architecture

ABSTRACT

The paper presents COMET software, which enables design of steel structural joints widely used in civil and industrial engineering. The conceptual basis of the project was the idea of creating a program with the following functions: automatic determination of all parameters of the joint which formally satisfy the requirements of design codes for the given internal force combinations; automatic determination of some parameters of the joint, taking into account the fact that other parameters are specified by the user and cannot be changed; implementation of all control verifications of whether the load-bearing capacity constraints as well as structural constraints are satisfied in the cases when all parameters of the joint are specified and cannot be changed.

Algorithm for designing each joint prototype has been presented as a set of operations implementing the rules for determining the interrelated values of the joint parameters. Each prototype is developed as an independent program that performs a full cycle of designing the joint and verification of the joint parameters according to the specified design codes.

Searching of unknown joint parameters has been implemented as a decision-making problem based on analysis of the joint mathematical model. Automatic searching of unknown joint parameters has been implemented as a multiple targeted improvement of a certain initial joint design in order to satisfy load-carrying capacity constraints taking into account the structural and other constraints. Successive improvement of the current joint design is performed on the basis of sensitivity analysis relative to variation of governing joint parameters.

In cases when the values of some joint parameters have to be taken as fixed (or user-defined), the program considers these parameters as the same kind of initial data. All other (unknown) parameters will be considered as design variables of the searching problem. Thus, the technology implemented in COMET supports the mode of active user decision making.

INTRODUCTION

Design and analysis of joints is one of the most important stages in the design of steel structures. Unlike the stress-strain state analysis on the basis of the design model, which follows strict rules of structural mechanics, "algorithms" for the analysis of joints use the traditional methods (taking into account the previous experience) of approximate solutions, which are based on a simplified representation of the behavior of joints. These methods are usually closely related to the set of proven designs of joints (prototypes) used for this type of structures.

Despite the variety of prototypes of joints of one type (for example, columns bases), the number of parameters, that need to be determined for each of them in the design process, is limited. Taking into account the peculiarities of the behavior of a certain prototype of the joint in the structure (e.g., the cross sections of structural elements coming into the joint, loads carried by the joint etc.), and the requirements of various design codes, the algorithm for designing each joint prototype should be presented as a set of operations implementing the rules for determining the interrelated values of the parameters. Each prototype is developed as an independent procedure that performs a full cycle of designing the joint, checking of the parameters according to the specified design codes, as well as the generation of a drawing of the designed joint. Taking into account the fact that, regardless of the selected prototype most of the parameters of the same purpose of the joints of the same type are determined according to the same rules, the software implementation of parametric prototypes comes down to the organization of information exchange between different software modules that serve to determine the specific parameters.

The focus on the use of parametric prototypes of joints that meet the above requirements has been adopted from the first programs developed by SCAD Soft Ltd. since the mid-1990s and implemented in software COMET (Karpilovsky et al. 1998). A similar approach to the solution of the problem of designing steel structural joints has been also used by other developers of CAD-CAE systems, for example, RFEM and RSTAB modules of Dlubal Software (2015), 'Connections' modules of Autodesk Robot Structural Analysis Professional (Sukhorukov 2009) or STK-SAPR and ESPRI of LIRA-SAPR.

CRITERIA FOR SELECTING PROTOTYPES FOR THE DEVELOPMENT

The set of parametric prototypes defines the scope of the program as well as the cost and time for its development. There are no strict rules for selecting the prototypes, and in the case of COMET it entirely depended on the developers' experience.

The complexity and high cost of the development of this kind of software have defined the search for designs of joints that would both meet the criteria of wide use in the design practice and provide the possibility to analyze joints,

which might not be the most common, but are quite difficult for most designers of joints.

The first criterion satisfies the business considerations of CAD-CAE system developers since the mass use of such joints in the design leads to the popularity of the program among ordinary designers. On the other hand, joints, which might not be that common, but, require highly skilled designers and create certain engineering problems, increase the rating of the software and the authority of the developers, which ultimately affects the commercial component of all the company developments.

Column bases (rigid and nominally pinned) are an example of joints which satisfy the criteria of wide use, at the same time the software also enables to analyze and design various types of beam splices with end-plates since it is difficult for most designers.

Regardless of the criteria for the selection of certain joints in parametric prototypes, a proper design study is an absolute requirement because the program operates only with the design details provided in advance at the algorithm development stage.

It should be noted that the design model of the joint is largely defined by the current practice. “Traditional” models are often simplified, since they were developed during the period of “manual” design demanding maximum simplification of the problem. Mass transition to the CAD-CAE design systems enables the use of more accurate design models. However, the results of such a “clarification”, often resulting in complication of the joint, and may require additional studies.

In some cases, this kind of clarification is inevitable. For example, the traditional calculation methods given in the codes are not always suitable for solving three-dimensional problems. In particular, it concerns rigid column bases for which the problem of determining the contact area of the base plate with concrete arises in bending in both principal planes. The internal solver of COMET uses the finite element method to solve this problem.

PARAMETRIC PROTOTYPES ORIENTATION AND ROLE OF A DESIGNER

The current version of COMET enables design of steel structural joints widely used in civil and industrial engineering (Karpilovsky et al. 2010, Perelmuter et al. 2010). The application is also used to perform a structural appraisal of a steel joint according to the requirements of Ukrainian codes (DBN B 2.6-163: 2010 or DBN B 2.6-198: 2014), Russian codes (SNiP II-23-81*, SP 53-103-2004 or SP 16.13330.2011) and European codes (EN 1993-1-8, EN 1993-1-1). Among other things, the selection of codes defines the set of prototypes of joints proposed for the analysis, which includes only the joints that are reflected in the text of the codes.

The COMET software provides the following groups of prototypes for steel structural joints: nominally pinned and rigid column bases, beam and rafter splices, hinged and rigid joints between columns and rafters, and truss joints.

The set of parametric prototypes for each type of joint has been determined on the basis of different requirements, the consideration of which has affected not only the selected designs, but also the parameters necessary for their implementation. A set of prototypes implemented for beam splices is shown as an example in Figure 1.

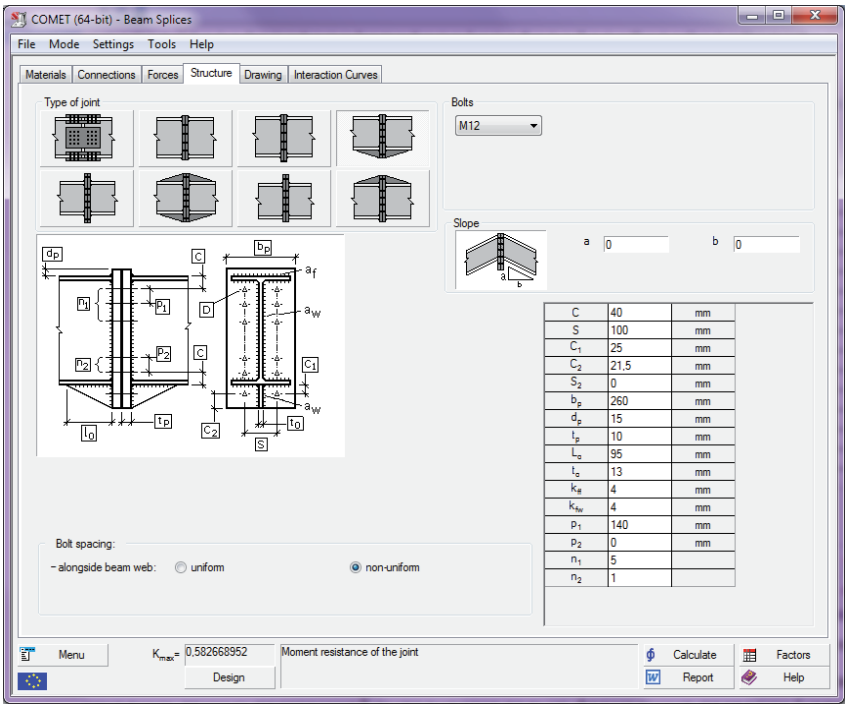

Figure 1. Set of prototypes for the design of beam splices.

The joint prototype is selected by the designer. Only formal checks are performed at the stage of the data input (e.g. correspondence of the set of force factors to the selected joint prototype). Once the calculation is completed, it is up to the designer whether to accept or reject the analyzed design. Given that the time of the calculation of joint is comparable with the time it takes to press a “button” invoking this operation, it becomes possible to analyze other options and make an informed decision.

INPUT AND CONTROL OF THE INITIAL DATA

Initial data include the information about the structural members connected in the considered joint, their sections and steel grades, joint's type (prototype), set of internal forces acting in adjacent sections of the connected structural members (see Figure 2) as well as the data allowing selection of the properties of the used bolted and welded connections (see Figure 3).

Taking into account the fact that the joint has to work in different design situations, the program enables specification of the necessary number of internal forces combinations. These combinations can be specified by the user or can be the result of the calculation performed by structural analyzer SCAD. The main requirement is the simultaneous action of forces included in one combination.

The check of the initial data is performed by the program both in the process of their specification (detection of formal errors) and in the design process. Diagnostic messages are generated on the basis of the results of these checks.

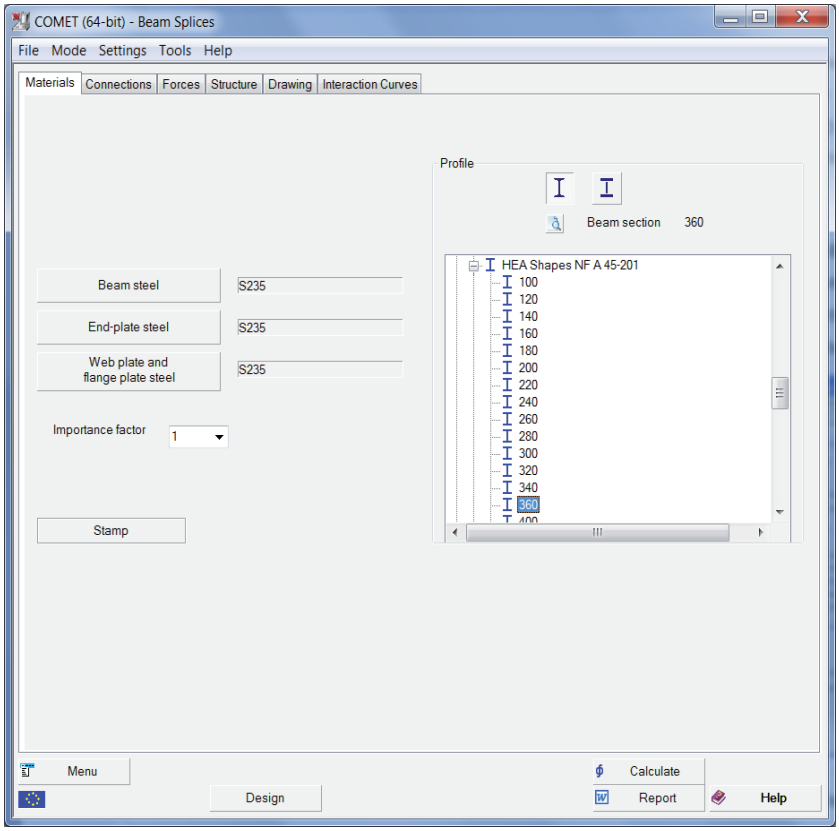

Figure 2. Dialog box for specifying the main initial data.

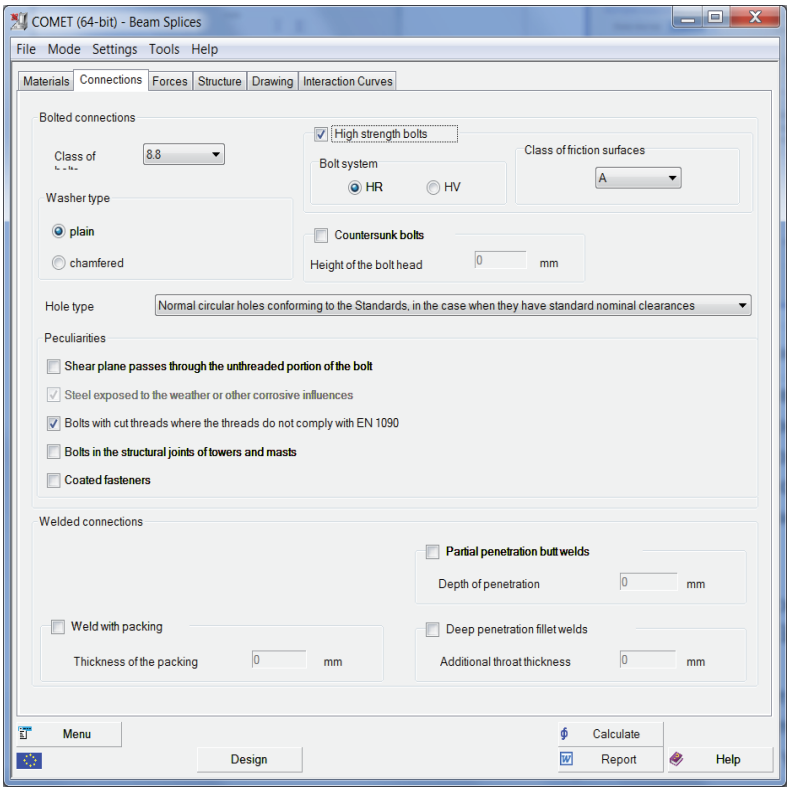

Figure 3. Dialog box to specify initial data for welded and bolted connections.

SOFTWARE IMPLEMENTATION

Conceptual provisions and flowchart

The conceptual basis of the project was the idea of creating a program with the following functions:

- automatic determination of all parameters of the joint which formally satisfy the requirements of design codes for the given internal forces combinations;
- automatic determination of some parameters of the joint, taking into account the fact that other parameters are specified by the user and cannot be changed;
- implementation of all control verifications of whether the load-bearing capacity constraints as well as structural constraints are satisfied in the cases when all parameters of the joint are specified and cannot be changed.

In fact, the role of the program can change from the "generator of all parameters" of the design specified by the user, taking into accounts the codes and external factors to the "simple check" of the capacity of the joint in accordance with the codes (the check of the parameters specified by the user). In cases when the values of some parameters have to be taken as fixed (user-defined), and all others are determined by the conditions of compliance with the codes, the program works according to the second variant. The program considers the parameters specified by the user as the same kind of initial data as the class of concrete or steel grade.

A generalized flowchart for solving the problem in the designer-software interaction mode corresponding to this concept is shown in Figure 4.

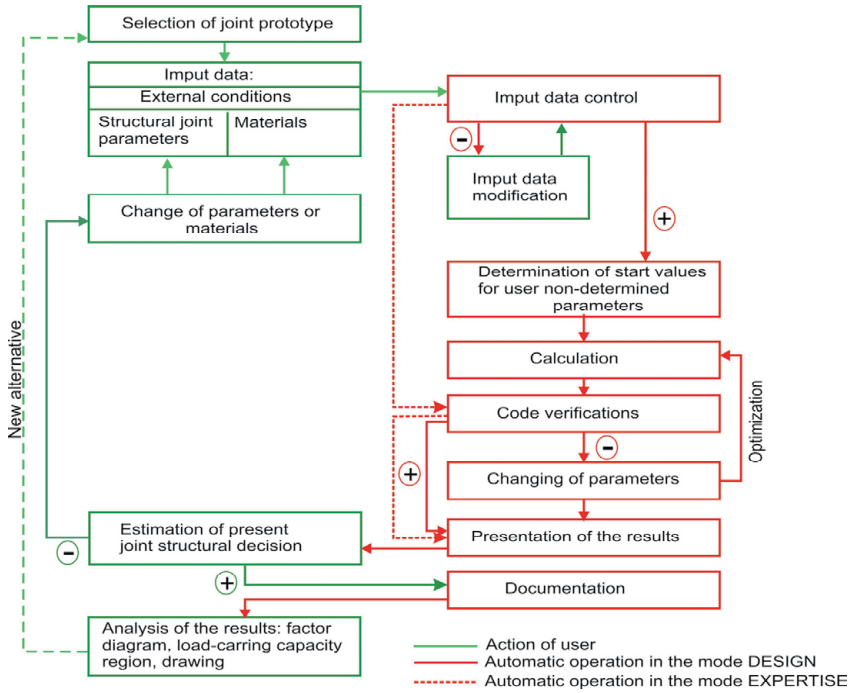

Figure 4. Generalized flow chart in the designer-software interaction mode.

A role of the structural engineer is an important feature of the concept of searching/checking the parameters of the joint adopted in the program. He/she is responsible for the choice of the design, completeness and correctness of the loads taken into account and acting on the structure with the considered joint, as well as the analysis of the applicability of the obtained solution. If, as a result of the analysis, the designer changes some parameters, the program will perform the check and the search for such values of other parameters that would ensure the operation of the joint and would not contradict the codes.

Software modes

As noted above, the program enables selection of the parameters of the joint on the basis of the design selected by the user and the conditions of its reliability and operability under the given operating conditions and materials (see Figure 5).

If the joint is already operating in the real structure, i.e. all its parameters and operating conditions are known, the check of the joint can be performed, the results of which enable a justified decision to be made about the possibility of the operation of the joint in the new conditions (for example, at high loads on the structure). Thus, two fundamentally different modes have been implemented in the program – Design and Calculate, which are invoked by the respective buttons.

If, as a result of the design, the parameters of the prototype provide the operability of the joint, but some of them cannot be accepted because of the (possibly not formalized) requirements the designer knows, the list of the initial data can be extended by specifying the desired values for such parameters. At the same time, all other parameters not subject to the above requirements are set to zero and the design mode repeats.

When setting the parameters, the program analyses their values and reports detected violations of the design requirements. These can be strict guidelines on the need to change the specified values, or warnings about the violation of the recommendations of codes that can be ignored.

Thus, the technology implemented in COMET supports the mode of active user decision-making. Such a mode can both satisfy experienced designers allowing them to achieve the necessary solution, and allow beginners to solve a design problem with minimal interference in the decision-making process.

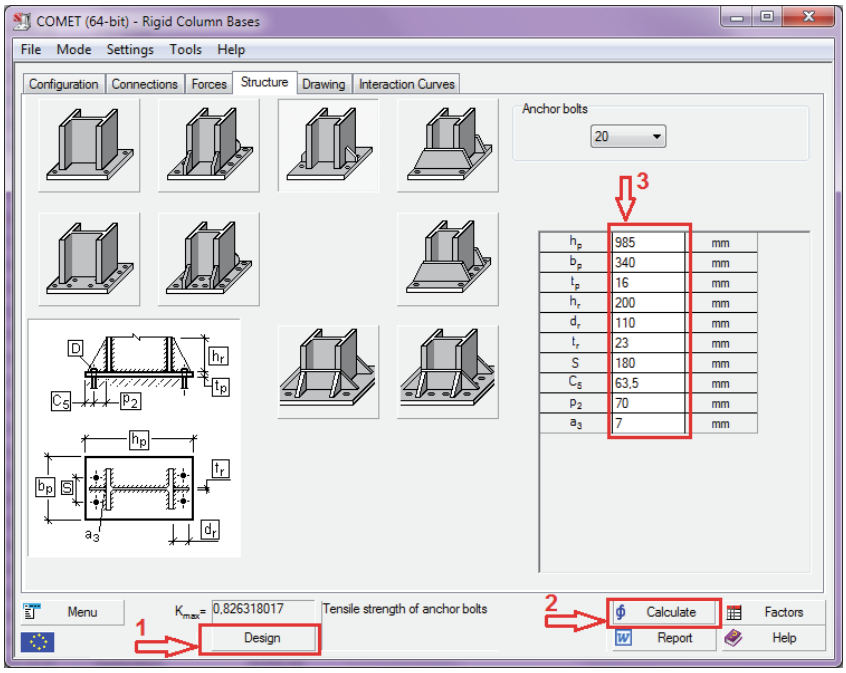

Figure 5. Control of the software mode: 1 - determination the preliminary design decision, 2 - calculation of variable parameters and verification of the design decision, 3 – specification of the values for user-determined (fixed) parameters.

Solution optimization

If the design check indicates there is a need to change the parameters, this is performed in the program on the basis of a sensitivity analysis. The basis of this approach is explained below.

Inequalities of the type $E_{d,i} \le R_{d,i}$ should be satisfied in all checks between the design values of the action effects $E_{d,i}$ and the design strength $R_{d,i}$ according to the limit state calculation method adopted in EN 1990. It is more convenient to represent these inequalities in the following form:

$$k_i = E_{d,i} / R_{d,i} \le 1,0 \quad (i = 1,\ldots,n) \tag{1}$$

where k_i is the utilization factor of the ith constraint, it is the reciprocal of the factor of safety. The value of the factor k_i is a function of the governing design parameters X_j $(j = 1,\ldots,p)$.

It should be noted that not all design parameters are independent. Some of them can be considered as governing, while others are unambiguously calculated from the known values of the governing parameters, and are not

considered further. Moreover, some values of the parameters can be forced by the user; they are fixed and are not considered in the following description as well.

Automatic selection of the unknown values of the internal parameters of a joint design is implemented as a multiple targeted improvement of a certain initial design of the joint in order to satisfy the bearing capacity limitations taking into account the structural and assortment limitations. Multiple improvement of the design is performed on the basis of the analysis of its sensitivity to variation of the controlled parameters of the joint design. The response of the system, represented by the values of the utilization factors of the load-bearing capacity constraints, is evaluated at each variation of a certain controlled parameter.

Let us consider the case when it is necessary to improve the design that does not satisfy the requirements of the codes, since its check has shown that some of the inequalities (1) are violated and the utilization factor of the constraints is greater than one. If an increment ΔX_s is given to one of the parameters, for example X_s, all utilization factors can change obtaining new values $k_{is} = k_i + \Delta k_{is}$. It is logical to first use the change of the parameter ΔX_r for which the value of the greatest utilization factor of restrictions improves the most, i.e. $k_{jr} = \min\limits_{s=1,\dots,p} \max\limits_{i=1,\dots,n} \left(k_i + \Delta k_{is} \right)$.

The problem can be simplified in certain situations:

- if a certain constraint utilization factor depends not on all governing parameters, the increments of the parameters which do not affect it are not checked;
- if different utilization factors depend on different groups of governing parameters, the problem is divided into a number of unrelated sub-problems.

PRESENTATION OF RESULTS

Results of the design and verification are given as a diagram of checked factors, drawing with a preliminary design of the considered joint, a family of graphs bounding the region of the load-bearing capacity of the joint in the coordinate system of the selected internal forces and the report in RTF-format.

Factors diagrams

Results of the load-bearing capacity verifications for compliance with the requirements of design codes are given in the form of a factors diagram. Each factor is accompanied by a reference to the respective section of the code, which regulates these requirements. The values of the factors are given in the form of the constraint utilization factors (see Figure 6).

Drawing

A graphical representation of the designed joint is given in the form of a simplified drawing, which describes the structure completely and in detail, including the specification (see Figure 7), but it does not take into account the manufacturer's technical requirements. In order to later amend the drawing it can be presented in DXF-format, a file that can be used by various graphic editors.

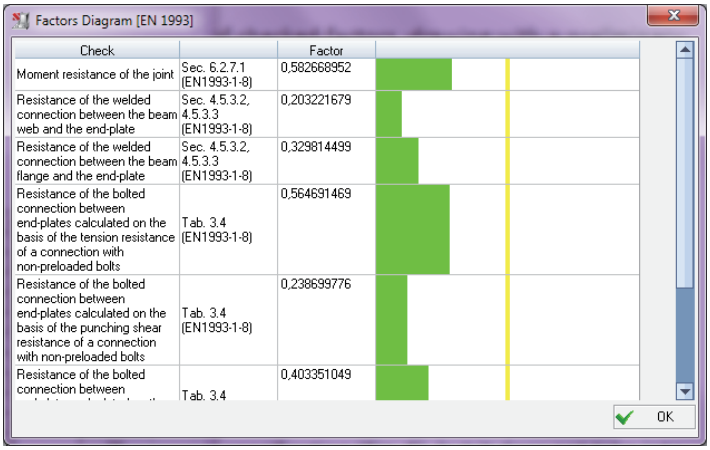

Figure 6. Factors diagram.

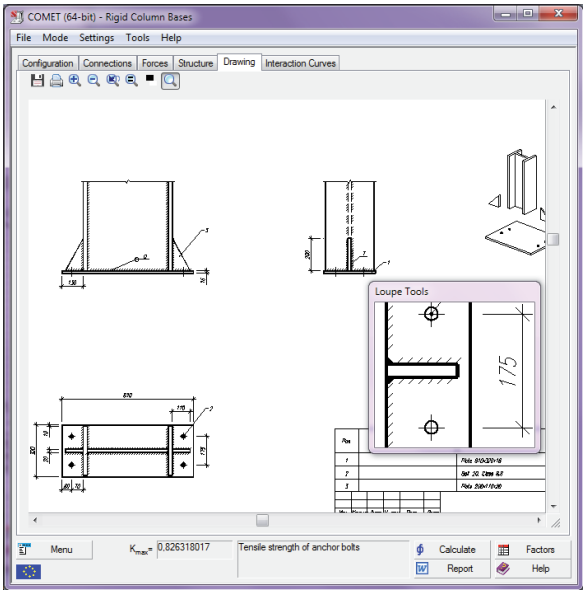

Figure 7. Design drawing on the screen.

Load-bearing capacity regions for structural joints

Load-bearing capacity region for the structural joint is a family of graphs in the coordinate system of the selected internal forces bounding the region where all utilization factors are less or equal to one or, in other words, where all inequalities (1) are satisfied (see Figure 8). Such a family of graphs gives us a representation of the load-bearing capacity of the designed joint in terms of the selected design code. Plotting each variant of such a region deals with a design verification of hundreds of internal force combinations. The authors believe that such a large-scale verification has never been performed before.

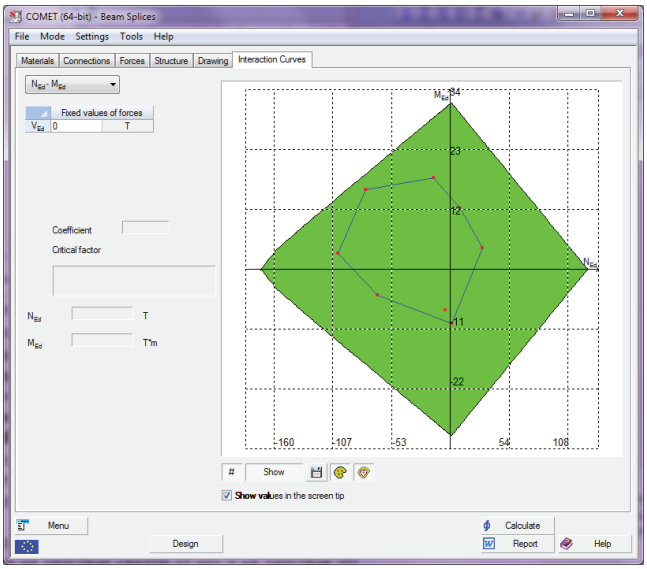

Figure 8. Plotting the load-bearing capacity region together with points corresponded to the acting internal forces in the joint and convex shell of internal forces.

The program also shows the position of points corresponding to the internal forces and to plot a convex envelope on the basis of these points thus bounding the part of the load-bearing capacity region, which corresponds to any linear combination of design internal forces in the considered joint.

Figure 9 shows variants of the load-bearing capacity region for different type of beam splices designed for the same set of internal forces. It can be seen in this case that the selection of the prototype has affected on the shape of the load-bearing capacity region.

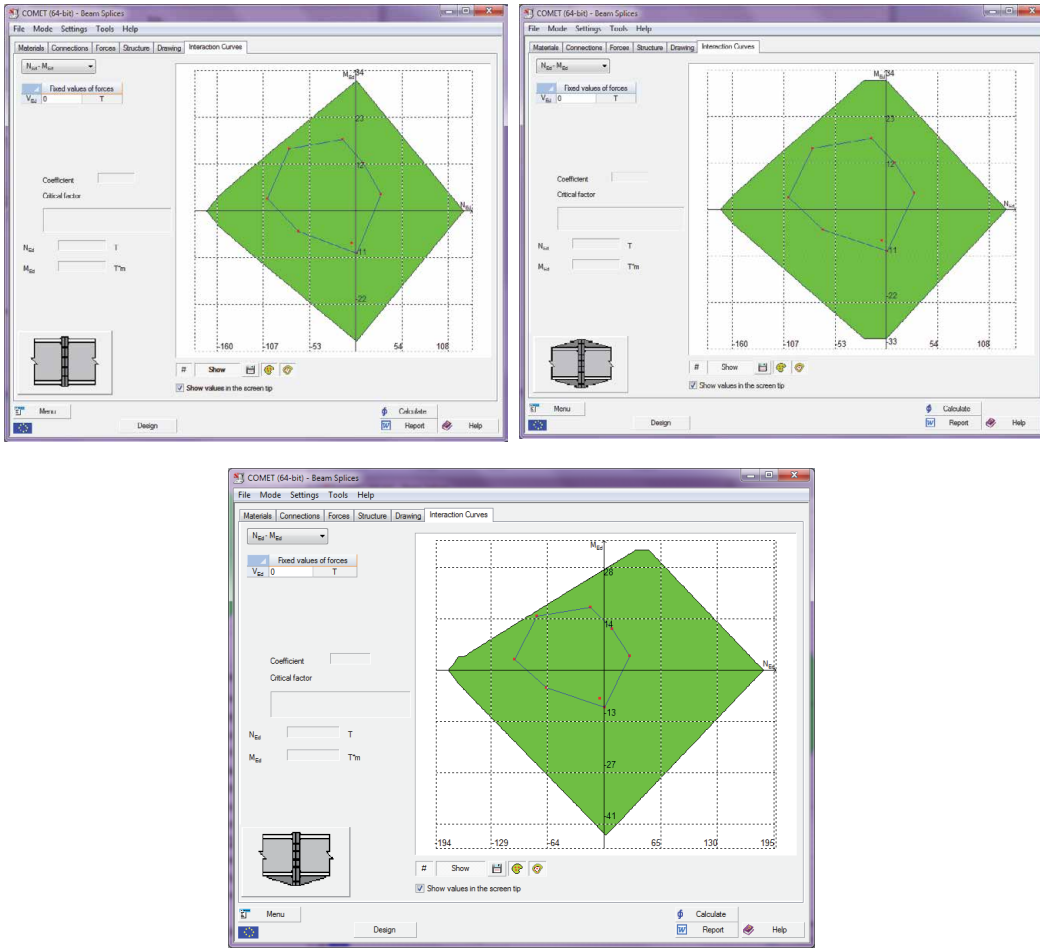

Figure 9. Variants of the load-bearing capacity regions for different types of beam splices joint.

CONCLUSIONS

Algorithm for designing each joint prototype has been presented as a set of operations implementing the rules for determining the interrelated values of the joint parameters. Searching of unknown joint parameters has been transformed to a decision-making problem based on an analysis of mathematical model of the joint. Automatic searching of unknown joint parameters has been implemented as a multiple targeted improvement of a certain initial joint design in order to satisfy load-bearing capacity constraints taking into account the structural and other constraints. Iterative improvement of current joint design is performed on the basis of sensitivity analysis relative to variation of governing joint parameters.

REFERENCES

Dlubal Software GmbH (2015). Add-on Module JOINTS. *Design of Connections in Steel and Timber Structures. Program Description*. Retrieved 18 Jan 2018 from http://www.dlubal.con/-/media/Files/website/documents/manuals/rfem-and-rstab-add-on-modules/connections/joints/joints-manual-en.pdf

Karpilovsky, V., Kryksunov, E., Perelmuter, A., & Permyakov, V. (1998). Software Application for Design and Analysis of Steel Structural Joints. Construction of Ukraine No. 5, 1998, 43-47.

Karpilovsky, V., Kryksunov, E., Mikitarenko, M., Perelmuter, A., Perelmuter, M., Fedorovskyy, V., & Yurchenko, V. (2010). *SCAD Office. Implementation of Design Codes in Computer-Aided Design Applications*. Moscow, SCAD SOFT.

Perelmuter, A., Kryksunov, E., Gavrilenko, I., & Yurchenko, V. (2010). Designing bolted end-plate connections in compliance with Eurocode and Ukrainian codes: consistency and contradictions. Modern Building Materials, Structures and Techniques. Selected papers. Vol. II. Vilnius: Vilnius Gediminas Technical University, Vilnius Technika. 733-743.

Sukhorukov, V. (2009). *Autodesk Robot Structural Analysis Professional. Moscow*, Association of Educational Civil Engineering Institutions of Construction.

RELIABILITY OF STEEL FRAMEWORKS OF INDUSTRIAL BUILDINGS

Pichugin S. F., DSc, Professor
pichugin.sf@gmail.com

Patenko Iu. E., PhD
maslova_yuliya@i.ua
Poltava National Technical Yuri Kondratyuk University, Ukraine

INTRODUCTION

The work focuses on the reliability assessment of single-storey industrial buildings with overhead travelling cranes. Problems of reliability assessment of such buildings are compared with the complex character of external loads. The nature of these loads is complicated and depends on many spatial and space-temporal factors.

Among all of the loads, which influence the design of industrial buildings, crane loads have the largest values. Often these loads define the architecture and spatial design of workshops, materials and weight of the supporting structures. Because of the problem of obtaining a probabilistic model of crane loads which will describe actual nature of the crane loads on structures of industrial buildings, the problem is not easy to solve. Therefore, the problem of development the probabilistic models is relevant and justified as well as the calculation the values of numerical characteristics of vertical and horizontal crane loads.

REVIEW OF RESEARCH SOURCES AND PUBLICATIONS

The results of extensive experimental investigations of crane loads are presented in the References (Pichugin 1998, Pichugin 2014b). Experimental data were processed using the technique of random variables and random processes which confirmed the probabilistic nature of crane loads. The problems of standardization and development of analytical models of crane loads are considered in works (Patenko 2016, Pichugin 1997, Pichugin 2016b). Comparative analysis of the values of crane loads which were defined according to national and international codes (EN 1991-1-3/2003, DBN V.1.2-2:2006, SNiP 2.01.07-85/1987) is presented in Pichugin (2010). The refined values of crane loads allow more accurate reliability assessment of industrial buildings (Patenko 2016, Pichugin 1997). The question of reliability of structures (ISO 2394:2015, ISO 13822:2010, ISO 13824:2009) is considered in Pichugin (2014a, 2005, 2016a and 2011a). The approaches to the reliability assessment were developed using probabilistic methods, which describe the behaviour of structures under external loads. Reliability assessment of steel frames of one-storey industrial buildings with overhead cranes is described

in (Patenko 2012, Pichugin 2015, Pichugin 2011b), where the spatial nature of the frameworks was refined. Furthermore, the detailed analysis of loads and review of Codes (FEM 9.511/1986) which classify parameters of overhead traveling cranes were done.

NUMERICAL CHARACTERISTICS OF CRANE LOADS

Numerical characteristics of vertical crane loads

Vertical load (Fig. 1) on the structures of different frames (columns, crane girders) was defined as:

$$\widetilde{F}_{\max} = \left[\frac{G_B}{2} + (\widetilde{Q} + G_{crab})\frac{L_{cr} - \widetilde{a}}{L_{cr}}\right]\frac{\widetilde{y}}{n_0}, \quad \widetilde{F}_{\min} = \left[\frac{G_B}{2} + (\widetilde{Q} + G_{crab})\frac{\widetilde{a}}{L_{cr}}\right]\frac{\widetilde{y}}{n_0}, \tag{1}$$

where G_B, G_{crab} – weight of the bridge and the crab of crane;

$\widetilde{Q}$ – hoisting load; L_{cr} – crane span;

$\widetilde{a}$ – approach of the crane hook; $\widetilde{y}$ – sum of the influence line ordinates;

n_0 – the number of wheels on one side of crane.

To the non-linear function (1) with three random arguments the procedure of statistical linearisation was applied. In this case the mathematical expectations $\overline{F}_1$ and $\overline{F}_2$ were determined by substitution instead of random arguments of the mathematical expectations of $\overline{Q}, \overline{a}, \overline{y}$. Thus, we got accurate result because all second derivatives that define the mathematical expectation are zeros.

To calculate the dispersion of maximum crane load the next coefficients were determined:

$$A_{1,\max} = \frac{dF_{\max}}{dQ} = \frac{L_{cr} - \overline{a}}{L_{cr}}\frac{\overline{y}}{n_0}; \quad A_{2,\max} = \frac{dF_{\max}}{da} = -\frac{G_{crab} + \overline{Q}}{L_{cr}}\frac{\overline{y}}{n_0};$$
$$A_{3,\max} = \frac{dF_{\max}}{dy} = \frac{1}{n_0}\left[\frac{G_B}{2} + (G_{crab} + \overline{Q})\frac{L_{cr} - \overline{a}}{L_{cr}}\right]. \tag{2}$$

Using the obtained coefficients, we defined the dispersion of vertical crane load as follows:

$$\widehat{F}_{\max} = \left(\frac{L_{cr} - \overline{a}}{L_{cr}}\frac{y}{n_0}\right)^2 \hat{Q}^2 + \left(\frac{G_{crab} + \overline{Q}}{L_{cr}}\frac{\overline{y}}{n_0}\right)^2 \hat{a}^2 + \frac{1}{n_0^2}\left[\frac{G_B}{2} + (G_{crab} + \overline{Q})\frac{L_{cr} - \overline{a}}{L_{cr}}\right]^2 \hat{y}^2. \tag{3}$$

For the estimation of the precision of dispersion we calculate the mixed derivatives:

$$\frac{d^2F_{\max}}{dQda} = -\frac{y}{L_{cr}n_0}; \quad \frac{dF_{\max}}{dQdy} = \frac{L_{cr}-a}{L_{cr}}\frac{1}{n_0}; \quad \frac{d^2F_{\max}}{dady} = -\frac{G_{crab}+Q}{L_{cr}n_0}. \tag{4}$$

The dispersion precision of maximum crane load was determined using the linearization procedure:

$$\Delta\widehat{F}_{\max} = \frac{1}{L_{cr}^2 n_0^2}\left\{\left[(L_{cr}-\overline{a})\hat{Q}\hat{y}\right]^2 + (\overline{y}\hat{Q}\hat{a})^2 + \left[(G_{crab}+\overline{Q})\hat{a}\hat{y}\right]^2\right\}. \tag{5}$$

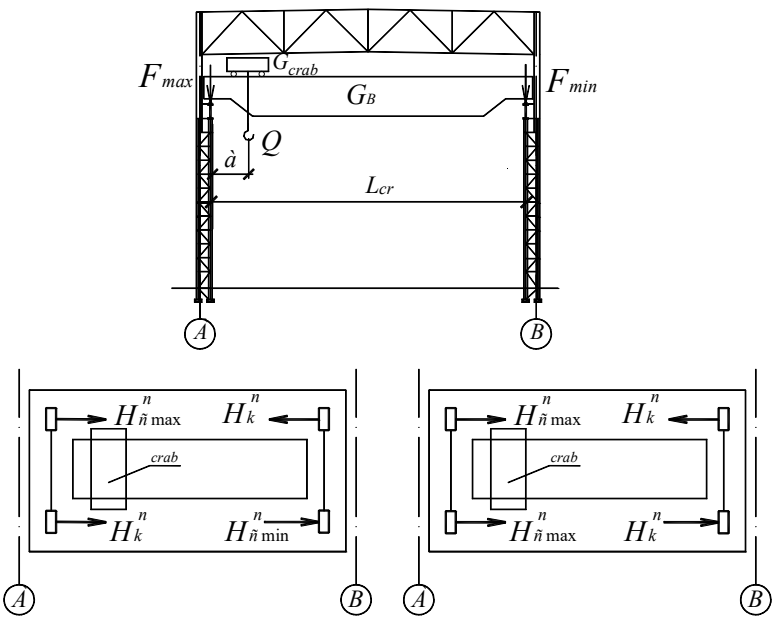

Figure 1. Schemes of crane loads: a) impose of vertical loads to the transverse frames; b) impose of horizontal loads to the crane wheels.

The precision of dispersion of minimum crane loads can be defined similarly. For the numerical evaluation, a crane with lifting capacity $Q = 50/10\,t$ was taken. The weight distribution was taken as normal with variation coefficient $V_Q = 1/3$, distribution y – uniform. The obtained precision of dispersion was very low (2,2% $\widehat{F}_{\max}$). The obtained numerical characteristics were used to construct a graph of normal distribution of the load on the column. This graph well corresponds to experimental polygons of loads.

Obtained formulas allow the use of simple random arguments $\widetilde{Q}$, $\widetilde{a}$ and $\widetilde{y}$ instead of complicated experimental study of vertical crane loads.

Furthermore, the available experimental data and *a priori* reasons followed by analytical determination of the characteristics of crane loads can be used.

Numerical characteristics of horizontal crane loads

To calculate the dispersion of minimum crane load we determined next coefficients:

$$A_{1,\min} = \frac{dF_{\min}}{dQ} = \frac{\bar{a}}{L_{cr}} \frac{\bar{y}}{n_0}; \; A_{2,\min} = \frac{dF_{\min}}{da} = -\frac{G_{crab} + \bar{Q}}{L_{cr}} \frac{\bar{y}}{n_0};$$
$$A_{3,\min} = \frac{dF_{\min}}{dy} = \frac{1}{n_0}\left[\frac{G_B}{2} + (G_{crab} + \bar{Q})\frac{\bar{a}}{L_{cr}}\right]. \tag{6}$$

Then the dispersion of minimum crane load can be defined as:

$$\hat{F}_{\min} = \left(\frac{\bar{a}}{L_{cr}} \frac{y}{n_0}\right)^2 \hat{Q}^2 + \left(\frac{G_{crab} + \bar{Q}}{L_{cr}} \frac{\bar{y}}{n_0}\right)^2 \hat{a}^2 + \frac{1}{n_0^2}\left[\frac{G_B}{2} + (G_{crab} + \bar{Q})\frac{\bar{a}}{L_{cr}}\right]^2 \hat{y}^2. \tag{7}$$

The mathematical expectation of lateral forces on the wheels of four-wheel crane (Fig. 1, b) can be fined using formula (8). These forces are limiting skewing of the bridge:

$$\bar{H}_k^n = 0{,}1\bar{F}_{\max} + \frac{\alpha\left(\bar{F}_{\max} - \bar{F}_{\min}\right)L_{cr}}{B}. \tag{8}$$

To determine the dispersion of lateral forces we can also apply the linearisation process and define the necessary coefficients. Then the dispersion of maximum lateral forces will be:

$$\hat{H}_k^n = \left[\left(0{,}1 + \frac{\alpha L_{cr}}{B}\right)\hat{F}_{\max}\right]^2 + \left(\frac{\alpha L_{cr}}{B}\hat{F}_{\min}\right)^2. \tag{9}$$

On the other side of crane will appear lateral forces with the following numerical characteristics:

$$\bar{H}_c^n = 0{,}1\bar{F}_{\max} \text{ or } \bar{H}_c^n = 0{,}1\bar{F}_{\min}; \hat{H}_c^n = 0{,}1\hat{F}_{\max} \text{ or } \hat{H}_c^n = 0{,}1\hat{F}_{\min}. \tag{10}$$

The obtained formulas allow the use of the numerical characteristics of horizontal crane loads in calculations and to use these characteristics for estimating the reliability of structures of industrial buildings.

Calculation of numerical characteristics of crane loads

For the definition the numerical characteristics of crane loads an industrial building (with a span of 24 m and a columns step 6 m) with a four-wheels traveling cranes was chosen. The cranes with medium operating mode and the separate drive base were considered. Crane span is $L_{cr} = 23{,}0\,m$ and a crane base is $B = 4{,}4\,m$. The mathematical expectations of maximum and minimum loads on crane wheels $\overline{F}_{\max} = 124{,}63$ kN, $\overline{F}_{\min} = 67{,}87$ kN were calculated by substituting in (1) the numerical characteristics of all parameters. The mathematical expectations of lateral forces on the wheels of the crane were calculated using formulas (8) and (10): $\overline{H}_k^n = 15{,}43$ kN; $\overline{H}_c^n = 12{,}46$ kN.

The mathematical expectations of horizontal load on a column from lateral forces: $\overline{H} = \overline{H}_k^n \cdot y_1 + \overline{H}_c^n \cdot y_2 = 23{,}32$ kN. We expressed the expectation and the standard for lateral forces using $0{,}1F_C^{WW}$, then:

$$\overline{X} = \frac{\overline{H}}{0{,}1F_C^{WW}} = 1{,}843\,,\ \hat{X} = \frac{\hat{H}}{0{,}1F_C^{WW}} = \frac{2{,}94}{0{,}1 \cdot 126{,}583} = 0{,}232\,,$$

where F_C^{WW} – load on the column of the crane without weight.

The obtained numerical characteristics of horizontal crane load correspond to the experimental values. For further calculations of the reliability of columns of industrial buildings the numerical characteristics of vertical and horizontal crane loads were worked out.

DESIGN MODELS OF FRAMEWORKS

The calculation of spatial models of frameworks (Fig. 2) for all loads, including crane loads were done using strength analysis of structures by the finite element method. Spatial design schemes of frames were formed out of spatial blocks of buildings, which included all transverse frames or intermediate blocks with the number of transverse frames from 7 to 10. As the distributive disks, the main elements which provide the spatial scheme of the frames were introduced in design models. Such elements are the bracing systems in the top and bottom chords of roof truss, crane girders with brake structure, longitudinal working platforms and bracing elements on the columns.

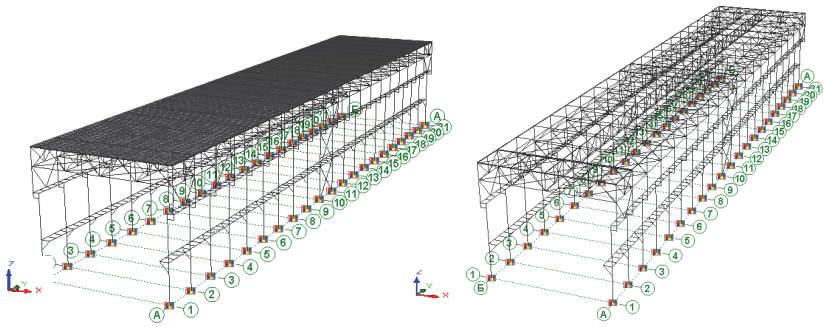

Figure 2. Spatial design models of industrial building: a) with a «heavy» coverage (prefabricated concrete panels); b) «light» coverage (profiled steel on purlins).

A comparison of internal efforts (bending moments and longitudinal forces) of frames at different design models has been made. Various cases of calculation were considered when the model contains elements which simulate the work of all possible bracing disks and individual bracings, and combinations of bracings.

It was noted that structures, which mainly provide spatial scheme and which should be taken into account in the formation of design models, are the covering of the building, the bracings on bottom chords of roof truss, crane girders with a braking structures and longitudinal working platforms. Consideration of other longitudinal structures of frames did not give a significant effect.

THE NUMERICAL RELIABILITY EVALUATION OF COLUMNS OF INDUSTRIAL BUILDINGS

The analytical model of crane loads was used in the calculation of reliability of columns in an example of multi-span industrial building. The spans of building are 24 *m*, the top elevation mark of the column is +14,000.

The columns of the building were designed for the resistance in the plane and out of the plane of action of compatible effect of dead and variable loads calculated according to Code DBN V.1.2-2: 2006 (Pichugin 2014a). The structures were loaded with random vertical loads: dead and snow loads applied with eccentricity, the vertical crane loads and horizontal loads, distributed wind loads. The results of probabilistic reliability calculation are shown in Fig. 3, 4 as the probability of no-failure of structures for 50 years, expressed in bels $P_L = -\lg[1 - P(t)]$.

The main aim of the reliability estimation was to identify the various parameters which affect the no-failure probability of structures. In particular,

two types of coverings for buildings were taken into account: «heavy» – prefabricated concrete panels and «light» – profiled steel.

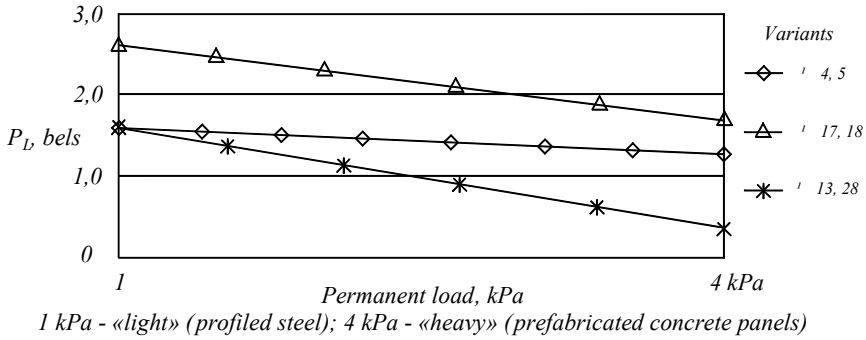

Figure 3. The dependence of the probability of no-failure of columns on the type of covering.

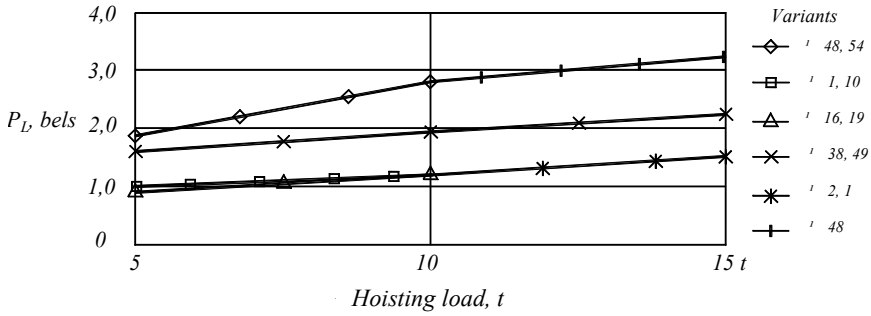

Figure 4. Dependence of the probability of columns no-failure on the duty of overhead cranes.

For each type of covering, various duty of overhead cranes (Fig. 4) and types of connection of column and girder (Fig. 5) were considered. In addition, the varied climatic loads were calculated (by considering the building, located in the II, III, V, and VI snow area of Ukraine and II, III and V wind area). For the extreme wind load effect on the outer columns, the parameters of middle and outer columns were analysed separately (for such columns different loading surface were considered). In total 56 variants of columns were worked out.

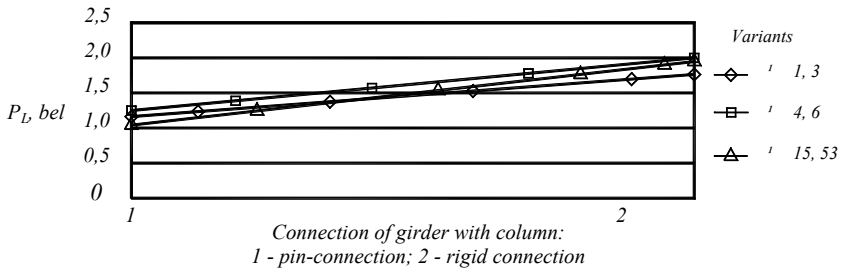

Figure 5. Dependence of the probability of no-failure of columns on the type of connection the girder and column.

CONCLUSIONS

The analytical probabilistic model of crane loads was established in the paper. This model allows obtaining of actual reliability parameters of buildings with overhead cranes.

Travelling cranes with the capacity from 5 up to 50 tons with different types of drive modes and duty of work were chosen for the calculations. The location of travelling cranes was considered in buildings with different columns spacing, different types of coverage and bracing structures that provide space work of frames.

Consideration of the spatial nature of frameworks in calculations has permitted detection of the reserve strength of frameworks of industrial buildings and identify the influence of bracing elements on the reliability assessments.

The calculation of spatial models of industrial buildings were done for combinations of all influencing loads, including crane loads. Spatial design models of frames were formed as spatial blocks of buildings, which included all transverse frames or internal blocks with 7-10 frames.

It was determined, that the structures, which mainly provide space behaviour and which should be considered while forming design models are the covering of buildings, bracing elements on the bottom of the roof truss, crane girders with braking force transferring girders and longitudinal working platforms.

To identify the quantitative impact of bracing systems on the reliability of frameworks the bracing blocks were removed alternately until the transverse frame of the building was obtained. The parameters of the plane frame were compared with the parameters of the frames in the space blocks. Probabilistic calculations of the columns as parts of frameworks models with bracing systems (crane girders with braking force-transferring girders, the bracings on bottom chords of roof truss) showed high reliability of structures of typical industrial buildings, for which the probability of failure within 50 years is $Q(t) = (1 \div 2) \cdot 10^{-7}$. The attaching of other elements, such as bracing elements

on the top chords of roof truss, purlins of coverage, horizontal beams of wall trelliswork in design models showed a minor influence on the reliability of frameworks. The probability of failure reduces steeply if the bracing elements of the roof truss and braking force-transferring girders were not taken into account in spatial models of the frameworks.

REFERENCES

ДБН В.1.2-2:2006. Навантаження і впливи: [Чинний від 2007-01-01] / Мінбуд України. К.: Вид-во «Сталь».

DBN V.1.2-2:2006. Navantazhennya i vplyvy: [Chynnyy vid 2007-01-01] / Minbud Ukrayiny. K.: Vyd-vo “Stal”".

EN 1991-1-3 (2003). Eurocode 1: Actions on structures. Part 3: Actions induced by cranes and machinery. Brussels: CEN.

FEM 9.511 (1986). Rules for the design of series lifting equipment; Classification of mechanisms. Fédération Européenne de la Manutention.

ISO 2394:2015. General principles on reliability for structures. Genève: International organization for standardization.

ISO 13822:2010. Bases for design of structures - Assessment of existing structures. Genève: International organization for standardization.

ISO 13824:2009. Bases for design of structures – General principles on risk assessment of systems involving structures. Genève: International organization for standardization.

Patenko, Iu. (2016). Determination of Accidental Crane Loads Parameters, International Scientific-Practical Conference of Young Scientists, Build Master Class. Kyiv: KNUCA.

Патенко, Ю.Е. (2012). Надійність сталевих каркасів одноповерхових виробничих будівель: автореф. дис. на здобуття наук. ступеня канд. техн. наук: спец. 05.23.01 «Будівельні конструкції, будівлі та споруди». Полтава: ПолтНТУ.

Patenko, Iu. E. (2012). Nadiynist´ stalevykh karkasiv odnopoverkhovykh vyrobnychykh budivel´: avtoref. dys. na zdobuttya nauk. stupenya kand. tekhn. nauk: spets. 05.23.01 ”Budivel´ni konstruktsiyi, budivli ta sporudy”. Poltava: PoltNTU.

Pichugin, S. F. (2014a). Reliability Analysis of Steel Structures, Proceedings of METNET Seminar 2014 in Moscow. Hämeenlinna: Hamk University of Applied Sciences. 115–122.

Pichugin, S. (1997). Probabilistic Description of Crane Load on Building Structures, XLIII Konferencja Naukowa KILiW PAN i KN PZITB. Tom III. Poznan-Krynica. 171–178.

Pichugin, S. (1998). Analysis of Bridge Crane Loads on Industrial Buildings, XLIV Konferencja Naukowa KILiW PAN i KN PZITB. Tom 7. Poznan-Krynica. 171–178.

Pichugin, S. F. (2005). Reliability of Building Structures. S.F. Pichugin & N.A. Demchenko. Poltava : PNTU.

Пічугін, С. Ф. (2010). Вплив кранових навантажень на каркаси виробничих будівель. С.Ф. Пічугін & Ю. Е. Патенко. Будівельні конструкції спортивних та просторових споруд: сьогодення та перспективи розвитку: зб. наук. пр. Київ: УКРНДІПСК. Вип. 5. 106–116.

Pichugin, S. F. (2010). Vplyv kranovykh navantazhen´ na karkasy vyrobnychykh budivel´. In S. F. Pichugin & Iu. E. Patenko. Budivel´ni konstruktsiyi sportyvnykh ta prostorovykh sporud: s´ohodennya ta perspektyvy rozvytku: zb. nauk. pr. Kyyiv: UKRNDIPSK. Vyp. 5. 106–116.

Пичугин, С. Ф. (2011a). Надежность стальных конструкций производственных зданий. [2-е изд.]. М.: Изд-во «АСВ».

Pichugin, S. F. (2011a). Nadezhnost' stal'nykh konstruktsiy proizvodstvennykh zdaniy. [2-ye izd.]. M.: Izd-vo "ASV".

Пічугін, С. Ф. (2011b). Оцінка надійності сталевих колон постійного перерізу виробничих будівель. С. Ф. Пічугін & Ю. Е. Патенко. Современные строительные конструкции из металла и древисины: сб. науч. тр. Одесса: ОГАСА. № 15, часть 2. 191–197.

Pichugin, S. F. (2011b). Otsinka nadiynosti stalevykh kolon postiynoho pererizu vyrobnychykh budivel´ In S. F. Pichugin & Iu. E. Patenko. Sovremennye stroytel´nye konstruktsyy yz metalla y drevysyny: sb. nauch. tr. Odessa: OHASA. № 15, chast´ 2. 191–197.

Пичугин, С. Ф. (2014b). Крановые нагрузки на строительные конструкции. Полтава: ООО «АСМИ».

Pichugin, S. F. (2014b). Kranovyye nagruzki na stroitel'nyye konstruktsii. Poltava: OOO "ASMI".

Пічугін, С. Ф. (2015). Визначення внеску в'язевих елементів у надійність каркасів виробничих будівель. С. Ф. Пічугін & Ю. Е. Патенко. Галузеве машинобудування, будівництво: зб. наук. пр. Полтава: ПолтНТУ. Вип. 1(43). 29–34.

Pichugin, S. F. (2015). Vyznachennya vnesku v´yazevykh elementiv u nadiynist´ karkasiv vyrobnychykh budivel´. S. F. Pichugin & Yu. E. Patenko. Haluzeve mashynobuduvannya, budivnytstvo: zb. nauk. pr. Poltava: PoltNTU. Vyp. 1(43). 29–34.

Пичугин, С. Ф. (2016a). Розрахунок надійності будівельних конструкцій Reliability Calculation of Building Structures [Текст]. Полтава: ТОВ «Асмі».

Pichugin, S. F. Rozrakhunok nadiynosti budivel´nykh konstruktsiy Reliability Calculation of Building Structures [Tekst]. Poltava: TOV “Asmi”.

Пічугін, С.Ф. (2016b). Ймовірнісна модель кранових навантажень на каркаси виробничих будівель. С.Ф. Пічугін & Ю.Е. Патенко. Стальзалізобетонні конструкції: дослідження, проектування, будівництво, експлуатація: Зб. наук. статей. Вип. 12. Полтава: ПолтНТУ. 189–195.

Pichugin, S.F. (2016b). Ymovirnisna model´ kranovykh navantazhen´ na karkasy vyrobnychykh budivel´ In S.F. Pichugin & YU.E. Patenko. Ctal´zalizobetonni konstruktsiyi: doslidzhennya, proektuvannya, budivnytstvo, ekspluatatsiya: Zb. nauk. statey. Vyp. 12. Poltava: PoltNTU. 189–195.

СНиП 2.01.07-85 (1987). Нагрузки и воздействия / Госстрой СССР. М.: ЦИТП Госстрой СССР.

SNiP 2.01.07-85 (1987). Nagruzki i vozdeystviya / Gosstroy SSSR. M.: TSITP Gosstroy SSSR.

BENDING TESTS OF VERY THICK PLATES WITH ADVANCED RESEARCH EQUIPMENT AND TECHNIQUES

Raimo Ruoppa, Raimo Vierelä, Marko Ylitolva, Rauno Toppila
Lapland University of Applied Sciences

Vili Kesti
SSAB Europe

ABSTRACT

The "ultimate bending machine" was built on the basis of a hydroforming machine and is located at the Tornio campus of Lapland University of Applied Sciences. Applying the machine for bending tests was engineered and implemented in cooperation with SSAB and special tools were designed and constructed for the tests. The maximum force of the press is 30 000 kN, which makes it possible to bend even 80-mm-thick plates.

With the press, bendability tests were carried out for 40-80-mm-thick steels. The test setup included an infrared camera, which was used to record the increase in the temperature of the plate. The influence of the forming speed on the temperature changes was studied as well. In some of the tests, the spring-back was also measured using video camera recording. The quality of the bends was evaluated by visual inspection and the minimum bending radius of each material was determined.

A demonstration with the online optical strain analysis tool GOM ARAMIS was also carried out. A steel plate was bent and the strains were measured through a mirror below the bending sample. A rectangular hollow section beam was also bent in the press and the strains were measured directly with the same optical strain analysis system. The results of the tests were encouraging and there are plans to apply the method in further studies.

INTRODUCTION

The usability of ultra-high-strength and wear-resistant steels has been studied for several years at Lapland University of Applied Sciences. Bendability tests have been carried out by using a commercial press brake and research techniques have been developed in cooperation with SSAB and the University of Oulu. In the bendability tests, the minimum bending radius (R_{min}) of the material, i.e. the smallest radius which is possible to be used without failure, is usually defined. The result of each test is evaluated by means of visual inspection. The spring-back, which usually takes place in three-point bending, is measured with a video camera.

As the strength and thickness of the steels being tested are increasing all the time, the demand for more powerful forming machines has arisen. At the beginning of the millennium, a hydroforming press was delivered to the VTT Technical Research Centre of Finland from Russia. Later on, the ownership of the machine was transferred to the Vocational College Lappia, which is a partner cooperating with Lapland University of Applied Sciences. The maximum force of the main cylinder is 30,000 kN, and the maximum pressure in hydroforming is 5000 bars. With the press, the aim was originally to research the hydroforming of tubes and sheets. However, it has mainly been used for traditional forming such as deep drawing and stretch forming. At the METNET seminar in Aarhus, the idea of using the press for bending tests was proposed (Toppila et al. 2011). In cooperation with SSAB, the design and construction of the necessary special tools were started.

Previously, bent samples were studied with the GOM ARGUS 3D optical strain analysis system in order to get more detailed information about the metallurgical phenomena involved in bending (Arola et al. 2015, Ruoppa et al. 2014). In this technique, a grid is marked on the surface of the sample before bending. After bending, on the basis of the change in the grid, a computer system calculates the strain distribution on the surface. In addition to ARGUS, the GOM system also has another optical strain measurement system called ARAMIS, which is capable of measuring strains online during the bending process. The system is based on marking of the stochastic pattern on the surface and its changes during plastic deformation. By using this technique, more information is available from the process.

MODIFICATION OF THE HYDROFORMING PRESS FOR BENDING TESTS

The basis of the design for the lower tool was that the die gap should be adjustable. The ultimate force of the press is 30,000 kN, which was set as the basis for the strength calculations. Figure 1a shows a 3D model of the tool. The tool was designed to consist of two halves, which were constructed by welding from 40- and 60-mm UHS steel cuttings with a nominal yield strength of 960 N/mm^2. The halves are assembled on top of T-slot plates and move towards and away from each other when the bolts are not tightened. The die gap varies from 100 to 800 mm. The strength of the tools was analyzed with FEM modelling using the maximum force of the machine. The stresses are shown in Figure 1b. It can be seen that the tools take the maximum force, with the maximum stresses being well below the strength of the material.

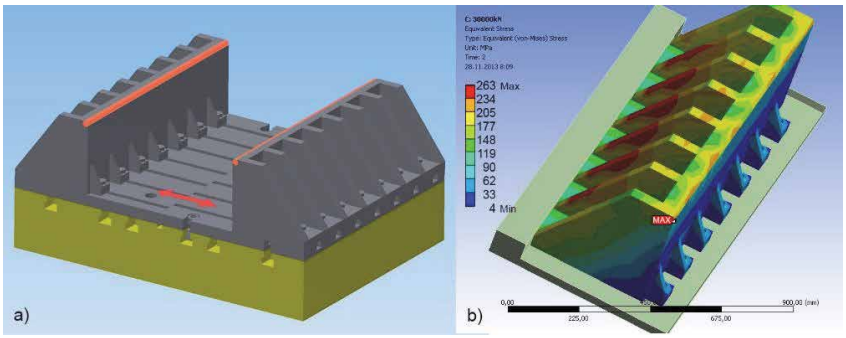

Figure 1. a) 3D model of the lower tool; b) stresses calculated by FEM in half of the lower tool with the maximum load of the press being used.

Figure 2a shows the hydroforming machine at the Tornio campus. The diameter of the main cylinder is about 1000 mm and the stroke of the piston is 500 mm. For the attachment of the punches, a beam was constructed from 60-mm-thick steel plate and it was fastened to the bed in the head of the piston. The press also has two side cylinders on both sides of the frame, which are used for moving the tools in order to adjust the gap of the lower tool. The cylinders also support the lower tool during the bending, thus resisting the horizontal forces which tend to separate the two halves away from each other'.

Figure 2. a) Hydroforming machine on the Tornio campus; b) bending of a thick steel plate.

In the press, the speed of the punch is adjustable and it is possible to record data such as the displacement and pressure of the cylinder. With this press and tool setup, it was now possible to bend even 80-mm-thick UHS steel plates.

FIRST BENDING TESTS OF THICK PLATES

The first bending tests for thick plates were carried out with the press above. The materials were SSAB's 50-mm Strenx 700, 45-mm Raex 400 and 450,

and 80-mm S355, the typical mechanical properties of which are shown in Table 1.

Table 1. Typical mechanical properties of the test materials.

Test material	$Rp_{0,2}$ N/mm^2	R_m N/mm^2	A_5 %
S355	355	500	23
Strenx 700	700	850	12
Raex 400	1000	1250	10
Raex 450	1250	1450	9

Samples were cut from the sheets so that the bending line was either longitudinal or transverse compared with the rolling direction (RD). With the 45- and 50-mm thicknesses, the bending length was 400 mm and with the 80-mm thickness, it was 600 mm. The die gap was set to be suitable for each case, taking into account the strength and thickness of the material and the punch radius used. The speed of the punch was in most cases 1.5 mm/s, which is, in practice, the maximum speed for bending tests carried out with the ultimate press. However, some tests were carried out with a lower speed, 0.2 mm/s, in order to study the influence of the speed on bendability.

Since the deformation of the material elevates the temperature, it may become significant for the forming properties, and this was also studied. For the measurement of the surface temperature, an infrared camera was assembled in front of the machine and placed sloping downwards towards the bending sample. Figure 3a shows the positioning of the camera and Figure 3b an example of the temperatures recorded during the bending test.

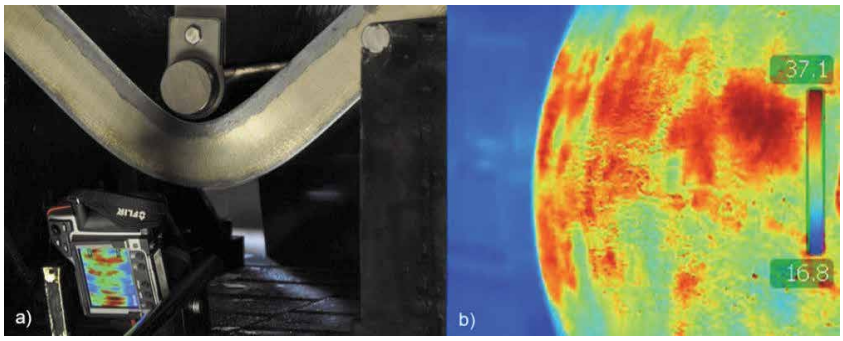

Figure 3. a) Bending of 80-mm S355, position of infrared camera;
b) example of temperature measurement in bending test of Raex 400.

The results of the bending tests are shown in Table 2. The minimum bending radius relative to thickness, R/t, was determined for each material and the average maximum temperatures recorded in the bending tests are also shown in the table.

Table 2. Results of the bending tests.

Material	Thickness mm	Punch speed Mm/s	Bending direction	Radius/ Thickness ratio	T_{max} ºC
S355	80	1.5	Longitudinal	0.4	55
		1,5	Transverse		55
		0.2	Longitudinal		35
		0.2	Transverse		35
Strenx 700	50	1.5	Longitudinal	1.5	38
		1,5	Transverse		38
		0.2	Longitudinal		27
		0.2	Transverse		27
Raex 400	45	1.5	Longitudinal	3.6	38
		1,5	Transverse	2.9	38
		0.2	Longitudinal	3.8	31
		0.2	Transverse	2.9	31
Raex 450	45	1.5	Longitudinal	4.2	38
		1,5	Transverse	3.6	38
		0.2	Longitudinal	4.2	31
		0.2	Transverse	4.0	31

During the tests, it was evident that different steel grades showed different behavior especially when too small a punch radius was used. Raex 400 and 450 showed a tendency for severe cracking when too small a radius was used, while Strenx 700 showed slightly smaller cracks, and an interesting phenomenon was also seen in the vicinity of the crack (the formation of ”valleys”). In general, the greater the strength of the steel, the greater the minimum bending radius and, especially with greater strength, usually greater in the longitudinal direction, as shown in Table 2 with Raex steels. It was found that the minimum bending radii R/t are in good agreement with the guaranteed values of thinner plates and the SSAB bending recommendations can also be used for the thicknesses under investigation.

One primary conclusion is that a faster bending speed leads to higher temperatures during bending. The biggest difference was seen in the thickest test samples (S355, 80mm). It is possible that thicker gauges are more prone to a temperature increase when the punch speed is increased. The peak temperatures in the vicinity of the cracks were 40-116°C. The speed may

have some influence on the minimum bending radius as Raex 450 in the longitudinal direction showed a tendency to crack with a greater punch radius when the speed was 0.2 mm/s.

The maximum bending force was measured in some tests by recording the pressure during the test. For the evaluation of the force, some equations have been published previously:

$$F = \left(0.5 + \frac{4 \times t}{W}\right) \times \frac{b \times R_m \times t^2}{W - (1.5 \times R_p)} \qquad (1) \qquad \text{(Ruoppa et al. 2014)}$$

$$F = \frac{b \times R_m \times t^2}{(W - R_d - R_p)} \qquad 2) \qquad \text{(SSAB 2015)}$$

where: R_m is the ultimate tensile strength (N/mm²)

b	is the bending length (mm)
t	is the sheet thickness (mm)
W I	s the die gap (mm)
Rd	is the die entry diameter (mm) and
Rp	is the punch radius (mm)

The forces calculated with Equations 1 and 2 were compared with the measured forces and the correlations between them are illustrated in Figures 4a and 4b. The data on which Equation 1 is based includes plate thicknesses from about 4 mm to 20 mm, leading to much lower forces. The graph shows that Equation 1 is also still quite reliable for greater thicknesses and forces. Equation 2 seems to be a little more accurate with lower forces but with greater forces, it deviates more from the measured values than Equation 1. However, both equations can be used for the evaluation of the force needed before bending.

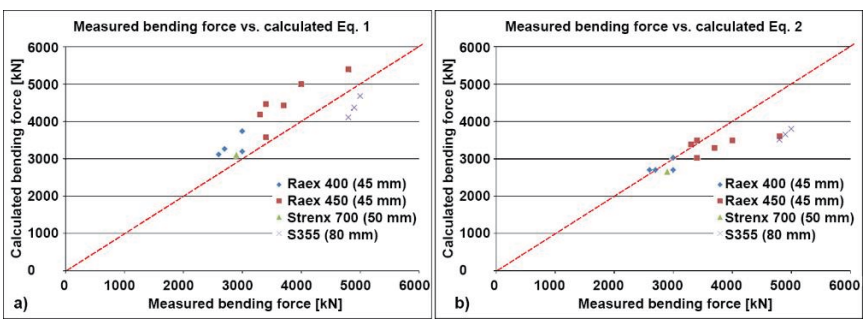

Figure 4. Measured vs. calculated force: a) Equation 1, b) Equation 2.

In three-point bending, spring-back typically takes place. After the punch is released, the angle of the plate opens as a result of the elastic deformation, which is, in addition to plastic deformation, always present during bending. It is important to know the amount of the spring-back in the bending process in order to reach correct dimensions in the final stage. The spring-back was measured by using a video camera. Two images are sampled from the video, one from the lower end of the punch and another after the release of the punch; see the photographs in Figure 5a. The spring-back angle is measured from the difference between the angles detected from the images.

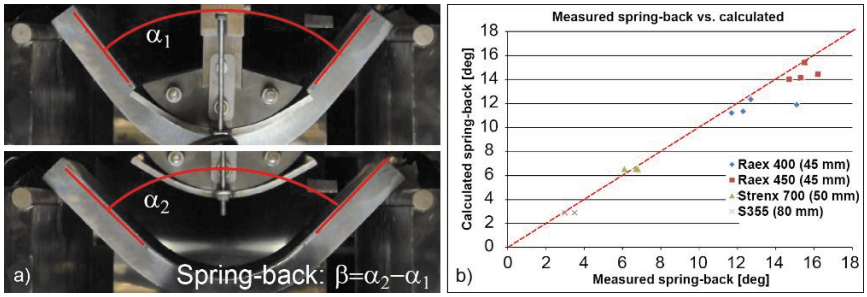

Figure 5. a) Principle of spring-back measurement, b) measured vs. calculated spring-back.

For the evaluation of the spring-back, the following equation is available:

$$\beta = C \times \left(\frac{R_e}{990.65}\right) \times \left(\frac{W}{t}\right) \qquad (3) \qquad \text{[Mäkikangas 2013]}$$

where: R_e is the yield strength (N/mm²)
t is the sheet thickness (mm)
W is the die gap (mm)
C is the constant (C=1.00 with W/t<25, C=1.10 with W/t≥25)

The spring-back was measured in some tests. In Figure 5b, the correlation between the measured and calculated spring-back is illustrated. This equation was based upon data where the thicknesses were relatively small, but from Figure 5b it can be concluded that the equation also works with greater thicknesses, as tested in this study.

DEMONSTRATION OF ARAMIS ONLINE OPTICAL STRAIN ANALYSIS

Lapland University of Applied Sciences has an optical strain analysis system, GOM ARGUS and ARAMIS, which is a non-contact optical 3D deformation measuring system, which analyzes, calculates and stores deformations. ARAMIS recognizes the surface structure of the measuring object in digital camera images and allocates coordinates to the image pixels. During the deformation of the measuring object, further images are recorded. Then ARAMIS compares the digital images and calculates the displacement and

the deformation of the object characteristics. ARAMIS is particularly suitable for three-dimensional deformation measurements under static and dynamic loads in order to analyze the deformations and strain of real components.

Before a test can be performed, ARAMIS must be calibrated to ensure the dimensional consistency of the measuring system. During the calibration, the sensor configuration is determined. This means that the distance of the cameras and the orientation of the cameras with regard to each other are determined. In addition, the image characteristics of the lenses are determined (e.g. focus, lens distortions). [ARAMIS manual 2008]

The GOM ARAMIS system was tested in the online measurement of strain during bending tests. Cameras were fixed directly to the bending machine in a vertical position, as shown in Figure 6.

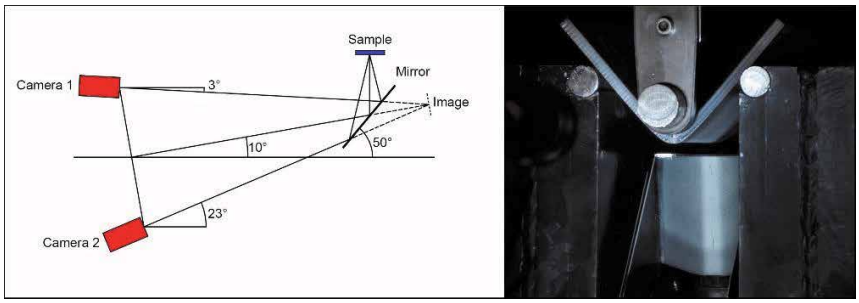

Figure 6. Positioning of cameras and mirror for ARAMIS testing in bending.

The centerline of the cameras was set to slope slightly downwards in order to avoid blinding of the upper camera during the bending test when the sample was moving downwards. The optimum angle was found to be 10 degrees, in which case the lower camera was sloping 23 degrees downwards and the upper camera 3 degrees upwards. The mirror was at a 50-degree angle relative to a horizontal line, in which case the image of the sample was perpendicular to the centerline; see Figure 6.

Some bending tests were carried out for the 10-mm Optim 960QC samples. The bending radius varied from 20 to 32 mm (R/t: 2.0t to 3.2t) and the sample was bent to about 90 degrees. The imaging was performed using a frame rate of 1/s. After computation, the results were shown in a video clip where the strain distribution is seen as different colors. Figure 7 illustrates some clips from the videos, where the angle varies. In Figure 7a, R/t was 3.2 (punch radius 32 mm) and in Figure 7b, R/t was 2.3 (punch radius 23 mm).

From the figures, it can be seen that with an increasing angle, the maximum strain increases as well. However, when R/t was 3.2, the maximum strain did not increase after a certain point, about 60 degrees in this case, but the strain spread over a larger area when the bending continued. When R/t was 2.3,

the maximum strain increased with an increasing angle all the time and the strain was concentrated more in the middle of the bend.

In the bending test with R/t of 3.2, no cracks were detected after bending through 90 degrees. With R/t of 2.3, when the bending angle increased, the measurement became unstable because of the high strain. Cracking of the surface was also detected after bending, which was also seen in the cameras of the ARAMIS system. This appears in the strain distribution chart as “blind spots” or holes, which means that the strain could not be measured in these areas; see the last image in Figure 7b.

ARAMIS was also tested in direct measurement of a beam, which was bent. Figure 8 shows the beam and cameras, which were positioned horizontal in this case.

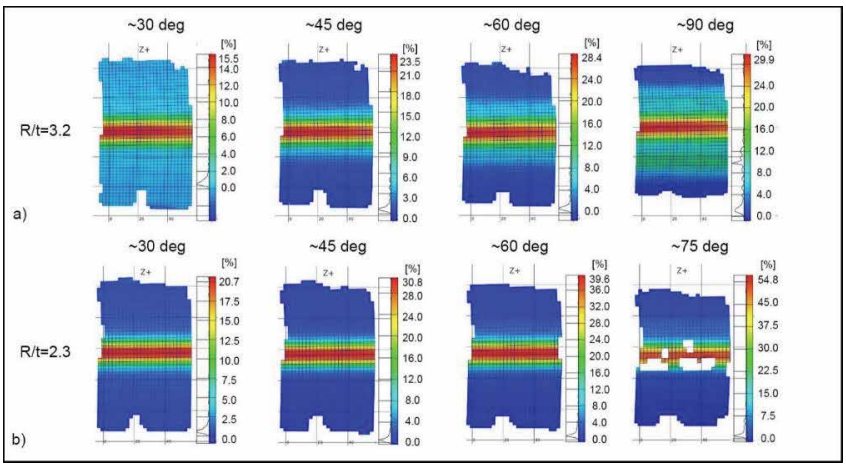

Figure 7. Strain distribution of the bend after bending with various angles and tools; a) R/t=3.2, b) R/t= 2.3. Material 10 mm Optim 960 QC.

Figure 8. Optical strain analysis in bending of a beam.

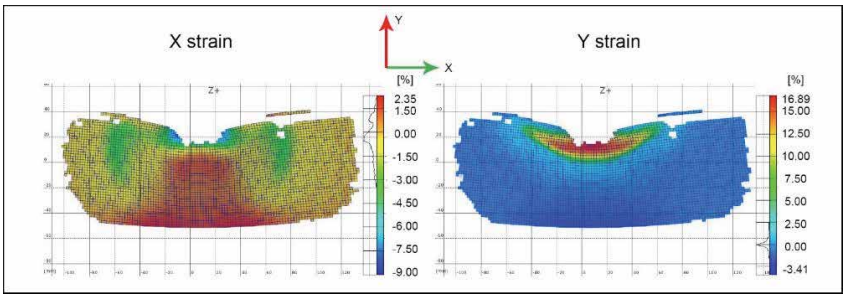

Figure 9. Strains in the X- and Y-directions on the surface of the beam.

In this case, the surface of the beam has a two-dimensional strain condition, contrary to bending, where the strain condition was one-dimensional "plane strain". Strain distributions on the surface of the beam in the X- and Y-directions are illustrated in Figure 9. At the bottom, the beam is straining in the X-direction and in the vicinity of the punch; the surface is straining in the Y-direction because of the buckling.

CONCLUSIONS

Three-point bending is the most common workshop process used to form steel plates. The need to bend thicker plates is increasing and it is vital to provide workshops with proper bending instructions for different steel grades. The new bending equipment at Lapland University of Applied Sciences was utilized to determine the bendability of thick plates. The test materials were 45mm Raex 400 and Raex 450, 50mm Strenx 700 and 80mm S355 steel grades. The quality of the bends was evaluated by visual inspection and the minimum bending radius, bending force and spring-back were determined. In addition, online temperature and strain measurements were carried out.

The results indicate that the minimum bending radii for thick plates are in good agreement with the guaranteed values for thinner gauges. It was also found that the bending force and spring-back equations can also be applied for bending of thick plates. An increase in the bending speed led to higher temperatures at the plate surface, which would be good to take into account when planning thick plate bending. The initial tests for online optical strain measurements were successful and the data gained from the tests can be used for, for example, validating bending simulations in the future.

ACKNOWLEDGEMENTS

The authors would like to acknowledge the financial support of MeriPohjola-hanke and TEKES – the Finnish Funding Agency for Technology and Innovation – for their support for the METNET Network.

REFERENCES

ARAMIS user manual-software v6.1, 27 October 2008. Retrieved 17 Jan 2018 from http://materials-science.phys.rug.nl/index.php/home/downloads/category/1-manuals?download=27%3Aaramis-v61

Arola, A-M., Kesti, V., & Ruoppa, R. (2015). The Effect of Punch Radius on the Deformation of Ultra-High Strength Steel in Bending. Proceedings of the 16th International Conference on Sheet Metal, 139-146, Erlangen, Germany, 16-18 March 2015.

Mäkikangas, J. (2013). Ultralujien levymateriaalien muovauksen erikoisosaaminen (ROLLE)- projektin loppuraportti (in Finnish). Oulu: University of Oulu.

Ruoppa, R., Toppila, R., Kesti, V., & Arola, A-M. (2014). Bendability tests for ultra-high-strength steels with optical strain analysis and prediction of bending force. Proceedings of the METNET Seminar 2014, Moscow, Russia, 21-22 October 2014.

SSAB (2015). Strenx, Hardox and Docol - Bending of High Strength Steels, Oxelösund, Sweden. Retrieved 15 August 2017 from https://ssabwebsitecdn.azureedge.net/-/media/files/en/general-multibrand/912-en-bending-of-high-strength-steel.pdf.

Toppila, R., Dolejs, J., Kauppi, T., Brtnik, T., Joutsenvaara, J., Vaara, P., & Ruoppa, R. (2011). Investigation of behavior of HSS using advanced techniques. METNET Seminar 2011 Aarhus, Denmark, 12-13 October 2011.

NUMERICAL STUDIES OF BEHAVIOR OF A CURVED STEEL AND CONCRETE COMPOSITE CABLE SPACE FRAME

L.I. Storozhenko, G.M. Gasii
Department of Structures from a Metal, Wood and Plastics
Faculty of Civil Engineering
Poltava National Technical Yuri Kondratyuk University, Poltava, Ukraine

ABSTRACT

The paper describes a study of the behavior of steel and concrete composite cable space frames under load. Composite cable space frames are a new kind of roof system for both long-span and short-span buildings, developed at Poltava National Technical Yuri Kondratyuk University.

The particular feature of the steel and concrete composite cable space frames lies in the fact that the bottom chord is made of flexible elements, while the top chord is made of rectangular reinforced concrete slabs. The flexible elements are made from short segments of steel cables that have special details at the ends through of which the segments are connected to each other. Due to the usage of steel cables, the total weight of the structure decreases, saving materials, and as a result, the total cost of construction decreases too.

INTRODUCTION AND PROBLEM STATEMENT

The development of the construction industry is accompanied by the introduction of new effective composite steel and concrete structures. These structures have the necessary strength characteristics and their use results in technical-economic benefits (Chilton 2007, Gasii et al. 2017).

Grid systems are the best known among long span and spatial structures. These systems have a great flexibility for shape finding. There is worldwide evidence of original shapes that have been achieved (Chilton 2007). In modern construction field, in most cases, there is a need to find more effective structural systems, including roof system. The main requirements for the structural elements of buildings are reliability, load capacity, architectural expression, aesthetics, ergonomics and good indicators of energy efficiency.

The effectiveness of steel and concrete composite cable space frames depends on the two materials used and also from the behavior under loads.

RECENT SOURCES OF RESEARCH AND PUBLICATIONS

A literature search shows that most of the large-span structures are made entirely of steel members, including space frames (Chilton 2007). However, there are examples of mixed steel systems (Ivanyk et al. 2014). In addition, steel-concrete composite structures are used widely for different buildings (Gasii 2014, Storozhenko & Gasii 2015). Likewise, steel and concrete composite cable space frames are used in many sectors of industrial and civil construction (Storozhenko et al. 2014).

Recently, steel and concrete composite cable space frames have been experimentally investigated (Gasii 2014, 2015, 2016a, 2016b, 2016c; Storozhenko & Gasii 2014, 2016). The behavior of steel and concrete composite cable space frames under load has been studied on both small-scale models (Storozhenko et al. 2012) and full-scale structures (Storozhenko et al. 2008, Storozhenko & Gasii 2017).

A review of previous studies shows that steel and concrete composite cable space frames have not fully investigated and there are few studies of the behavior of the steel and concrete composite cable space frames under load. The aim of the present study is to investigate the behavior of the steel and concrete composite cable space frames under uniformly distributed load using numerical methods.

THE MAIN MATERIAL AND RESULTS

Numerical study includes modeling of the steel and concrete composite cable space frames that have similar physical and mechanical properties of materials of structures that were tested earlier experimentally (Figure 1) (Storozhenko & Gasii 2017).

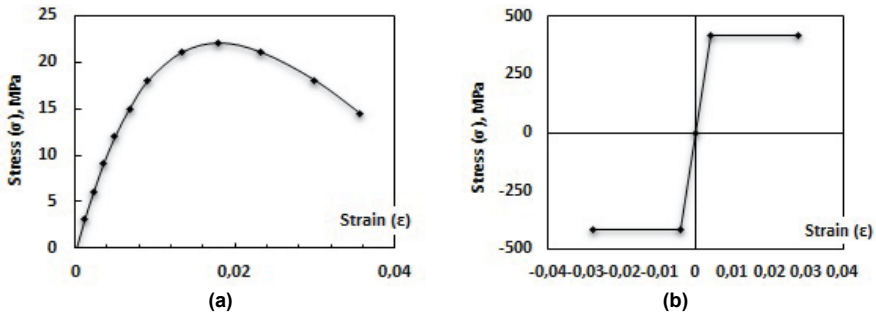

Figure 1. The stress-strain curve: a) concrete; b) steel.

Geometric scheme of the steel and concrete composite cable space frame was created as a spatial system of plates and rods (Figure 2). The load q was applied to the top chord. The scheme has pinned and roller supports (Figure 3).

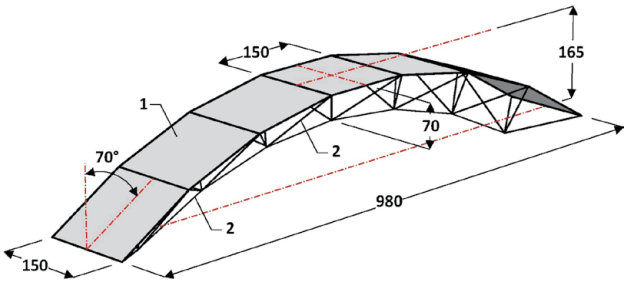

Figure 2. The geometric scheme of the curved steel and concrete composite cable space frame: 1 – plate; 2 – rod.

Meshing models of the curved steel and concrete composite cable space frame were made according to recommendations in (Perelmuter 2014): the ratio of the maximum to the minimum length of the element ; the ratio of the maximum to the minimum angle between the sides of the element $\frac{L_{max}}{L_{min}} = 1$; finite element form factor .

$\frac{\alpha_{max}}{\alpha_{min}} = 1$; finite element form factor $\frac{L_i^2}{S} = \frac{150^2}{150^2} = 1$.

To achieve accurate results and to ensure convergence of results, the model of the steel and concrete composite cable space frame was calculated a number of times with different meshing degrees. In all, four models were analyzed (Figure 4).

The results are presented in Table 1 and Table 2. Figure 5 shows the deflection of the steel and concrete composite cable space frame under uniformly distributed load. The deflections of both the top and the bottom chord are shown in Figure 6.

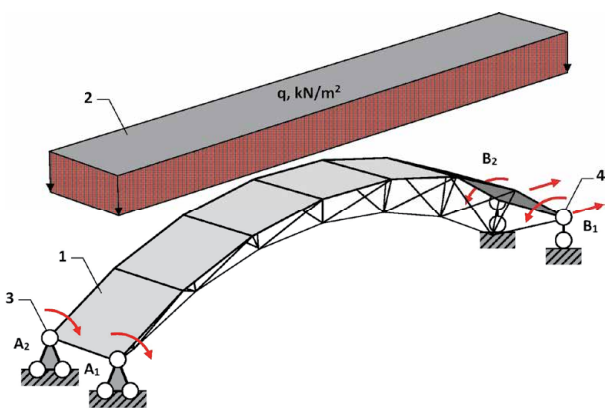

Figure 3. Loading diagram: 1 – model of the curved steel and concrete composite cable space frame; 2 – uniformly distributed load; 3 – pinned support; 4 – roller support.

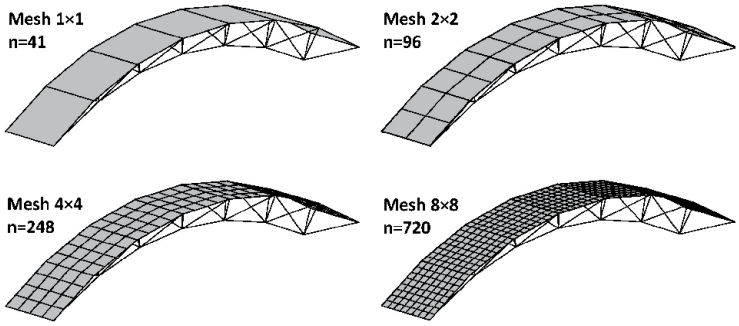

Figure 4. Meshing degrees of model of the steel and concrete composite cable space frame.

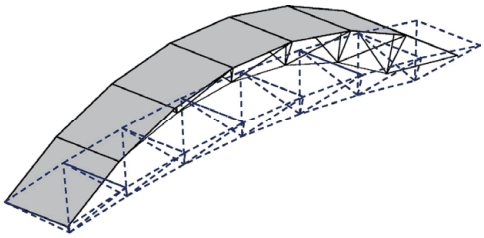

Figure 5. The deflection of the curved steel and concrete composite cable space frame under uniformly distributed load.

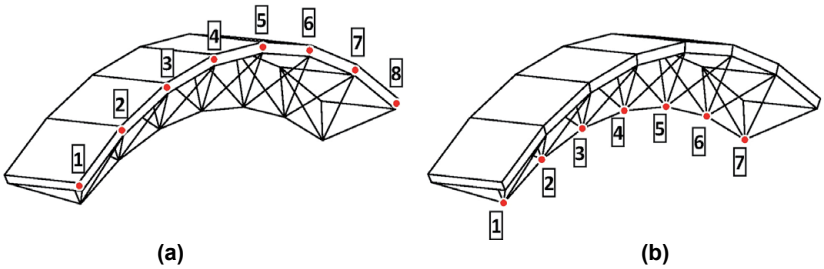

Figure 6. Numbering nodes of chords of the curved steel and concrete composite cable space frame: a) top chord; b) bottom chord.

Table 1. Node vertical displacements of the top chord of the analyzed frame.

Model	Node vertical displacements, mm					
	2	3	4	5	6	7
Model 1 (1×1)	1,96	3,65	4,62	4,62	3,65	1,96
Model 2 (2×2)	1,97	3,66	4,63	4,63	3,66	1,97
Model 3 (4×4)	1,98	3,67	4,64	4,64	3,67	1,98
Model 4 (8×8)	1,98	3,67	4,65	4,65	3,67	1,98

Note. Displacements of nodes 1 and 8 equal 0.

Table 2. Node vertical displacements of the bottom chord of the analyzed frame.

Model	Node vertical displacements, mm						
	1	2	3	4	5	6	7
Model 1 (1×1)	1,51	3,09	4,21	4,62	4,21	3,09	1,51
Model 2 (2×2)	1,52	3,10	4,23	4,63	4,23	3,10	1,52
Model 3 (4×4)	1,52	3,11	4,24	4,64	4,24	3,11	1,52
Model 4 (8×8)	1,52	3,11	4,24	4,65	4,24	3,11	1,52

Tables 1 and 2 show that the result of the solution are nearly the same. The maximum difference is about 1%. Therefore, we can use any model for finding the displacement of the steel and concrete composite cable space frame.

The results indicate the reliability of the data. The results of numerical studies were compared with experimental results and are shown in Figure 7 and Figure 8.

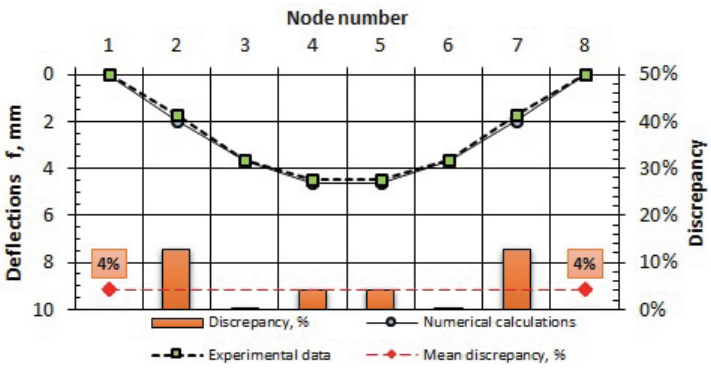

Figure 7. Comparison node vertical displacements of the top chord of the structures obtained by numerical and experimental studies.

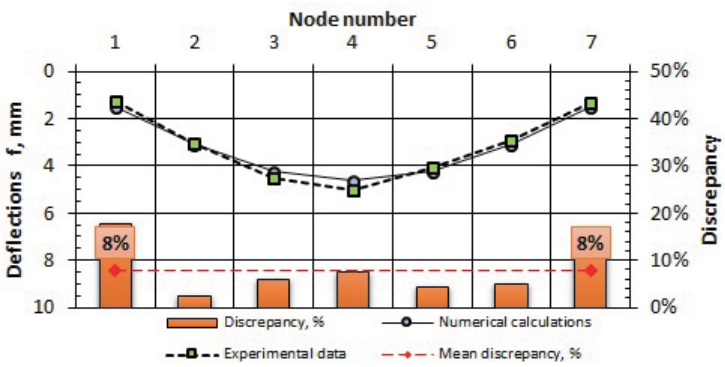

Figure 8. Comparison node vertical displacements of the bottom chord of the structures obtained by numerical and experimental studies.

The analysis of the results shows that under uniformly distributed load, the maximum horizontal displacement of the steel and concrete composite cable space frame is 5.34 mm, and the maximum vertical displacement is 4.63 mm.

DISCUSSION AND CONCLUSIONS

As a result of the numerical study, the displacements in the nodes of the steel and concrete composite cable space frame under uniformly distributed load were obtained, which did not exceed the ratio 1/190. Comparison of numerical data with experimental data shows the differences 4% and 8% for the top and bottom chords, respectively.

REFERENCES

Chilton, J. (2007). *Space grid structures*. Boston: Architectural Press.

Гасій, Г. М. (2013). Зведення структурних сталезалізобетонних покриттів. Актуальні задачі сучасних технологій. Тернопіль: ТНТУ. 73–74.

Gasii, G. M. (2014). Technological and design features of flat-rod elements with usage of composite reinforced concrete. *Metallurgical and Mining Industry* 2014(4), 23–25.

Gasii, G. M. (2016a). Comparative characteristics of the spatial grid-cable steel-concrete composite slab. Вісник Національного університету «Львівська політехніка». Теорія і практика будівництва, 2016(844), 260–265.

Gasii, G. M. (2016b). The flat double-layer grid-cable steel-concrete composite structure. Proceedings of the METNET Annual Seminar in Castellon, Spain, on 11–12 October 2016, 56–62.

Gasii, G. M. (2016c). Types of Steel and Concrete Composite Cable Space Frames. Наука та прогрес транспорту. Вісник Дніпропетровського національного університету залізничного транспорту імені академіка В. Лазаряна, 2016(6), 158–165.

Gasii, G., Hasii, O., & Zabolotskyi, O. (2017). Estimate of technical and economic benefits of a new space composite structure. In MATEC Web of Conferences, 2017, Vol. 116, 02014.

Ivanyk, I., Vybranets, Y., & Ivanyk, Y. (2014). Research of composite combined prestressed construction. *Acta Scientiarum Polonorum* 2014(2), 81–88.

Перельмутер, А. В. (2014). Беседы о строительной механике. Издательство SCAD Soft, ACB.

Стороженко, Л. І., Ермоленко, Д. А., Гасій, Г. М., & Гладченко Ю. Л. (2012). Експериментальне дослідження моделей структурно-вантової сталезалізобетонної конструкції. Збірник наукових праць [Полтавського національного технічного університету ім. Ю. Кондратюка]. Сер.: Галузеве машинобудування, будівництво, 2012(3), 243–249.

Стороженко, Л. І. & Гасій Г. М. (2015). Нові композитні матеріали кріплення гірничої виробки. Науковий вісник Національного гірничого університету 2015(4), 28–34.

Стороженко, Л. І., Гасій Г. М., & Гапченко, С. А. (2014). Нові сталезалізобетонні структурно-вантові конструкції. ACADEMIC JOURNAL Series: Industrial Machine Building, Civil Engineering, 2014(1), 91–96.

Storozhenko, L. I. & Gasii G. M. (2014). Experimental research of strain-stress state of ferrocement slabs of composite reinforced concrete structure elements. *Metallurgical and Mining Industry* 2014(6), 40–42.

Storozhenko, L. I. & Gasii, G. M. (2016). Analysis of stress-strain state of the steel-concrete composite ribbed slab as a part of the spatial grid-cable suspended structure. Academic journal. Industrial Machine Building, Civil Engineering, 2016(2), 81–86.

Стороженко, Л. І. & Гасій Г. М. (2017). Методика експериментального дослідження великогабаритного зразка просторової структурно-вантової сталезалізобетонної конструкції. Збірник наукових праць [Полтавського національного технічного університету ім. Ю. Кондратюка]. Серія: Галузеве машинобудування, будівництво, 2017(2), 270–276.

Стороженко, Л. І., Тимошенко, В. М., & Гасій, Г. М. (2008). Результати експериментальних досліджень сталезалізобетонного структурного покриття. Ресурсоекономні матеріали, конструкції, будівлі та споруди. 376–381.

LOAD-BEARING CAPACITY AS AN INTERACTIVE ANALYSIS TOOL IN SCAD OFFICE

Igor Gavrilenko, Sergij Girenko, Anatoly Perelmuter
Michail Perelmuter, Vitalina Yurchenko
SCAD Soft, Kyiv, Ukraine

ABSTRACT

Load-bearing capacity as a mathematical region for structural sections and joints in terms of design codes is considered in this paper. The main attention has been paid to an important property of the region, namely, its convexity. The paper presents a case when internal forces with no ultimate design values can be unfavorable for a non-convex load-bearing capacity region of a cross-section.

An algorithm for automatic generation of load-bearing capacity regions for structural sections, connections and joints has been presented and implemented in the SCAD Office software package. The program is able to show the position of points corresponding to the specified internal forces and to plot a convex shell on the basis of these points thus bounding the part of the load-bearing capacity region, which corresponds to any linear combination of design internal forces in the considered cross-section or structural joint. Construction of load-bearing capacity regions of a section or joint combined with a convex shell of specified internal forces is a flexible tool for the analysis of loading conditions.

Load-bearing capacity region for cross-sections is also a means for critical analysis of code-based requirements and regulations used for verifications of cross-sections. Unexpected properties of the design often occur here, which are caused by some simplifications and inconsistencies with the code requirements. Specifically, these effects often arise due to some kinds of strict logical transitions from one design situation to another (e.g., depending on the sign of a force). This leads to an abrupt change of requirements, which does not correspond to the physical nature of the phenomenon, which is usually associated with continuous changes. In Eurocode it often relates to the change of the section class (for example, the transition from Type 3 to Type 4), which occurs abruptly under a change of the load combinations.

Finally, load-bearing capacity regions has been also used in the process of software development as an instrument for critical analysis of traditional approaches to design and calculation of steel structural joints.

INTRODUCTION

Many modern software packages can generate interaction surfaces for various pairs (or triples) of internal forces in a bar element section. Examples include Strelets-Streletsky & Vodopyanov (2009), Abdelhamid Charif (2009), Charalampakis & Koumousis (2008), Fafitis (2001), Rodriguez-Gutierrez & Dario Aristizabal-Ochoa (1999) and Sulimowski & Klowan (1980). A maximum allowable in terms of strength combination of internal forces acts on this surface. Most often it is a triple of forces (M_y, M_z, N) acting in a cross-section of a reinforced concrete element. When it comes to the criteria that define the maximum allowable combination, some software packages are oriented toward a certain strength condition (for example, the classic von Mises condition), while other programs link the analysis to the strength requirements given in the codes.

However, in both cases, the demonstration of interaction surfaces is performed only to provide a geometric illustration of the phenomenon and does not imply any active user operations. SCAD Office, on the contrary, actively uses the generation of the load-bearing capacity regions, which differ in that they take into account the full set of code requirements (strength, general and local stability, crack resistance, etc.) to a certain structure for which the region is generated, and they also enable to use the interactive mode of their analysis. Moreover, the load-bearing capacity regions can be generated not only for the cross-sections of bar elements, but also for the joints of structural members.

LOAD-BEARING CAPACITY REGION OF SECTIONS

Design code requirements (strength conditions, general and local stability, limit slenderness, etc.) to a certain design section of a structure can be written in the form of a certain system of inequalities, each of which depends functionally on the values of internal forces $\vec{S} = \{S_1, S_2, ..., S_n\}$ that can arise in the considered section from the action of the design combinations of loadings:

$$\mathbf{\Phi}\left(\vec{S}\right) \le 1;$$

or

$$\begin{cases} f_1\left(S_1, S_2, ..., S_n\right) \le 1; \\ f_2\left(S_1, S_2, ..., S_n\right) \le 1; \\ \quad ... \\ f_j\left(S_1, S_2, ..., S_n\right) \le 1; \\ \quad ... \\ f_m\left(S_1, S_2, ..., S_n\right) \le 1; \end{cases}$$

where n is the total number of possible internal forces in the section; m is the number of inequalities that describe the design code requirements. The

value of the left-hand side of the inequality $\xi_j = f_j\left(S_1, S_2, ..., S_n\right)$ will be called *the utilization factor of restrictions*.

Each code requirement $f_j\left(\vec{S}\right) \le 1$ defines a certain region in the *n*-dimensional space of internal forces, and the intersection of all standard inequalities $\mathbf{\Phi}\left(\vec{S}\right) \le 1$ forms the load-bearing capacity region of the section $\mathbf{\Omega}_s$ in terms of the considered codes (see Figure 1). The maximum utilization factor of **restrictions** for each point of the load-bearing capacity region of the section **is** $\xi_{\max} = \max\left\{\xi_j \middle| j = \overline{1,m}\right\} \le 1$.

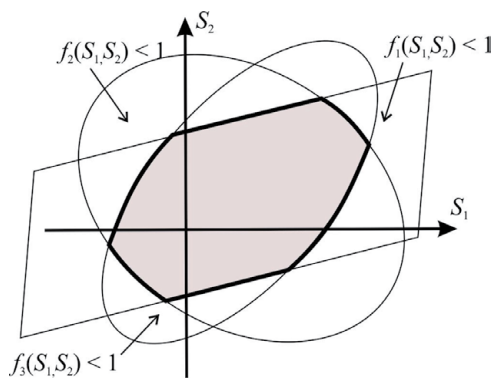

Figure 1. Formation of the load-bearing capacity region of a section in the two-dimensional space of internal forces.

Thus, *a load-bearing capacity region of a section* $\mathbf{\Omega}_s$ is a certain region in the *n*-dimensional space of internal forces, all points of which correspond to a combination of these internal forces, under the action of which the cross-section satisfies *all the requirements of the considered design codes*. Unlike the classic interaction curves, the boundary of the load-bearing capacity region of the sections is not only the strength requirements of the section, but the entire set of limitations governed by the requirements given in the design codes (including the conditions of general and local stability, limit slenderness, crack resistance requirements etc.).

PROPERTIES OF THE LOAD-BEARING CAPACITY REGION OF A SECTION

One of the most important properties of the load-bearing capacity region is its convexity. It should be noted that it is the convexity of this region that allows us to limit ourselves in the linear calculation for the checks of this section for the action of only those combinations of internal forces in the cross-section for which the extreme (minimum or maximum) values are characteristic. The positive result of such checks automatically means that all other conceivable combinations of loads will be acceptable. This statement follows from the very

definition of the concept of "convexity of a region". One of its definitions says that a region is convex if and only if for an arbitrary pair of points *A* and *B* belonging to it all points belonging to the segment *AB* belong to this region as well.

The absence of the convexity property of the load-bearing capacity region of the considered section can lead to many undesirable consequences related to the fact that, traditionally, evaluating unfavorable combinations of internal forces, engineers either do not consider some actions at all (in the case when they have an unloading effect) or take them fully into account. This rule is entirely valid for a convex load-bearing capacity region, while for a non-convex region a combination with intermediate (not extreme) values of internal forces can turn out to be an unfavorable one.

Let us illustrate this with an example. Let us consider a section for which a non-convex load-bearing capacity region is characteristic (Figure 2), under the action of two independent loadings $\tilde{\mathbf{N}}$ and $\grave{\mathbf{E}}$. The point *P* in Figure 2 corresponds to a pair of internal forces arising in the considered section under the action of the load $\tilde{\mathbf{N}}$, and the point *Q* – from the action of the load $\grave{\mathbf{E}}$. It is not difficult to see that the standard requirements are met when the section is checked for the action of each of the loads $\tilde{\mathbf{N}}$ and $\grave{\mathbf{E}}$ separately, and also when checking the section for the action of their total sum ($\tilde{\mathbf{N}} + \grave{\mathbf{E}}$), since the points *P, Q*, as well as the point *P* + *Q* belong to the load-bearing capacity region of the section. However, under the action of the "incomplete" linear combination of loadings ($\tilde{\mathbf{N}} + \lambda\grave{\mathbf{E}}$), when $\lambda < 1$, the requirements of the codes are violated, since a pair of internal forces appears in the considered section. This pair of forces is shown in Figure 2 as a point $P + \lambda Q$, which does not belong to the load-bearing capacity region.

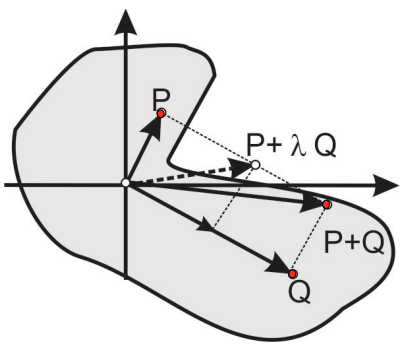

Figure 2. Checking the section for a combination of loads with "non-extreme" values.

There is a firm belief in the engineering environment that the load-bearing capacity region of a section is convex. This consideration is based on the following theories:

- according to Drucker's postulate, the boundary yield surface is convex in the space of internal forces for an ideal elastically plastic system (Kachanov 1969, 366);
- according to the Papkovich theorem, the stability region is convex in the space of loads on the system (Papkovich 1941, 85).

Although these theories are obviously established, they, unfortunately, do not correspond to the properties of the above-mentioned load-bearing capacity region of the section $\mathbf{\Omega}_S$, which is entirely defined by the design codes. Neither the classical theory of plasticity, for which Drucker's postulate is valid, nor the bifurcation (Euler's) theory of equilibrium stability, for which the Papkovich theorem is proved, is used in the design codes. Moreover, when generating the load-bearing capacity region $\mathbf{\Omega}_S$, in addition to the strength and stability conditions regulated by the design codes, it is also necessary to consider other code requirements (conditions of limit slenderness, crack resistance, etc.), which leads us far beyond the validity of the above-mentioned theories.

It should be noted that the absence of the convexity property of the load-bearing capacity region of a section is often observed in the geometrically nonlinear stability analysis. An example illustrating this is given below (Perelmuter & Slivker 2010, 73–76).

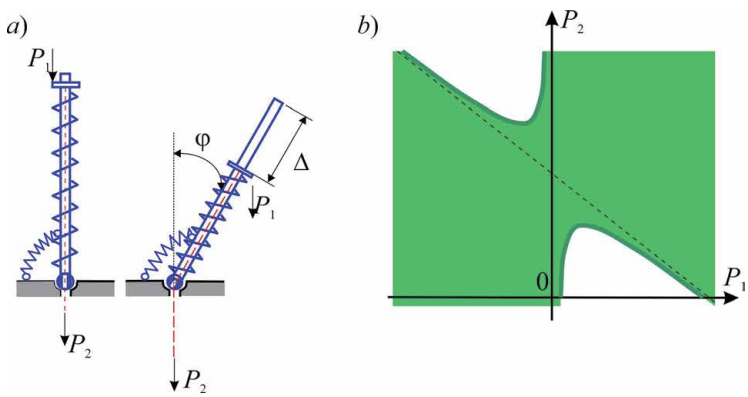

Figure 3. Example of a system with two degrees of freedom (Perelmuter & Slivker 2010, 73–76).

Figure 3*a* shows a rigid bar elastically clamped in its initial cross-section by a spring with the rotational stiffness γ. A friction-free spring of stiffness c slides along the bar. The following two forces are applied directly to this spring: a vertical one P_1 and a force P_2 directed toward the bearing hinge. The

mechanical realization of the force P_2 can be imagined as the tension of a rope that runs over a pulley at the bearing hinge.

The stability region shown in Figure 3*b*, is not convex (the reason for this is a nonlinear formulation of the problem), although the origin is within the stability region. However, it should be noted that this region does not appear to be star-like with respect to the null point. This means that there are paths of proportional loading (motion along a line starting in the null point), which first leave the stability region and then enter it again. The stability regions of ordinary designs are almost always star-like, and even if they are not, the use of the "secondary strength" has no practical value. Therefore, it is postulated in the SCAD Office analysis that the load-bearing capacity regions are star-like, and the "secondary" load-bearing capacity regions (even under the assumption of their existence) are not sought.

COMPUTER-AIDED GENERATION OF THE LOAD-BEARING CAPACITY REGION

ARBAT, KRISTALL and DECOR programs enable generation of the load-bearing capacity regions for sections of load-bearing bar elements of reinforced concrete, steel and timber structures, respectively.

Sections of bar elements, where six internal forces (longitudinal force, bending moments with respect to the two principal axes of inertia of the section, corresponding transverse forces, and torque) can appear under the load, have a load-bearing capacity region in the form of a six-dimensional geometric object, which is difficult not only to analyze, but even to represent. The best way to display the load-bearing capacity region of sections is by performing its orthogonal projection onto a certain plane (pair) of internal forces. The generation of a two-dimensional projection of the load-bearing capacity region of a section is performed according to the algorithm given below.

The user selects a pair of internal forces (for example, a pair "longitudinal force N – bending moment M_y"), in the coordinate system of which an orthogonal projection of the load-bearing region will be generated. The remaining internal forces in the section (M_z, Q_y, Q_z, M_x) are fixed at a certain level (they are specified by the user or take zero values). At a certain fixed value of the ratio $e = M_y/N$ (in fact, on the ray e), the point most distant from the origin is sought, where all the code-based requirements are still satisfied. For such a point, a certain inequality from the system $\mathbf{\Phi}\left(\vec{S}\right) \le 1$ takes a limit value $f_j\left(\vec{S}\right) = 1$, therefore it belongs to the boundary of the two-dimensional orthogonal projection of the load-bearing capacity region of the section.

The entire boundary of the load-bearing capacity region is created by scanning the rays e, which change their value no less than every degree. In this way, two-dimensional orthogonal projections of the load-bearing capacity region are generated for any pair of internal forces selected by the user ($M_y - M_z$, $M_y - Q_z$ etc.). This method of generating a load-bearing capacity region assumes that

the region is star-like, which is a hypothesis (see above), on the one hand, and a restriction of the software implementation, on the other hand.

The generated region is an interactive tool for communicating with the user. Using the cursor, one can examine a two-dimensional projection of the region. A certain set of internal forces corresponds to each position of the cursor. Their values are displayed in the respective fields. Depending on the change in the position of the cursor (changes in the respective pair of internal forces), the maximum value of the utilization factor of code-based restrictions-inequalities $\xi_{\max}$ corresponding to these forces is output, as well as the type of the inequality for which it is calculated (Figure 4). Clicking the right mouse button on the region enables the entire list of performed checks to be seen together with the values of utilization factors of restrictions $\xi_j \forall j = 1, m$ for the set of internal forces that corresponds to the cursor position on the generated load-bearing capacity region of the section.

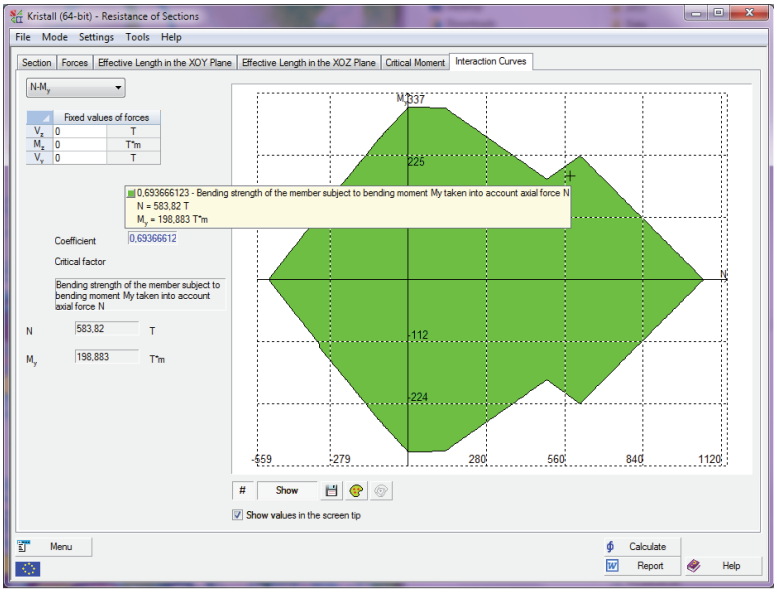

Figure 4. Interactive mode of exploring the load-bearing capacity region of the section.

LOAD-BEARING CAPACITY REGION OF SECTIONS AS A TOOL FOR THE ANALYSIS OF CODES

Several thousand calculations are performed during the computer-aided generation of the load-bearing capacity region of a section, which is apparently the largest check of the considered section. Moreover, the shape of the load-bearing capacity region of the section as well as the character of its boundaries in many cases enables performing a more detailed analysis of the requirements of the codes than can be done in other ways. The analysis of the boundaries

of the region enables the checking of the consistency and completeness of the standard requirements. In this case, it is easy to identify the inconsistency of certain provisions of the codes, particularly the non-smoothness of the transition between the approximations used.

For example, let us consider the design code for steel structures (SP 16.13330.2011). We will generate the load-bearing capacity region for a cross-section in the form of a symmetric welded I-beam with a 400×10 mm web and 200×10 mm flanges made of steel with the design strength R_y = 2050 kg/cm². The effective length of the bar in both principal planes of inertia is 600 cm, the service factor and the importance factor are taken as γ_c = 1,0 and γ_n = 1,0. The load-bearing capacity region Ω_{SNiP} of this section in accordance with the codes SP 16.13330.2011 is shown in Figure 5.

The boundary of the load-bearing capacity region Ω_{SNiP} on the *DEFGH* section is defined by the strength condition under the combined action of tension and bending, on the *CD* and *IH* sections – by the condition of stability of in-plane bending, and on the *IKABC* section – by the condition of stability out of the bending moment plane.

The non-convexity of the boundary of the load-bearing capacity region Ω_{SNiP} on the *IKABC* section is related to the change in the type of dependence of the coefficient *c* on the value of the relative eccentricity *m*. This coefficient is included in the condition for checking the out of plane buckling of a beam under bending and compression. It should be noted that the non-convexity of the *IKABC* section of the load-bearing capacity region Ω_{SNiP} does not appear when the element has small out-of-plane slenderness, for such design cases the condition of stability out of the bending moment plane is not a determining factor.

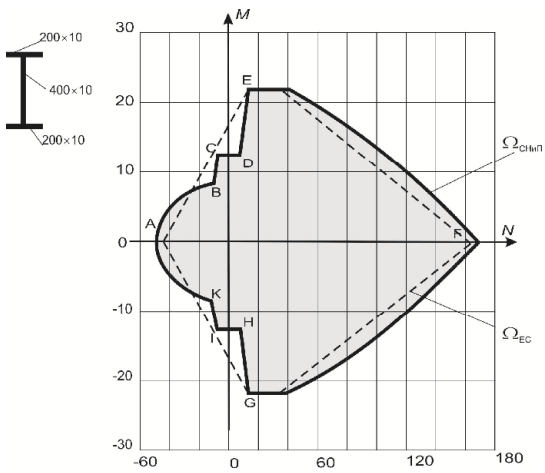

Figure 5. Load-bearing capacity region of a steel section: Ω_{SNiP} – according to SP 16.13330.2011; Ω_{EC} – according to EN 1993-1-1:2005 (2006).

The configuration of the *CDE* and *IHG* sections of the load-bearing capacity region Ω_{SNiP} is determined by the codes specifying that the stability of in-plane bending of a bar should be checked only at the values of the relative eccentricity $m_x > 20$, when the stability check of such a bar has to be performed as for a flexural member. Sections of the boundary *DC* and *JK* of the load-bearing capacity region Ω_{SNiP} correspond to these values (Figure 5).

The dashed line in Figure 5 shows the load-bearing capacity region Ω_{EC} of a cross-section calculated according to the requirements of EN 1993-1-1: 2005 (2006). The load-bearing capacity region of this section is convex, because the section operates within the limits of elastic deformation of steel.

Figure 6 shows the load-bearing capacity region of a steel I-beam with an 800 × 10 mm web and 360 × 20 mm and 240 × 20 mm flanges generated in accordance with the requirements of EN 1993-1-1: 2005. Here the non-convexity of the load-bearing capacity region of the section is related to the requirements of EN 1993-1-1: 2005, concerning the classification of sections. In the stress state corresponding to the appearance of compressive stresses in one of the flanges, the section ceases to be classified as a Class 2 section (plastic deformations of steel, calculation using the plastic moment of resistance) and passes into Class 3 of sections (elastic deformations of steel, calculation using the elastic moment of resistance). The jumps AB and CD correspond to these transitions. A similar jump-like change in the boundary of the load-bearing capacity region can occur at the transition of the section from Class 3 to Class 4.

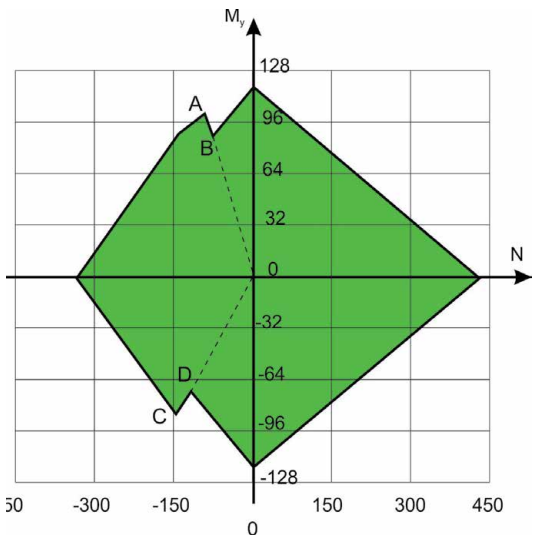

Figure 6. Load-bearing capacity region of a steel section according to EN 1993-1-1.

Another instructive example is given in Figure 7, which shows the load-bearing capacity region of a reinforced concrete section calculated according to the deformation model without taking into account the random eccentricity

(variant *a*) and with taking into account (variant *b*). The eccentricity is obviously taken into account in the variant given in the codes, since there is no physical model that would violate the smoothness of the boundary of the load-bearing capacity region. Indeed, the recommendations of the codes that for a statically indeterminate system the value of the eccentricity of the longitudinal force is taken equal to the value e obtained from the static analysis but not less than a certain fixed value of the random eccentricity e_0, does not in any way explain the fact that the random eccentricity (this factor is quite objective) disappears somewhere when $e > e_0$. In addition, for a statically determinate system, the value $(e + e_0)$ is introduced into the calculation.

The number of examples could be increased, but the ones given here indicate a very real situation when the load-bearing capacity region acquires a strange configuration. As the analysis shows, in many cases there are some inconsistencies in the formulation of requirements for the elements of load-bearing structures, due most likely to insufficient adjustment of the formulations themselves.

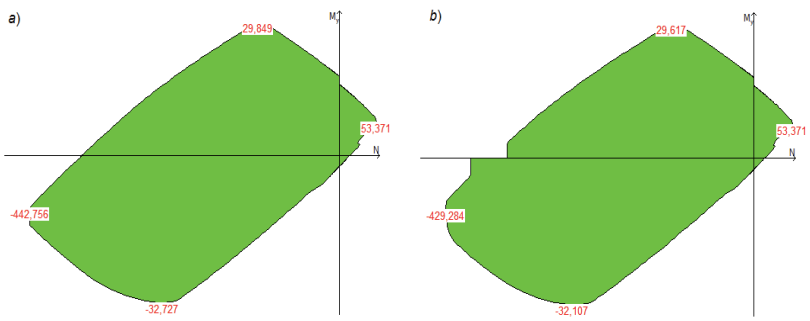

Figure 7. Effect of random eccentricity on the shape of the projection of the load-bearing capacity region of a reinforced concrete section.

The origin of such inconsistencies is related to the fact that the traditional approach based on the manual calculation generated all sorts of "simplifications", which allowed some checks to be skipped or to replace the general case with a certain particular case (as at $m < 20$ for steel elements under bending and compression).

Moreover, the use of "logical switches" that change rules without an exact physical basis leads to an abrupt change in the algorithm, as in the classification of cross-sections in the Eurocode. Modern technologies enable to detect such inaccuracies and determine ways to improve the codes.

LOAD-BEARING CAPACITY REGION OF JOINTS

The design and calculation of the joints of beam elements is, apparently, one of the most important stages in the design of steel structures. Unlike the analysis of the stress-strain state based on a structural design model, which obeys the strict rules of structural mechanics, the "algorithms" for calculating joints use traditional (taking into account the previous experience) methods of approximate solution, which are based on simplified notions about the operation of joints. Thus, the design models of joints of steel structures are largely determined by the existing design traditions. As a rule, these techniques are closely related to a set of service-tested designs of joints used for this type of structures.

Similar to the definition of the load-bearing capacity region of a section introduced earlier, we introduce the definition of the load-bearing capacity region of a joint.

A *load-bearing capacity region of a joint* $\mathbf{\Omega}_{\mathbf{J}}$ is a certain region in the *k*-dimensional space of internal forces, all points of which correspond to a combination of these internal forces, under the action of which the joint satisfies *all the standard requirements*. The boundary of the load-bearing capacity region of the joint is the entire set of limitations governed by the requirements given in the codes (including the strength conditions of the sections of the load-bearing structural elements adjacent to the considered joint, the strength conditions for the structural elements of the joint – wing plates, cantilever stiffeners, base plates and end-plates, the strength conditions of bolted and welded connections in a joint, etc.). The dimension k of the load-bearing capacity region of the joint is defined by the number of load-bearing structural elements l adjacent to the considered joint, as well as by the total number n of internal forces that may occur in the sections of these elements, $k = l \times n$.

COMET (Karpilovsky et al. 2014) enables computer-aided generation of the load-bearing capacity regions of the joints of steel structures in terms of the considered codes for rigid and nominally pinned column bases, beam splices, beam-to-column joints, and for truss panel points.

When the calculation of the joints of steel structures is performed according to the codes, the considerations and hypotheses that were developed during the times of manual calculation and served as a means of simplifying the manual calculations of engineers are used here. "Traditional" models are often very coarse, because they were developed during the "manual" design period, which required maximum simplification of the problem. The use of these conservative simplifications in the computer analysis often indicates the inconsistency of individual hypotheses.

The shape of the load-bearing capacity region of the joints, as well as the character of its boundaries, has made it possible in many cases to analyze the traditional approaches to the calculation of the joints of steel structures

in more detail. The analysis of the boundaries of the region has shown that the simplifications of the formulations of the regulations of the type “can be ignored” (as, for example, an indication of the possibility of neglecting the end-plate stiffeners when determining the geometric properties of the support section of the girder and the distribution of normal stresses in it, which is given in (Recommendations for the Calculation, Design, Manufacture and Installation of End-plate Joints of Steel Structures 1989) or “can be taken” (as, for example, the forces in anchor bolts can be taken as equal to their load-bearing capacity or averaged over the sections of uniform distribution of the reaction of the foundation concrete under the base plate), in most cases lead to various kinds of non-convexities in the load-bearing capacity region of the joints.

Therefore, software implementation of the calculation of the load-bearing capacity of joints of steel structures required the developers to avoid any simplifications of regulations. Moreover, in some cases, the refusal to simplify the formulations of the regulations was inevitable. For example, the traditional methods of calculating the joints of steel structures given in the codes are not always oriented toward solving three-dimensional problems.

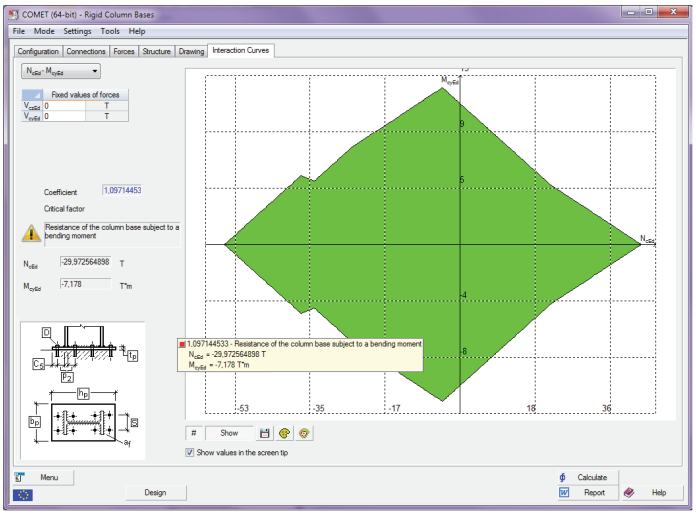

Figure 8. The load-bearing capacity region of the rigid column base using an equivalent reinforced concrete section when calculating the stress distribution in the foundation concrete and the forces in the anchor bolts.

In particular, this refers to the rigid column bases, for which the problem of determining the contact region of the base plate with the foundation concrete arises under bending in both principal planes. In the case when there are commensurate bending moments in the support section of the column and, respectively, tensile forces arise in the anchor bolts, the stress distribution in the foundation concrete, as well as the forces in the anchor bolts, are calculated in COMET by the finite element method using an equivalent reinforced concrete section with the dimensions equal to those of the base

plate and the arrangement of the working reinforcement, corresponding to the arrangement of anchor bolts in the base (Figure 8). For such an equivalent section, the stresses at the characteristic points below the base plate are determined, in particular, depending on the length of the perpendicular dropped to the neutral axis of the section.

Thus, the massive transition to CAD-CAE design systems enables the use of more accurate design models of steel structural joints in everyday practice. However, the results of this "refinement", often leading to a complication of the joint, may require additional justifications.

LOAD-BEARING CAPACITY REGION OF SECTIONS

Risks related to the non-convexity of the load-bearing capacity region seem to deprive us of the grounds for using the methods given in the codes. However, the vast experience in using the recommendations of these documents speaks in favor of the fact that these dangers do not realize. Apparently, the real variants of loading turned out to be such that the system avoided the "dangerous zone". This fact points to the possibility of analyzing the closeness of the real set of internal forces to those boundary of the load-bearing capacity region, where the property of non-convexity is manifest.

An almost identical analysis can be performed using additional tools provided by SCAD Office components. These tools enable a display of the entire set of verified loading options (combinations of internal forces specified by the user), in the form of a set of points, each of which corresponds to one of the loading options (Figure 9). A convex hull of these points is also shown, i.e. a set of loadings that are linear combinations of the given (basic) loadings. Despite the fact that these combinations were not subjected to a direct check, in the case when the convex hull of loadings does not leave the load-bearing capacity region of the section, it can be ensured that the various loadings combined from the basic ones are not unsafe.

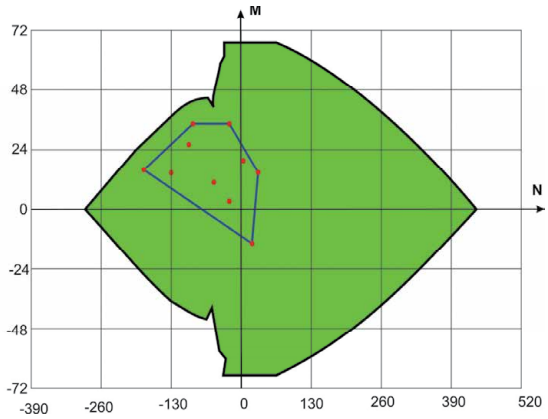

Figure 9 Given (basic) loadings and their convex hull, combined with the load-bearing capacity region of the section.

It should be noted that when operating only with two-dimensional orthogonal projections of the load-bearing capacity region, it is possible to "see" the projections of some points (combinations of internal forces) belonging to this region (for which the maximum utilization factor of restrictions does not exceed one) as displayed outside the projection boundary of the load-bearing capacity region (as, for example, point 1 in Figure 10). There may also be an erroneous "vision" of a different kind, when the projection of the point lies within the boundaries of the projection of the load-bearing capacity region, and the point itself does not belong to the region (see, for example, Point 6 in Figure 10). In order to identify such situations, the projections of the points in which the utilization factor of restrictions exceeds one, are displayed in red on the projections of the load-bearing capacity region.

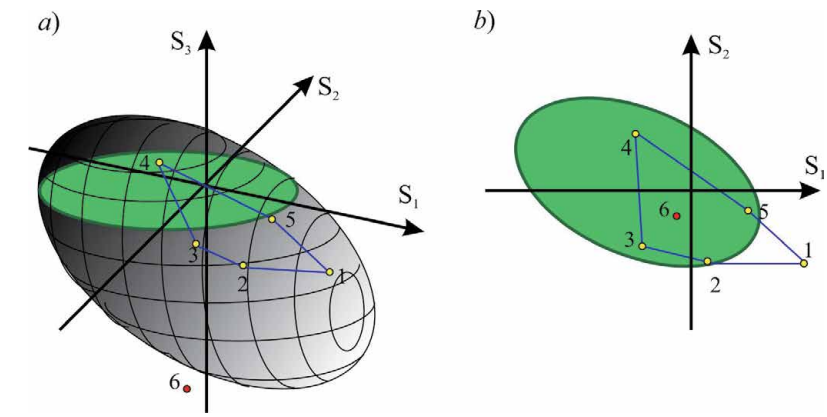

Figure 10. Illustration of possible design situations.

However, we cannot be completely sure that the used set of basic loadings is accurate, since all our calculations operate with the initial data determined only with limited accuracy. We can only assume that the real set of possible variants is not very far from the convex hull of the base loadings. Thus, the complete immersion of the convex hull of the base loadings in the load-bearing capacity region is only a necessary condition, and a more cautious recommendation is that the convex hull of the base loadings should be located at a sufficient distance from the non-convex section of the boundary.

As a measure that defines the concept of "sufficient distance" the following procedure is suggested. The modulus of the internal force vector for each base point can be determined thus:

$$|S| = \sqrt{\left(S_1/S_1^0\right)^2 + \left(S_2/S_2^0\right)^2 + \ldots + \left(S_n/S_n^0\right)^2},$$

where S_i^0 denotes the value of the ith force at the boundary of the load-bearing capacity region. Forces S_i were calculated on the basis of a set of initial data

on the loads on a structure, which, generally speaking, are approximate, since it is hardly possible to take into account all the circumstances of structural loading without exception and with an exact precision. Assuming that the initial data are determined with the usual engineering practice accuracy of up to 5%, we can say that the convex hull of the base loadings is at a sufficient distance from the dangerous boundary if it does not approach it by a distance less than $0,05|S|$.

CONCLUSIONS

Load-bearing capacity region for structural sections and joints in terms of design codes has been considered. Algorithm for automatic generation of load-bearing capacity regions for structural sections, connections and joints has been presented and implemented in SCAD Office software package.

The main attention in the paper has been focused on those design cases where the load-bearing capacity region of a section or a joint is non-convex and internal forces other than at the ultimate design values can be unfavorable. Construction of load-bearing capacity regions combined with a convex shell of specified combinations of internal forces has been proposed as flexible tool to indicate risky design cases. Load-bearing capacity region of a section has been also proposed for a critical analysis of code-based requirements and regulations used for verifications of structural cross-sections.

REFERENCES

Abdelhamid Charif (2009). *RC-BIAX Software*. Riyadh: King Saud University.

Charalampakis, A. & Koumousis, V. (2008). Ultimate strength analysis of composite sections under biaxial bending and axial load. *Advances in Engineering Software* 2008(39), 923–936.

EN 1993-1-1:2005 (2006). Eurocode 3. Design of Steel Structures. Part 1-3: General rules and rules for building. Brussels: CEN.

Fafitis, A. (2001). Interaction surfaces of reinforced-concrete sections in biaxial bending. *Journal of Structural Engineering*, ASCE 127(7), 840–846.

Kachanov, L. (1969). *Fundamentals of the Theory of Plasticity*. Moscow: Nauka.

Karpilovsky, V. et al. (2014). SCAD Office. Implementation of SNiP in Computer-Aided Design Applications. Moscow: SCAD SOFT.

Papkovich, P. (1941). *Structural Mechanics of Ships. Part 2. Complex Bending and Stability of Rods. Bending and Stability of Plates*. Leningrad: Publishing House of *Shipbuilding* Industry.

Perelmuter, A. & Slivker, V. (2010). *Handbook of Mechanical Stability in Engineering. Volume 1. General Theorems and Individual Members of Mechanical Systems*. Moscow: SCAD SOFT.

Recommendations for the Calculation, Design, Manufacture and Installation of End-plate Joints of Steel Structures (1989). *TsBNTI Minmontazhspetsstroy USSR*.

Rodriguez-Gutierrez, J. & Dario Aristizabal-Ochoa, J. (1999). Biaxial interaction diagrams for short RC columns of any cross section. *Journal of Structural Engineering*, ASCE, 125(6), 672–683.

SP 16.13330.2011 (2011). "SNiP II-23-81* Steel Structures". Moscow.

Strelets-Streletsky, E. & Vodopyanov, R. (2009). Software Package for the Computer-aided Analysis and Design of Reinforced Concrete Structures. *CAD and Graphics* 2009(3), 68–71.

Sulimowski, Z. & Klowan, E. (1980). Decisive sets of internal forces. XXVI Conference Proceedings KILiW i KN PZITB. Wrocław-Krynica, 1980 (in Polish).

FIRE TEMPERATURE DISTRIBUTION IN TRAPEZOIDAL COMPOSITE FLOORS

Kuldeep S Virdi
Professor Emeritus of Structural Engineering
City, University of London

ABSTRACT

The paper describes a finite difference approach for calculating temperature distribution in trapezoidal composite floors exposed to fire. It is shown how the applicable differential equation is transformed to the finite difference form and the manner in which the inclined boundaries of the trapezoidal section are handled. The computer program developed is briefly described. Calculated results are compared with those from two sets of published experimental results.

INTRODUCTION

The design of structures in fire has long been based on experimentally established rules. However, fire testing of structural components is becoming increasingly expensive. With the developments in the power and accessibility of computers, there has been an increasing shift towards the use of numerical methods, validated by sufficient number of well-designed experiments. The predominant numerical method in use is the finite element method (FEM). Several commercial FEM packages of software are available which enable sufficiently accurate analysis to be carried out. These programs give rapid results, especially for linear elastic analysis. In the FEM approach, modelling of geometry does not pose a serious obstacle. For geometric and material non-linear analysis, however, these programs require considerable effort in terms of data preparation and also actual computations. An alternative approach, based on the finite differences (FD), offers a simpler formulation. However, with finite difference, modelling of geometry creates an obstacle to the development of general-purpose software. It has been found that efficient solutions can be obtained using finite differences, but the software can normally be applied to a restricted form of geometry. It is in this light that this paper presents a finite difference formulation of the problem of heat transfer in trapezoidal floors slabs, such as the one shown in Figure 1.

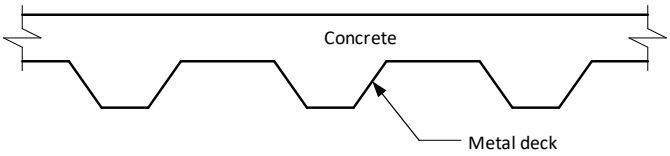

Figure 1. Typical trapezoidal floor slab.

Composite floors using profiled steel sheeting, allow rapid construction. Steel deck eliminates the need for expensive formwork. The use of metal decking provides a safe working platform during construction provides weather protection under the metal decking and speeds up the work of other trades.

ANALYSIS FOR THE FIRE LIMIT STATE

Analysis of structural systems exposed to non-uniform heating under fire is a three-step process involving estimate of fire exposure, heat flow analysis for calculating internal temperatures, and a strength analysis to calculate deflections and eventual failure as the temperature grows. The traditional approach for the first stage is normally prescribed in the form of standard fire curves, which describe the temperature of the compartment at a given time after the initiation of the fire. Since the introduction of Eurocodes, the use of natural fire curves (BS EN 1991-1-2:2002) instead of the standard fire curves has been increasingly adopted in designs since they have been shown to result in more economical, yet perfectly safe, designs. In the second stage, the classic heat flow equation is solved to determine the temperature distribution within the structure. The effects of the heat radiation and the heat convection from fire to the structure surface are accounted for via the boundary conditions. The temperatures influence the strains, which in turn, affect the stresses. Due account needs to be taken of the interaction between thermal strains and strains due to deformation of the structure. In the third stage, the equilibrium-deflected shape of the structure is calculated to be in equilibrium with the applied loading, including the thermal effects. As stated above, this paper focuses on a finite difference approach for calculating the temperature distribution in trapezoidal composite floors exposed to fire.

COMPARTMENT FIRE TEMPERATURES

The intensity of fire temperatures developing in a compartment depend on the fire loading as prescribed on the basis of combustible material in the compartment expressed as mass of timber in kg/m^2. The level of fire loading is linked with the usage of the compartment. The other critical parameter is the amount of ventilation surface expressed as a fraction of the total surface of the compartment. Guidance is available in Eurocode 1 (BS EN 1991-1-2:2002) to calculate the compartment temperature with time using these parameters. An alternative, traditional, approach is to use a standardised fire curve such as ISO 834, also included in Eurocode 1 for fire, defined by the following equation:

$$T_f = T_0 + 345 \log_{10}(8t + 1) \tag{1}$$

where, T_f is the temperature of the fire in the compartment, T_0 is the ambient temperature before the fire, and t is the time (in minutes) since the commencement of the fire. The temperature unit is degree Celsius. The

numerical results in the paper are for a standard fire curve, even though the computer program described later is capable of handling natural fires.

HEAT FLOW CALCULATIONS

In the context of trapezoidal composite floors, it is assumed that heat flow is two-dimensional. A common scenario is that the fire is fully developed in the volume under the floor. Even when simulating localised fire, the assumption can be justified if the two-dimensional heat flow is calculated at sufficient number of points, as in the present work.

The thermal analysis for structural fire problems can be separated into two parts. In the first part, heat transfers across the boundary from the fire into structural members by convection and radiation. The other part relates to the heat transfer within structural member by conduction. The differential equation for heat conduction in two dimensions is the well-known Fourier equation:

$$\frac{\partial}{\partial x}\left(K\frac{\partial T}{\partial x}\right)+\frac{\partial}{\partial y}\left(K\frac{\partial T}{\partial y}\right)+Q=\rho c\frac{\partial T}{\partial t} \tag{2}$$

where T is the temperature, t is the time, K is the thermal conductivity, ρ is the density of the material, c is the specific heat of the material and Q is the internal heat energy. The thermal properties of concrete and steel (thermal conductivity, specific heat, and specific mass) are temperature-dependent. The thermal conductivity decreases as a function of temperature; the specific heat increases as a function of temperature. Some standards allow computations to be performed using constant values for the thermal properties. The internal heat energy does not apply to solid concrete/composite floors

Equation (2) can be solved by the finite element method or by the finite difference method. The finite-difference method has been used extensively for heat conduction problems (Mills 1994) because it is quite easy to implement. The method used here is based on the finite difference procedure given in Lie (1992), adapted for the geometry of the trapezoidal cross-section. Since the geometry of a typical trapezoidal metal deck floor is repetitive, only the section shown in Figure 2 is used in the analysis, using symmetry about the left axis and continuity on the right side.

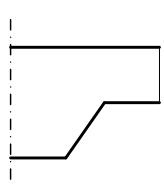

Figure 2. Part of the cross-section selected for temperature distribution analysis.

There are several finite element computer programs that solve the heat conduction equation with fire-boundary conditions such as FIRES-T3 (Iding et al. 1977) and TASEF (Sterner & Wickstrom 1990). The finite difference approach was adopted by Lie (1992) for the temperature distribution calculations in reinforced concrete columns.

A paper by (Hamerlinck & Twilt 1989) investigated the influence of specific heat of steel on the thermal behaviour of composite slabs. It was concluded that as the steel sheet is very thin, the influence of its heat capacity on the heat transfer was negligible. It has been assumed in this paper that the steel sheet at high temperatures loses its strength completely, and the floor is then reduced to a reinforced concrete slab. Thus in the modelling described below, the steel sheet is ignored.

THERMAL PROPERIES OF MATERIALS

Material properties used here are as specified in Eurocode 4 Part 1.2. The relevant properties for concrete are its density, specific heat and conductivity.

$$\rho = 2350 \qquad kg/m^2 \tag{3}$$

$$C = 900 + 80\left(\frac{T}{100}\right) - 4\left(\frac{T}{100}\right)^2 \qquad J/kg\,K \tag{4}$$

$$K = 2 - 0.24\left(\frac{T}{100}\right) + 0.012\left(\frac{T}{100}\right)^2 \qquad W/m\,K \tag{5}$$

Properties of steel are not quoted here as the thin sheet of metal decking is assumed to store negligible heat energy and is neglected in the calculations.

FINITE DIFFERENCE APPROXIMATION OF HEAT CONDUCTION EQUATION

As a first step in the solution of the problem by finite differences, the domain in which the differential equation applies is divided into a mesh with gridlines parallel to the Cartesian axes. A part of the grid is shown in Figure 3. The figure shows that the spacing of horizontal and vertical gridlines (Δy and Δx, respectively) can be different in size. The figure also shows that, when the differential equation is approximated by the finite difference formulae at point (i,j), its influence extends over the shaded area. It is assumed that heat is conducted through the lines marked as Top, Bottom, Left and Right. In the present problem, there is no internal heat generated within the floor, hence the term Q in Equation (2) becomes zero, as do the contributions Q_{in} and Q_{out} shown in Figure 3.

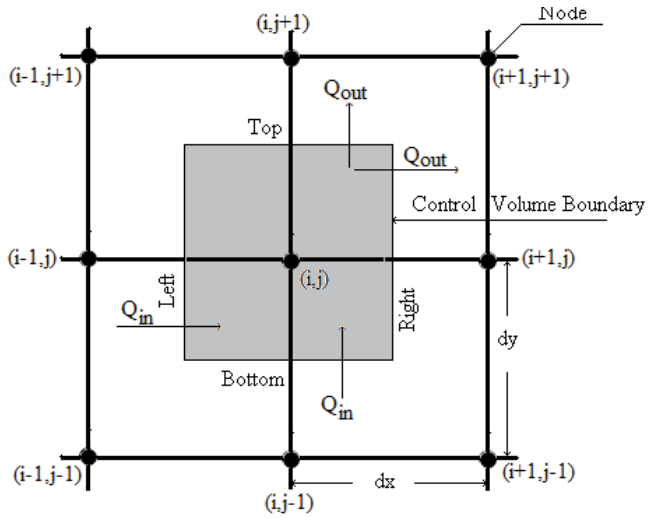

Figure 3. Part of the grid shown, centred around the point (*i,j*) defined by vertical grid line *i* and the horizontal grid line *j*.

Without going into basics of the finite difference formulae, in the same way as Equation (2) is derived, with Q=0, the principle of conservation of energy can be applied. Thus, the rate of heat conduction into the control volume equals the rate of heat conduction out of the control volume and the rate of energy stored inside the control volume. In finite difference form, using the time step as Δt, at the temperature T^m at the mth time step, as shown below:

$$-K\left\{\frac{T_{i,j}^m - T_{i-1,j}^m}{\Delta x}\Delta y + \frac{T_{i,j}^m - T_{i,j-1}^m}{\Delta y}\Delta x\right\} = -K\left\{\frac{T_{i,+1j}^m - T_{i,j}^m}{\Delta x}\Delta y + \frac{T_{i,j+1}^m - T_{i,j}^m}{\Delta y}\Delta x\right\} + \rho c \Delta x \Delta y \frac{T_{i,j}^{m+1} - T_{i,j}^m}{\Delta t} \tag{6}$$

Rearranging the above equation, the temperature at the next time step is determined as given below:

$$T_{i,j}^{m+1} = T_{i,j}^m + \frac{\Delta t}{\rho c \Delta x \Delta y}\left\{\frac{K(T_{i,j+1}^m - T_{i,j}^m)}{\Delta y^2} + \frac{K(T_{+1i,j}^m - T_{i,j}^m)}{\Delta y^2} + \frac{K(T_{i,-1j}^m - T_{i,j}^m)}{\Delta x^2} + \frac{K(T_{i,j11}^m - T_{i,j}^m)}{\Delta y^2}\right\} \tag{7}$$

The above equation could have been obtained directly from equation (2). The equation also shows the power of the finite difference method. It will be noted that the complicated differential equation has been reduced to a simple algebraic equation. Also, in this particular case, the problem can be solved without iteration. A sufficient condition is that the time step has to be less than a critical value given by:

$$\Delta t < \frac{\rho c \{\min(\Delta x, \Delta y)\}^2}{2K} \tag{8}$$

The significance of the sufficient condition is that it is not a necessary condition, so minor variation from the critical value does not jeopardise convergence.

Where the material properties change with temperature, the applicable conductivity parameters used, for determining the flux towards the left, right, top or bottom, are the harmonic mean (rather than the mean) of the value at point (*i,j*) and the neighbouring point depending upon the direction being considered. This is based on the proposal by (Patankar 1980).

Thus, for the left, right, top and bottom faces of the control volume in Figure 3,

$$K_{left} = \frac{2K_{i,j}\,K_{i-1,j}}{K_{i,j}+K_{i-1,j}},\ K_{right} = \frac{2K_{i,j}\,K_{i+1,j}}{K_{i,j}+K_{i+1,j}},\ K_{bottom} = \frac{2K_{i,j}\,K_{i,j-1}}{K_{i,j}+K_{i,j-1}} \text{ and } K_{top} = \frac{2K_{i,j}\,K_{i,j+1}}{K_{i,j}+K_{i,j+1}} \tag{9}$$

Boundary Conditions

At the boundaries of the floor, both exposed to fire and ambient, emissivity of the surfaces has to be considered. As an example, Figure 4 shows the lower horizontal boundary of the floor, which is exposed to heat radiation and convection.

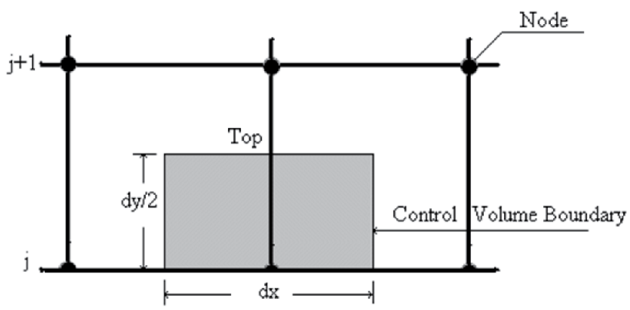

Figure 4. Control Volume for a lower boundary.

The control volume is Δx (Δy/2) shown as the shaded area in Figure 4. When writing the energy balance condition at point (*i,j*), the heat transfer rate from the boundary into the volume is given by:

$$Q_{i,j}^{m} = \sigma\,\varepsilon_f\,\varepsilon_c\,\{(T_f^m + 273)^4 - (T_{i,j}^m + 273)^4\}\,\Delta x \tag{10}$$

Where, $Q_{i,j}^{m}$ is the heat flow in the *y* direction at point (*i,j*) at time *m*, σ is the Stefan-Boltzmann Constant, ε_f is the emissivity of the fire and ε_c is the emissivity of concrete. Rearranging the control volume energy balance equation gives the following equation for temperature at the next time step:

$$T_{i,j}^{m+1} = T_{i,j}^{m} + \frac{2\Delta t}{\rho c \Delta x \Delta y}\left\{\frac{K(T_{i,j+1}^{m} - T_{i,j}^{m})}{\Delta y}\Delta x + \frac{K(T_{i+1,j}^{m} - T_{i,j}^{m})}{\Delta x}\frac{\Delta y}{2} + \frac{K(T_{i,j}^{m} - T_{i-1,j}^{m})}{\Delta x}\frac{\Delta y}{2} + Q_{i,j}^{m}\Delta x\right\} \quad (11)$$

A similar equation can be written for the upper horizontal boundary, where the heat flow due to radiation will be zero, as there is no fire at that surface.

$$T_{i,j}^{m+1} = T_{i,j}^{m} + \frac{2\Delta t}{\rho c \Delta x \Delta y}\left\{\frac{K(T_{i,j}^{m} - T_{i,j-1}^{m})}{\Delta y}\Delta x + \frac{K(T_{i+1,j}^{m} - T_{i,j}^{m})}{\Delta x}\frac{\Delta y}{2} + \frac{K(T_{i,j}^{m} - T_{i-1,j}^{m})}{\Delta x}\frac{\Delta y}{2}\right\} \quad (12)$$

The equation for an inclined boundary is obtained using the same procedure of writing the energy balance equation. Consider the control volume shown in Figure 5. An assumption is made that a node always exists at a boundary. This can be easily achieved by choosing Δx and Δy to match the slope of the inclined boundary. Also, as there is no right or bottom edge, it is assumed that there is no conduction along those two sides. The heat input from the boundary is based on the length of the inclined boundary.

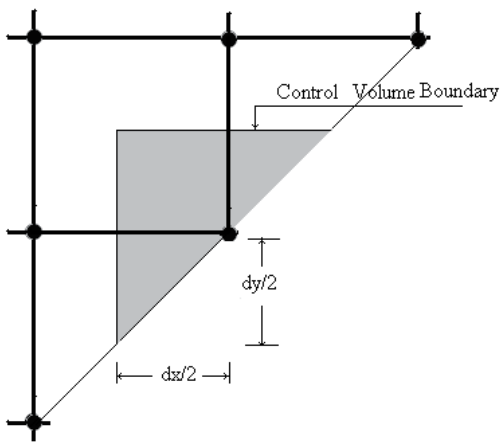

Figure 5. Boundary control volume for an inclined node.

The equation for the temperature at the next time step for an inclined boundary can be shown to be as follows:

$$T_{i,j}^{m+1} = T_{i,j}^{m} + \frac{4\Delta t}{\rho c \Delta x \Delta y}\left\{\frac{K(T_{i,j+1}^{m} - T_{i,j}^{m})}{\Delta y}\Delta x + \frac{K(T_{i,j}^{m} - T_{i-1,j}^{m})}{\Delta x}\Delta y + Q_{i,j}^{m}\sqrt{\Delta x^2 + \Delta y^2}\right\} \quad (13)$$

COMPUTER IMPLEMENTATION

The equations developed above are sufficient to carry out the computations for the response to fire of composite floors exposed to fire. The flow chart of the computations is shown in Figure 6. The calculations start at the boundary nodes at the lowest level, sweeping left to right and then progressing to the higher levels one by one.

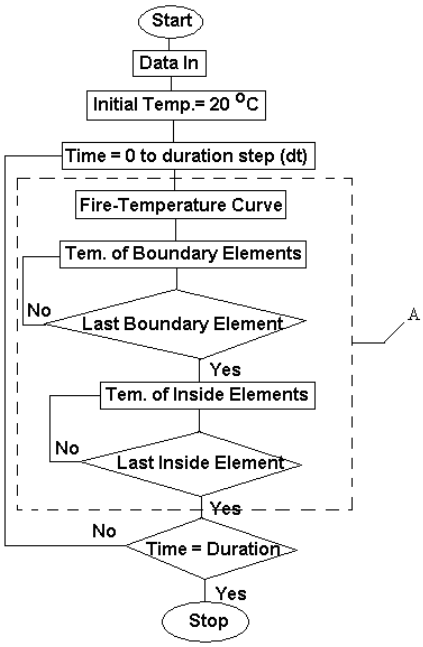

Figure 6. Flow chart of the computations.

A computer program, labelled COMFLEF has been written in Visual Basic to carry out the calculations. The program has a user-friendly interface and requires a small amount of input data to define the problem. Some key features are described below.

Geometry

The cross-section is divided into five zones, four of which are rectangular and one triangular, as shown in Figure 7. Only three horizontal and two vertical dimensions are sufficient to define the cross section. Corresponding to the five dimensions, the five values of the number of gridlines define the complete mesh. The horizontal and vertical grid equidistant spacing are deduced. It may be added that the heat balance equations are suitably adjusted at nodes where the grid spacing at the left and right or above and below are unequal.

The node numbers are generated going from the bottom to the top and then from the left to the right. As stated earlier, the metal deck is ignored in the calculations as if the concrete surface was directly exposed to the fire.

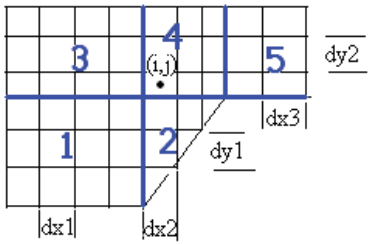

Figure 7. Cross-section divided into 4 rectangular and 1 triangular zones.

Boundary Conditions

It is assumed that the bottom surfaces are exposed to fully developed fire. The top surface is exposed to ambient temperature. The left and right side are assumed to be lines of symmetry.

Material Thermal Properties

The program has built-in material properties for concrete (and steel, although not required in this application) as specified in BS EN 1994-1-2/2005.

VALIDATION

The method described above has been validated against experimental fire tests carried out by Hamerlinck & Twilt (1989) and by Abdel-Halim et al. (1999). Comparison is made between experimental results for temperature distribution within the floor slab with results from the program COMFLEF.

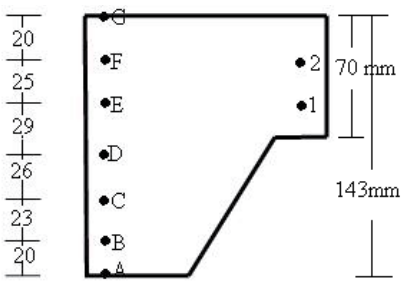

Figure 8. Locations of points where temperatures were measured (Abdel-Halim et al. 1999).

The trapezoidal metal deck specimens had dimensions of 1600×700 with a total depth of 143 mm. The concrete used was normal weight concrete of grade B25 (C25 in Eurocode nomenclature). The slabs were subjected to a standard fire. Figure 8 shows the location of points where the temperatures were measured in the experiment.

The distribution of temperatures down the depth is compared in Figure 9 for fire at 120 min. It will be seen that the calculated temperatures are fairly accurate

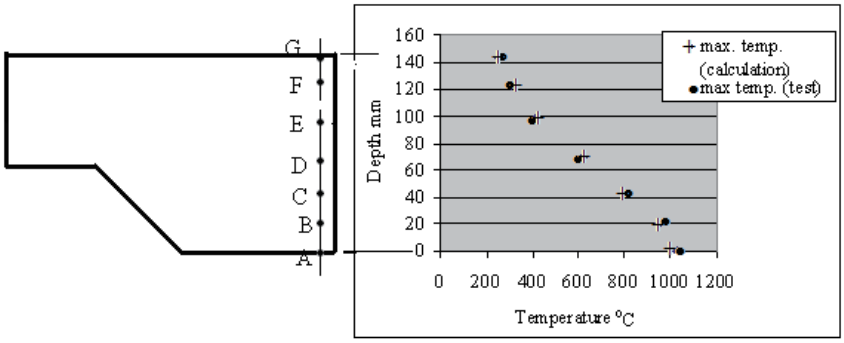

Figure 9. Comparison of computed temperatures with measured values at 120min of fire.

The cross-section and the location of selected points for measuring concrete temperatures in the tests by Abdel-Halim, Hakmi and O'Leary are shown in Figure 10 for their Sample 1, in which a light steel mesh was provided for fire resistance and to control cracking.

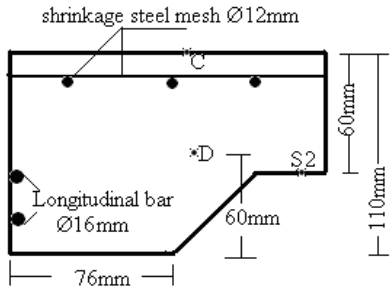

Figure 10. Cross-section of Test Sample 1 in (Abdel-Halim et al. 1999).

Figure 11 shows plots of the development of temperatures at various locations against time. It will be seen that the computed results follow the measured values at most locations. In all cases, the experimental results show a lag, and this is attributed to moisture in the concrete, which was not taken into account in the present analysis. Clearly, the computed results are conservative.

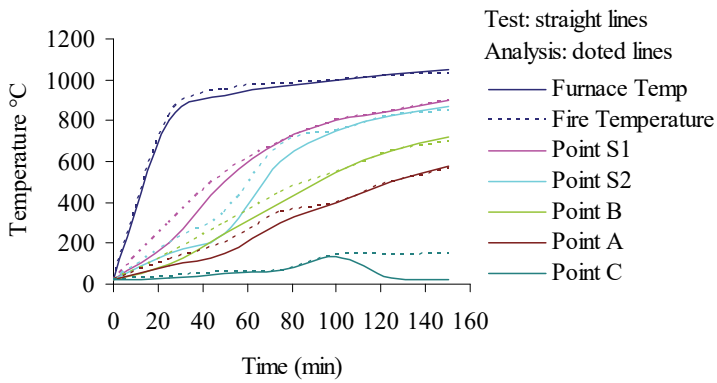

Figure 11. Comparison between calculated and measured growth of temperatures at selected points for Sample 1 in (Abdel-Halim et al. 1999).

CONCLUSION

A method of analysis of calculating temperature distributions in composite floors exposed to fire has been presented. The method uses the finite difference approximation to solve the Fourier equation of heat conduction. An effective solution has been obtained for dealing with inclined boundaries in the context of gridlines parallel to Cartesian axes. A computer program COMFLEF based on the method has been described in outline

The results from the computations based on the finite difference approach have been validated against experimental results from two previous publications. Excellent correlation was obtained for the temperature distribution within the cross-sections as well as for growth of temperatures at several points in the cross-section for up to 120min fire duration.

An indication has been given for using the temperature distributions calculated from the described method for mechanical response of composite floors.

ACKNOWLEDGMENT

Assistance given by a former doctoral student, Mrs Samia Nama, working under the author's supervision is gratefully acknowledged.

REFERENCES

Abdel-Halim, M. A. H., Hakmi, M. R., & O'Leary, D. C. (1999). Fire resistance of composite floor slabs using a model fire test. *Engineering Structures,* 21, 176–182.

BS EN 1991-1-2:2002 (2002). *Eurocode 1 – Actions on Structures – Part 1-2: General Actions-Actions on structures exposed to fire*. Brussels: CEN.

BS EN 1994-1-2 (2005). *Eurocode 4 – Design of composite steel and concrete structures – Part 1-2: General Rules - Structural Fire Design*. Brussels: CEN.

Hamerlinck, A. F. & Twilt, L. (1989). *ECSC sponsored research on The Behaviour of Fire-Exposed Composite Steel/Concrete Slab. Test Report BI 89-016,* s.l.: TNO Delft, The Netherlands.

Iding, R. H., Bresler, B., & Nizamuddin, Z. (1977). *FIRES-T3, A computer program for the fire response of structures-thermal.* Berkeley: Fire Research Group.

Lie, T. T. (1992). *(ed.). Structural fire protection - ASCE Manuals and Reports in Engineering Practice No 78*. New York: ASCE.

Mills, A. F. (1994). *Heat and Mass Transfer*. McGraw-Hill Education

Patankar, S. V. (1980). *Numerical Heat Transfer and Fluid Flow*. Washington DC: Hemisphere Publishing Corp.

Sterner, E. & Wickstrom, U. (1990). *TASEF - Temperature Analysis of Structures Exposed to Fire, Report 1990:05.* Boras: Swedish National Testing and Research Institute.

ALL ROADS LEAD TO ROME?
Vision-Based Scenario Evaluation concerning Sustainable Residential Areas.

Dr. Tarja Meristö
FuturesLab CoFi, Laurea University of Applied Sciences

Jukka Laitinen
FuturesLab CoFi, Laurea University of Applied Sciences

ABSTRACT

This paper introduces a methodological review and concrete results concerning the scenarios for sustainable residential areas and their ability to reach the desirable vision in each case. The data collection for the future scenarios and for the shared vision took place during the scenario process facilitated by the writers of this paper in the context of ELLI project. The results will open new views to the future when developing energy efficient residential areas from sustainable perspectives. The results include also a methodological evaluation of the power of the vision and scenarios in the context of regional strategic planning. As a conclusion, a set of scenarios with various abilities to reach the vision will be presented.

INTRODUCTION

Futures research as a part of strategic planning will open new opportunities to the future (Meristö 1990), but that will also map risks and surprises concerning wild cards and black swans (Taleb 2006). The future is not facts "what will happen in the future" but more a description of "what might happen in the future". The futures work includes not only possible and probable scenarios but also the vision of the desirable future (Amara 1981).

In this paper we will focus the future of sustainable residential areas, which by definition are physical and functional entities containing building blocks, services and people. These, all together, will form an area with all dimensions of sustainability, i.e. economic, social and environmental aspects of it. Energy-efficient residential areas are in focus in the project ELLI, financed by ERDF and coordinated by Häme UAS, where we at Laurea have developed scenarios for energy-efficient areas to the year 2036. The process lasted from Autumn 2016 to Spring 2017, including three futures workshops with regional decision makers from various case areas in Finland (Laitinen & Meristö 2017, Meristö & Laitinen 2016).

Planning sustainable areas has a long history. Especially natural resources and parks as well as cultural and holy places have been decades among

protected areas (Eagles et al. 2002). Planning sustainable areas includes both developing infrastructure and services, which will require multiple criteria decision-making concerning all the actors in this field (Osinski 1999). Concerning sustainable residential areas, also building systems and materials will play an important role, e.g. passive building system can lead to energy-efficiency without extra input from the residents (Blumenfeld & Thumm 2014). Research on alternative paths towards sustainable and energy-efficient residential areas has not been done a great deal and that is why this paper is intended to open new routes to the field.

RESEARCH DESIGN AND FRAMWORK

The framework for this paper combines futures research, especially scenario planning to strategic planning and visionary leadership (Meristö 1991, Nanus 1992). The timeframe is reaching up to the future for the next 20 years.

The main research question in this paper is: *Do all the scenarios lead to the vision?* The sub-research questions are as follows: *Are there any missing opportunities or threats, which these scenarios do not cover? Who are the key interest groups committed to the vision? Whose voice matters?*

Vision is defined as a value-based perception of the future, where the actors concerning the subject in focus will commit to (Kamensky 2000). Vision is a guideline to the future and it helps decision-makers to make a choice between several alternatives and assumptions which are behind alternative scenarios (Meristö 1990). Vision is far beyond the strategic planning horizon, still the vision sentence should include concrete conditions of the future and the communication of the vision should be clear. Otherwise the commitment will not be complete: *only shared vision will come true in the course of time* (Nanus 1992).

Scenario is an alternative development path to the future in the long run. Scenario as a word will come from the theatre world, where it means description of the play, detailed moves on the stage, actors´ roles and positions during the play and so on. The same illustration applies to the future scenario, too. On the stage there will be the real world actors from different groups like companies, citizens, government or NGOs and the scene will base on alternative assumptions from the operating environment relevant to the subject in focus. As a result from scenario process, there will be a wide range of scenarios from possible to probable ones, from desirable to unthinkable ones, if the process has been well facilitated (Meristö 1991).

Scenario selection as a basis for the decision-making and strategy formulation is not an automatic process, where only to calculate the best expected outcome in the future. Scenario selection is more sophisticated combination of art and science, where multi-criteria decision-making approaches are needed. From Amara´s (1981) point of view, the future can be influenced by individual choices. In reality, actors making these choices will form a complex ecosystem

with many dynamic connections, having relationships with each other. Only a part of these connections are transparent, and a lot of reasoning will happen in black boxes behind closed doors or inside the head and heart. These hidden assumptions often will be called taboos, i.e. issues not mentioned loudly or even if any discussion will be held, it does not lead to any practical consequences (Kettunen 2009). Scenario selection is therefore a process, where we have to estimate the interests and power game of actors in the ecosystem, but also to recognize the risk behavior profile of the decision-maker and the ability to carry the risks in the organization in focus (Meristö 1991).

There is no universal ranking for scenarios, rather, each case is connected to the decision-maker and his or her mindset, risk profile and reference group. The ranking list of scenarios can vary from one evaluation point to another: Regarding e.g. three dimensions of sustainable development (Bruntland 1987) the preferred future might differ from economic, social or ecological perspectives. Also the key actors in alternative perspectives will change. Action scenario approach will bring to the board key actors from the whole ecosystem of energy-efficient resident areas: citizens/residents and NGOs at the grass-root level, governmental actors from international, national and local level as enablers and regulators, but also companies and enterprises in planning phase, but also in construction phase as well as in use and maintain phase during the whole life-cycle of the buildings and residential areas as a whole.

Triple helix (Figure 1) context combined with sustainable development dimensions (Meristö & Laitinen 2014) will give the first alternatives of the criteria for good decisions concerning the energy-efficient residential areas in the real life, i.e. in the multi-actor context with different interests. Secondly, the decision-makers´ and their organization´s mindset have to be taken into consideration when developing criteria for good decisions concerning the scenario selection as a basis for the strategy development (Meristö 1991). Ability and willingness to take risks are the key elements of this mindset, which will define the result of scenario selection: Forecaster will follow the probable line with no risk, Risk-taker will choose the most attractive alternative with high risk, Risk-avoider will avoid the selection of scenarios, but will prepare himself for the future in all cases, Realist will focus on fast action with flexibility created for the alternatives not chosen, Future-maker will build a strong network to achieve the desired future whereas the last attitude is Beef-cattle focusing on waiting and hoping for a better future (Meristö 1991).

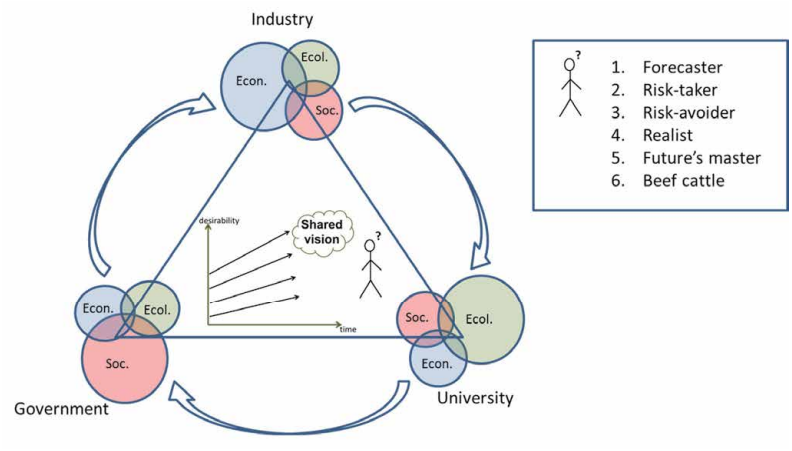

Figure 1. Framework for the study: combination of triple helix, sustainable development, shared vision and selection of scenarios (based on Meristö 1991; Meristö 1990 and Meristö & Laitinen 2014).

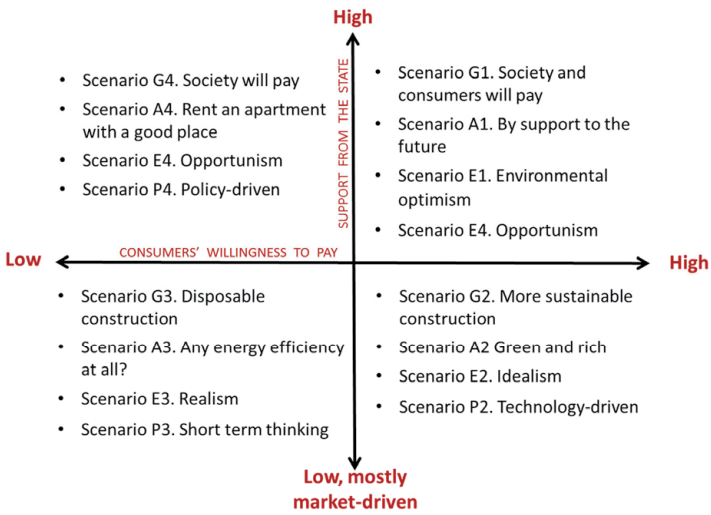

Figure 2. Alternative scenarios for the case areas in Finland: a summary.

RESULTS

Scenario work will always produce some alternatives which without special pressure do not lead towards the vision. The shared vision is the basis for motivation to make an ambiguous choice among scenario alternatives. Those alternatives not selected will need considerations against the selected one: need for flexibility for surprises have to be estimated (Meristö 1990). Surprises are often risks, but also opportunities which can be exploited in a strategy prepared for the future.

Project ELLI defines the vision of the energy-efficiency in residential areas as "a residential area with carbon-neutral community strategy including sustainable values in construction, city-planning, labor and investment policy and citizen-centric service design…"

The constructed scenarios for the three different case areas and for the energy-efficient residential area in general will differ from each other concerning on the one hand *the consumers´ willingness to pay for green* and environmental friendly solutions, and on the other hand t*he society´s support for the energy-efficient* regional development. Both these two drivers can be positive or negative by value, i.e. consumers are willing to pay or not and society will give support or leave that to the market. These two axes will form *a fourfold table*, where each quarter is one basis for scenario assumptions. The case area scenarios and the scenarios in general have been put to the table in each quarter as follows (Figure 2).

The case areas in focus are a region called Askonalue in City of Lahti (A), another region called Engelinranta in City of Hämeenlinna (E) and third one Peltosaari area in City of Riihimäki (P). More generally described is still a common description of energy-efficient residential area in Finland (G).

Each area will have these four alternative scenarios for the future. All the constructed scenarios for the different case areas do not lead to the vision. Like scenario building process, also the scenario evaluation has happened in the facilitated futures workshops consisting of actors from this field, including decision-makers from the specific residential areas in focus. In Table 1, scenarios are listed based on their favorability towards the vision. The grey area in the table includes those scenarios not leading to the vision. A special threat for the energy-efficient residential areas seems to be a situation, where both society and consumers are reluctant to pay for the green and carbon-free solutions.

Table 1. Scenarios towards the vision in ELLI case areas.

Generally, residential area with energy efficient goals (G)	Askonalue Lahti (A)	Engelinranta Hämeenlinna (E)	Peltosaari Riihimäki (P)
Scenario G1. Society and consumers will pay	Scenario A1. By support to the future	Scenario E3. Realism	Scenario P1. Visionary view
Scenario G2. More sustainable construction	Scenario A4. Rent an apartment with a good place	Scenario E1. Environmental optimism	Scenario P2. Technology-driven
Scenario G4. Society will pay	Scenario A2 Green and rich	Scenario E2. Idealism	Scenario P3. Short term thinking
Scenario G3. Disposable construction	Scenario A3. Any energy efficiency at all?	Scenario E4. Opportunism	Scenario P4. Policy-driven

The results can be illustrated by a figure describing scenarios and vision in the same picture. It is easy to notice, how well or not the scenario alternatives

will lead towards the vision in the course of time. As an example, the general description of an energy-efficient residential area and its scenario alternatives towards the vision is shown in Figure 3.

Scenario 1 *Society and consumer will pay* will lead best towards the vision, and also Scenario 2 *More sustainable construction* will provide opportunities for the energy-efficient residential areas in the future. Scenario 4 *Society will pay* will slowly lead towards the vision, but Scenario 3 *Disposable construction* will clearly stay under from the desirable future with its challenging vision.

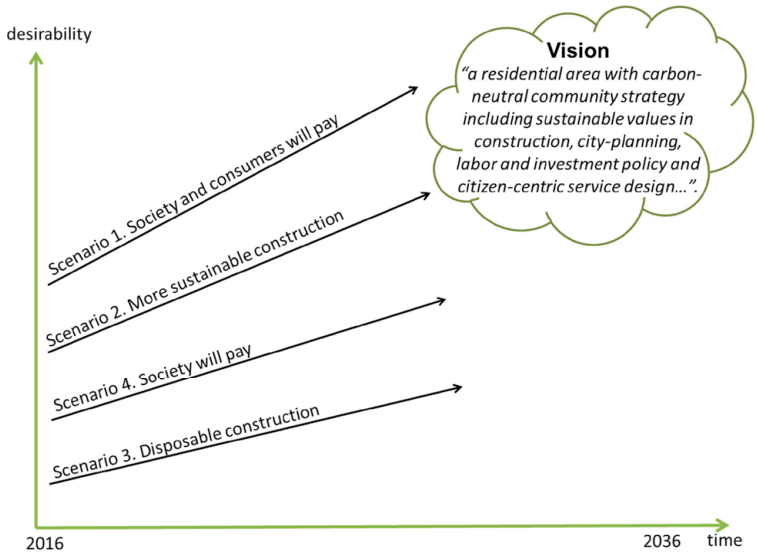

Figure 3. Vision of the energy-efficient residential area generally with scenario ranking towards the vision (based on Meristö 1990).

The best scenario will not automatically lead towards the vison, but it will require specific actions with careful planning and timing, too (see Laitinen & Meristö 2018).

CONCLUSION

The results will open new views of the future when developing energy efficient residential areas from sustainable perspectives. First the triple helix context have to be taken into consideration. Secondly, all the dimensions of sustainable development have to be checked through all different interest groups: citizens, NGOs, government, municipalities, companies from different business fields as well as international agreements states and unions have been committed. Third, personal features in decision making process are important to notice e.g. risk aversion vs. risk taking. Also, the commitment to the vision has to be clarified: only the shared vison can become real in practice, too.

The results include a methodological evaluation of the power of the vision and scenarios in the context of strategic regional planning. If the scenarios are too general by nature, they cannot act as guidelines towards the vision. Also, when approaching the future only via one or two main actor groups in the governmental context, the regional planning cannot face all the challenges related to the energy-efficient residential areas. By open, citizen-centric and participatory design processes small and large opportunities and threats can be handled by scenario work. In the case of many disagreements of goals and tools, at least time-bounded prioritization can be done over the traditional planning period and beyond (see e.g. Kettunen & Meristö2010).

REFERENCES

Amara, R. (1981). Searching for Definitions and Boundaries. *The Futurist*.

Blumenfeld, A., & Thumm, W. T. (2014). Passive Building Systems versus Active Building Systems. In *Building Innovation 2014*. Washington DC: EXPO 2014.

The Brundtland Report (1987). Report of the World Commission on Environment and Development: Our Common Future. Oslo: UN.

Eagles, P., McCool, S., & Haynes, C. (2002). Sustainable Tourism in Protected Areas. Guidelines for Planning and Management. World Commission on Protected Areas, Best Practice Protected Area Guidelines Series No. 8. Gland & Cambridge: IUCN.

Kamensky, M. (2000). *Strateginen johtaminen*. (in Finnish; Strategic Management). Helsinki: Talentum.

Kettunen J. (2009). *Uudistu ketterästi*. (in Finnish; Agile Renewal). Helsinki: Talentum.

Kettunen, J. & Meristö, T. (eds.) (2010). Seitsemän tarinaa ennovaatioista - Rohkeaa uudistaa ennakoiden.(in Finnish; Seven Stories about Proactive Innovations – Winner Takes the All) Helsinki: Teknologiainfo Teknova.

Laitinen, J. & Meristö, T. (2018). Rome was not built in one day - Future-oriented regional development towards energy-efficient residential areas. Proceedings of the METNET Seminar 2017 in Cottbus, Germany (Forthcoming).

Laitinen, J. & Meristö, T. (2017). Applying Visionary Concept Design to Energy Efficient Residential Areas. Proceedings of the METNET Seminar 2016 in Castellón. HAMKin julkaisuja 4/2016. Häme University of Applied Sciences, Hämeenlinna, Finland.

Meristö, T. (1990). Futures Research and Strategic Planning - Do They Go Together? Proceedings XI World Conference of WFSF, Budapest, Hungary, 312–320.

Meristö, T. (1991). Skenaariotyöskentely yrityksen johtamisessa. (in Finnish with English summary Scenarios in Strategic Management). Acta Futura Fennica. VAPK-kustannus.

Meristö, T. & Laitinen, J. (2014). Sustainability as a Business Opportunity Today and Tomorrow: Triple Helix Perspective. Proceedings of the METNET Seminar 2013 in Luleå. HAMKin julkaisuja 1/2014. Häme University of Applied Sciences, Hämeenlinna, Finland.

Meristö, T. & Laitinen, J. (2016). Cleantech Business Opportunities in the Future. Proceedings of the METNET Seminar 2016 in Castellón. HAMKin julkaisuja 4/2016. Häme University of Applied Sciences, Hämeenlinna, Finland.

Nanus, B. (1992). *Visionary Leadership: Creating a Compelling Sense of Direction for Your Organization*. San Francisco: Jossey-Bass Publishers.

Osinski, H. (1999). Planning Sustainable Land Use in Rural Areas at Different Spatial Levels Using GIS and Modelling Tools. *Landscape of Urban Planning* 46(1-3), 93–101.

Taleb, N. N. (2007). *The Black Swan: The Impact of the Highly Improbable*. London: Allen Lane.

ROME WAS NOT BUILT IN ONE DAY
Future-oriented regional development towards energy-efficient residential areas

Jukka Laitinen
FuturesLab CoFi, Laurea University of Applied Sciences

Dr. Tarja Meristö
FuturesLab CoFi, Laurea University of Applied Sciences

ABSTRACT

Often, there are visions about the desired future as in the case of energy efficiency of residential areas but the challenge is how to achieve that vision. The research question in this paper is how to transform the vision into practical actions applied in regional development. As a methodological tool we apply "steps towards the vision" framework. It includes the action proposals to reach the vision but it also defines the responsible actors and timing of the action proposals. The results consist of the vision and steps towards the vision for a general energy-efficient residential area in Finland. In a general model, the planned actions will start from national level and they will continue via municipality level to local level and finally to individual level. As a practical example, we will also introduce the steps towards the vision in the case area of Engelinranta located in the city of Hämeenlinna. In that case, the future is highly dependent on the decisions of city concerning e.g. town planning, plot completion and technical plan. As a conclusion, it can be said that "steps towards the vision" approach helps to manage the long-term time frame by dividing the future development path into smaller steps with action plans, where also the responsible actors will be defined as well as the timing of actions.

INTRODUCTION

The vision of the world 2050 highlights the climate change and the need to decrease CO_2 emissions at all levels. The importance of energy efficiency has been recognized both in EU and national level (Ministry of Economic Affairs and Employment 2017). The energy efficiency of the buildings, and broadly considering residential areas, has a remarkable role when looking for solutions to the problems caused by climate change, because 40% of the energy consumption and 36% of CO_2 emissions in the EU related to the buildings (European Commission 2016). Approximately 70 – 80 % of greenhouse gas emissions of buildings are from daily energy consumption and the remaining 20 – 30 % from building materials and construction. In addition to technical performance, when evaluating the energy efficiency and carbon footprint of buildings, other important factors are user-oriented design, solutions

that prolong the lifetime of the building, quality of construction, users' consumption habits and solutions that increases use efficiency (Sarapää 2014).

In this paper we will focus on energy efficiency of residential areas with their desired futures. There is not much earlier research of developing energy-efficient residential areas. Earlier studies concerning energy-efficiency have more focused on buildings (e.g. Thorpe 2011, Laustsen 2008) than on complete residential areas. The aspect for the development of residential areas is something other than energy efficiency, e.g. participatory landscape planning (Tress & Tress 2003). However, there are some studies dealing with the systemic view to the problem (e.g. Kalaisevam & Parameshwaran 2014, Säynäjoki et al. 2012). Also as a part of ELLI project research group from Lappeenranta University of technology combined energy efficiency and residential area perspectives by using lifecycle modelling in their research work (Leino et al. 2017).

Often, there are visions about the desired future also in the case of energy efficiency of residential areas, but the challenge is how to reach that vision. Thus, our research question in this paper is how to transform the vision into practical actions applied in regional development. In practice, it's not always so clear how to fulfill the needed requirements to reach those visions.

This paper first introduces the research design behind the paper including the framework and the methodological process. Then we introduce the results that consist of the vision and steps towards the vision for a general energy-efficient residential area in Finland. We also complete the general results with a pilot residential area to understand more deeply local conditions. As a conclusion, we introduce the general requirements for future-oriented regional development. Finally we will make some methodological considerations of this steps towards the vision process, including the coverage of participants, the role of facilitators as well as the background information needed concerning the future alternatives.

RESEARCH DESIGN

The framework for this paper consists of futures research combined with a co-creation process and the timeframe is up to the future for the next 20 years. The data for this research paper have been collected during 2016 and 2017 in the ongoing ELLI project (Figure 1). At first, change factors related to the future energy efficient residential were recognized. Then, alternative scenarios were created based on the chosen driving forces. The scenarios were created for three different case areas: Askonalue in City of Lahti, Engelinranta in City of Hämeenlinna and Peltosaari in City of Riihimäki. In addition to the three case areas, scenarios for a general energy-efficient residential area in Finland were created during the process.

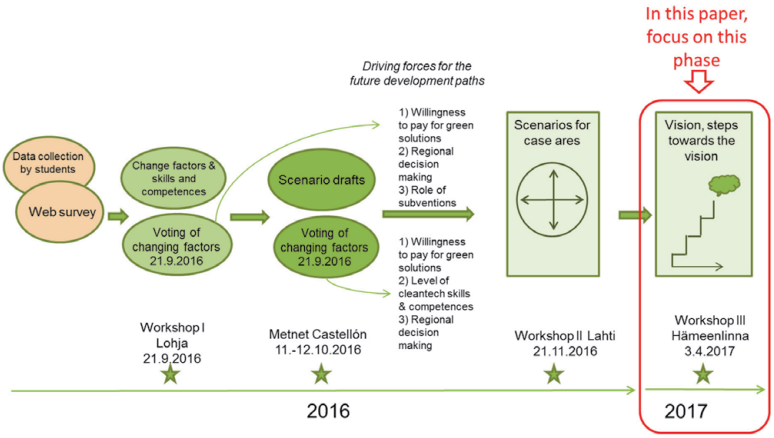

Figure 1. Background for the paper: process and focus.

The focus in this paper is the last step of the process in which the vision and the steps towards the vision were defined. As a methodological tool we apply "steps towards the vision" framework. It includes the action proposals to reach the vision, but it also defines the responsible actors and timing of the action proposals. Theoretical and practical background for the process will lie on the action scenario approach (Meristö 1991), where the aim is not only to create alternative scenarios for the future, but to make decisions based on these scenarios. It means that every scenario alternative has to be analyzed carefully, including threats and opportunities as well as interest groups in each scenario. Then, for strategic decisions, the actors have to estimate for each alternative required resources, skills and timing, but also attitudes towards each scenario especially in case it is not the desirable one. Actions based on threats and opportunities recognized in scenarios can vary from the aggressive to the defensive, and the strategy development at regional level can be a challenge, if the shared vision is not found (see e.g. Meristö et al. 2000).

In practice, we have approached the problem of energy-efficient residential areas at two levels: first, the general level of the theme and then, the implementation level in each of the three case area. In this paper we will introduce *first the results of the general level group work*, including the vision and steps towards the vision following the most desirable scenario path, where both consumers and state will pay for and support development and implementation of green solutions. In the general model, the assumptions will start from national level and slowly they will continue through society via municipality level to local level and finally to individual level, where the last step towards the vision in the best case will be an integrated view from sustainable and responsible resident areas including e.g. construction with materials, energy alternatives, city planning and ways of living and consuming. After the general description we will *focus on practical steps towards the vision in one specific residential area* as a case study, namely case Engelinranta in the City of Hämeenlinna.

As a basis for this case study will be the most realistic scenario selected in a practical group work during the futures workshop held and facilitated in spring 2017. One of the hidden basic assumptions there is that the national decisions will support development of energy-efficient residential area e.g. in taxation policy as well as in rules and regulations.

RESULTS

In our scenario process, alternative scenarios for the future energy efficient residential areas were created before the steps towards the vision were defined for the chosen scenario. The driving forces for the scenarios were the role of subventions and residents' willingness to pay for the green solutions. In the case of a general energy-efficient area in Finland, the vision will be achieved best in a scenario in which both the society and the consumers share the costs. Due to the common interests and proactive attitudes of the society and consumers, sustainable construction and carbon neutrality are realized more probably compared to other alternative scenarios. On the other hand, if consumers are reluctant to spend money for green solutions and the society is not supporting energy-efficiency, the development leads easily to traditional solutions with high carbon footprint.

In our project, the vision of the future energy-efficient residential area was defined as follows (Meristö & Laitinen 2018):

> *"The future energy-efficient residential area is located in a city which aims for carbon neutrality and applies the values of sustainable construction. The residential area is economically, socially and ecologically sustainable including workplaces, many kind of residents and safe and accessible environment. The residents are seen as a resource – citizen driven innovations create user friendly solutions for living, services, logistics, heating and recreation".*

When aiming to reach the vision, actions need to be planned properly. The implementation of actions requires real actors with well-defined responsibilities. The timing of the selected actions is important, too. Figure 2 illustrates the steps towards the vision in the case of a general energy-efficient residential area. Every step describes the needed actions, responsible actors and the timing of those actions. In this case, the time frame is 20 years to the future but the step-by-step approach helps to achieve the vision. The order of the actions is also essential. If the actions of some certain step are not implemented, the vision will not be reached.

The path towards the future can be divided into five steps (from A to E) when approaching the vision. First, the national level decision-making process (A) has to take into consideration support activities for green solutions by taxation, investment subventions or even direct investments to promote that kind of work. This has to happen within the following five years, otherwise the favorable development is not possible in a wide scale during the given

time horizon, i.e. next twenty years. Also, in less than five years´ time period, the next two steps (B, C) have to be taken at the municipal and local levels to promote the sustainability in city planning and in construction business in practice. Consumers and citizens (D) are in the key role, when trying to generate *design for all solutions* in this field. Without individual choices and preferences no change in the mindset will happen. This will require a longer time, from five to ten years, because of the diversity of people even in a small country as Finland. Finally, all different actors need a shared vision to go further, i.e. an integrated ecosystem (E) towards eco-efficient residential area is necessary for continuous co-creation process to achieve the vision in the course of time, at least from five to ten years ahead.

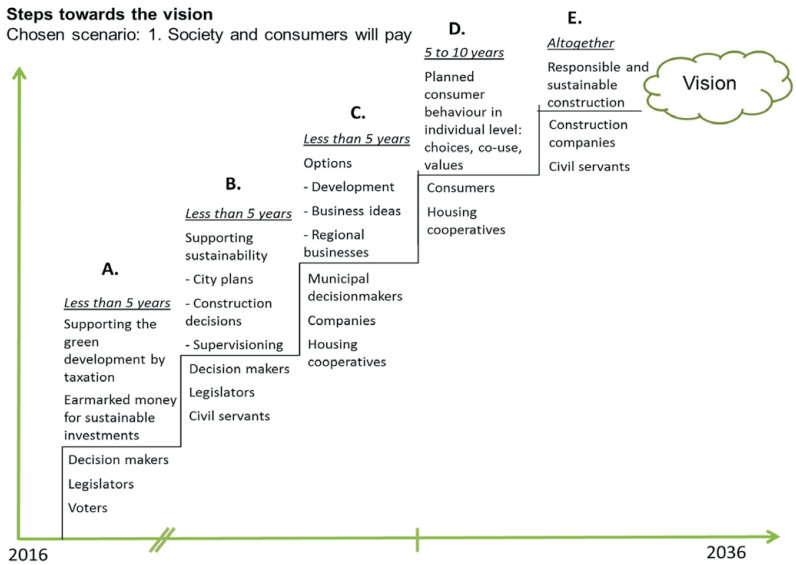

Figure 2. Steps towards the vision: actions and responsibilities (a general energy-efficient residential area in Finland).

The baseline scenario for this step by step approach is scenario number 1, where both society and consumers are willing to pay for green solutions (Meristö & Laitinen 2018). What if –questions for the other scenario alternatives are e.g. what it the society is not supporting, what if the consumers only promote sustainability but the acceptance in real life is low, what if the local regulations and practices vary from case to case? Navigation marks for the next 5 years concerning the first three steps A-C is needed, otherwise the favorable development in practice is not possible.

During the Elli-project the “steps towards the vision” approach was applied also to the real case areas. Figure 3 illustrates the steps towards vision in Engelinranta area which is located in the city of Hämeenlinna. The steps are defined for the scenario in which citizens are not willing to pay much extra for the green solutions and the government subsidizes green development only

to a small extent, so the solutions are mainly market driven. However, the implicit assumption in Engelinranta case is that society is still taking care of basic preconditions for the sustainable development.

The future of Engelinranta is highly dependent on the decisions of city of Hämeenlinna concerning e.g. town planning, plot completion and technical plan. However, commercial actors have also an important role in many phases in cooperation with the city of Hämeenlinna. For example, energy companies and consultants participating in the energy vision and the plans related to it.

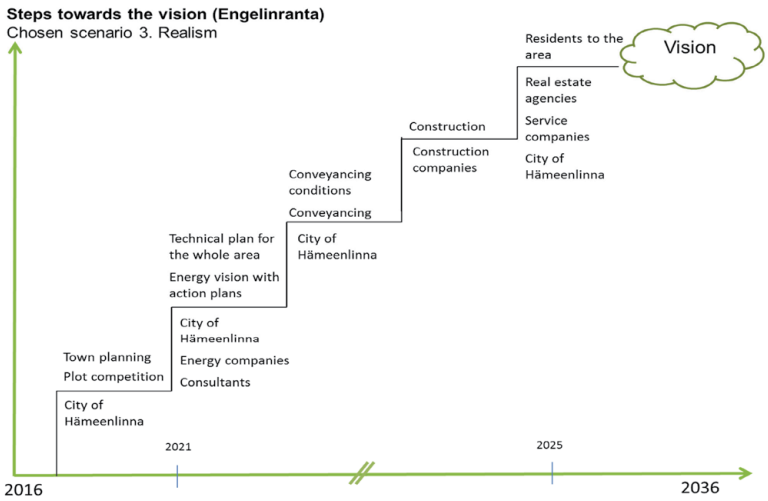

Figure 3. Steps towards the vision: actions and responsibilities (case Engelinranta).

CONCLUSIONS

In the future-oriented regional development it is important that wide range of stakeholder groups are participating in the process. Active participation enhances the dialogue between actors, enables the achievement of the shared vision of the future and also improves actors' commitment to the regional development. In Elli project we have applied the action scenario process (Meristö 1991) and many kind of actors have been involved, including companies, municipal decision makers, regional development organizations and researchers. The role of facilitators is also important in the future-oriented regional development process because they give guidance to participants and collect the background information needed concerning the future alternatives. Facilitators, as outsiders, can also raise up the discussion above the everyday problems and focus more on the holistic view of the future.

In the regional planning the time frame is often very long, especially in the case of planning future energy-efficient residential areas. "Steps towards the vision" approach helps to manage the long term time frame by dividing

the future development path to smaller steps with action plans, where also the responsible actors will be defined. The steps also improve the timing of actions. Often steps may have different requirements at the time because different actors have different time frames: e.g. political decision makers may plan the future considering the election periods. On the other hand, private commercial actors may have shorter time frame depending on profit potential. Research community quite opposite to these can raise up long-term issues challenging e.g. the next generation, as it has happened e.g. in relation to the discussion about climate change or megatrends like urbanization at world level, which both are relevant when planning energy-efficient residential areas for the future. Although the length of steps can vary, they all have to be accomplished to achieve the vision. Time-line in the picture is illustrative and in real life the time frame can be shorter or longer depending on the speed with which the different actors will take care of their responsibilities.

REFERENCES

European Commission (2016). Energy efficiency – Buildings. Retrieved 11 Sep 2017 from https://ec.europa.eu/energy/en/topics/energy-efficiency/buildings

Kalaiselvam, S. & Parameshwaran, R. (2014). Thermal Energy Storage Technologies for Sustainability. Systems Design, Assessment and Applications. Oxford: Elsevier.

Laustsen, J. (2008). Energy Efficiency Requirements in Building Codes, Energy Efficiency Policies for New Buildings. IEA Information Paper. OECD/International Energy Agency (IEA).

Leino, M., Claudelin, A., & Korpijaakko, E. (2017). Tulevaisuuden energiatehokkaat asuinalueet: Askonalue. (Energy-efficient residential areas in the future, case Asko area). In S. Vanhamäki & E. Korpijaakko (eds.). Perspectives to Energy Efficiency and to Residential Areas in the Future (Näkökulmia energiatehokkuuteen ja tulevaisuuden asuinalueisiin). Lahti: LAMK Publications 30. (In Finnish.)

Meristö, T. & Laitinen, J. (2018). All roads lead to Rome? Vision-Based Scenario Evaluation concerning Sustainable Residential Areas. Proceedings of the METNET Seminar 2017 in Cottbus, Germany (Forthcoming).

Meristö, T., Kettunen, J., & Hagström-Näsi C. (2000). Metsäklusterin tulevaisuusskenaariot. (The Future Scenarios of Forest Cluster), Tekes Teknologiakatsaus 95/2000. (In Finnish.)

Meristö, T. (1991). Skenaariotyöskentely yrityksen johtamisessa. (Scenario Working in Company Management). Acta Futura Fennica No 3. Helsinki: VAPK-kustannus. (In Finnish.)

Ministry of Economic Affairs and Employment (2017). Government report on the National Energy and Climate Strategy for 2030. Publications of the Ministry of Economic Affairs and Employment.

Sarapää, N. (2014). Development of eco-efficiency criteria in plot competitions. Master of Science Thesis. Tampere University of Technology. (In Finnish.)

Säynäjoki, A., Heinonen, J., & Junnila, S. (2012). A scenario analysis of the life cycle greenhouse gas emissions of a new residential area. Environmental Research Letters, 7(3).

Thorpe, D. (2011). Solar Technology. The Earthscan Expert Guide to Using Solar Energy for Heating, Cooling and Electricity. New York: Earthscan.

Tress, B. & Tress, G. (2003). Scenario visualisation for participatory landscape planning - a study from Denmark. Landscape and Urban Planning, 64(3), 161–178.

Technical Note
SELECTION OF FINITE ELEMENT FOR DESIGNING METAL BUILDING STRUCTURES

D. O. Kuzmenko
Master of Engineering Science (Belarusian-Russian university, the Republic of Belarus)

V. M. Fridkin
Doctor of Engineering Science, professor (Moscow State University of Railway Transport of Emperor Nicholas II)

I. M. Kuzmenko
Candidate of Science, assistant professor (Belarusian-Russian university, the Republic of Belarus)

INTRODUCTION

Modern engineering buildings have various types and design variants (Bogdanov 2011, 6–16; Kuzmenko 2003, 47–50; Kuzmenko 2006, 198–202; Kuzmenko 2014; Kuzmenko, Fridkin, & Markov 2015, 40–51; Kuzmenko & Fridkin 2017, 171; Fridkin 2011, 171; Fridkin, Chesnokov, & Kokosadze 2015, 119). Load-carrying elements of the metal engineering structures are designed as "linear" elements that are manufactured from metal sheets which are connected in tri-dimensional beams by "nodal" load-carrying elements (gusset plates). Each gusset plate connects adjacent beam elements as tri-dimensional beams and finally in tri-dimensional structures. Other than simple building structures (e.g. industrial building door frames that consist of door bolts, columns, trusses etc.) under model engineering which do not require high processing capacity, estimation of wide-span bridges or floor structures of entertainment facilities demands a vast amount of calculations.

Structures, representing linear systems, can be calculated with the help of volume, shell or beam finite elements. One can deal with complicated structures (that do not have a uniform section, but with structural elements with a complicated form, made from different materials) only with the help of volume finite elements, with some minor exceptions which can be analysed using shell elements. Nowadays there are several software programs that allow, within a certain period of time, calculation of any engineering structure for external loading.

The software programs of CAE/CAD systems can solve any problem within a short period of time; therewith they allow making changes to the structure if this is necessary after the calculations. The results of experimental verification of the accuracy of numerical models are presented in Lagerev (2014, 36-40). In Shimanovsky (2008, 61) the influence of the finite element size on the accuracy of statistical estimation was considered. The requirements that are specified in developing the computer models to the mesh definition of the finite elements are described in Bogdanov (2013, 119). However, there are no

direct comparisons of the various types of finite elements and their influence on the accuracy, calculating speed and resource-intensiveness of the problem being solved in these publications.

THE MAIN TYPES OF THE FINITE ELEMENTS AND THEIR FEATURES

Finite element types used in various software programs, for example, in CAE / CAD Ansys Work Bench, are described in Basov (2002, 2005). From all the variety of types of finite elements (FE) for solving the static problem of calculating skeletal systems, in the opinion of the authors, it is sufficient to use FE types of BEAM, SHELL and SOLID. The size of the finite element of the BEAM, SHELL and SOLID types is standardized by the segment length between the nodes of the element. By that, it is meant that the whole element has a uniform section, geometrical characteristics and material characteristics.

All volume BEAM types have two nodes that can have three or six degrees of freedom on the main coordinate axes. All volume SHELL types have from four to eight nodes that can have three or six degrees of freedom on the main coordinate axes. The element SOLID type can change its shape (cube, tetrahedron, hexahedron), depending on the problem to be solved. All volume SOLID types have from eight to twenty nodes that can have three or six degrees of freedom on the main coordinate axes.

Comparative analysis of the accuracy and resource capacity of the solution of the problem of load-bearing linear elements of metal building structures can be done using finite elements BEAM 188, SHELL 181 and SOLID 186. We give a detailed description of each of these FE.

BEAM 188 (Figure 1a) – three-dimensional linear beam element with finite deformations. Element is suitable for direct modelling of beam structures with a moderate ratio of length to thickness. It is built on the basis of Timoshenko's beam. It takes into account the effects of tangential (shear) deformations. It has six or seven degrees of freedom in each node. This includes movements in the direction of the X, Y and Z axes and rotations around the X, Y and Z axes. Under certain conditions, a seventh degree of freedom (cross-sectional distortion) is added. This element is suitable for linear as well as nonlinear problems with large rotations and (or) large deformations.

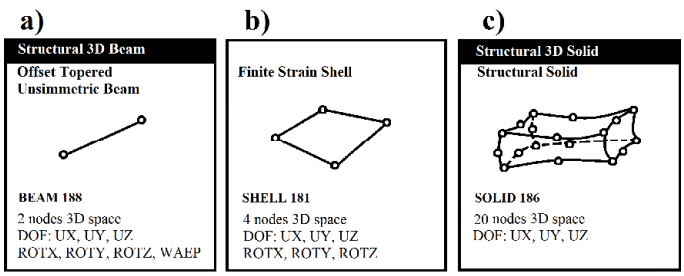

Figure 1. The finite elements used in the study.

The element has, by default, the ability to account for the change in stiffness when loaded. This makes it possible to use this element to study stability problems in compression, bending, and torsion (by applying eigenvalues and by studying the loss of stability by the method of searching along the length of the arc).

SHELL 181 (Figure 1b) – multilayer shell with finite deformations. The element is well suited for calculating shell models with small or moderate thickness. The element has four nodes and six degrees of freedom in each node: moves in the direction of the X, Y, and Z axes of the nodal coordinate system and rotations around the X, Y, and Z axes of the nodal coordinate system. Elements of triangular shape can be used only as transition elements in grids.

This element can be used in linear problems and in nonlinear problems with large rotations and (or) deformations. In nonlinear problems, the change in shell thickness is taken into account. As applied to the element, full and truncated variants of numerical integration are supported. The element can be used to calculate multilayer or three-layer shells.

SOLID 186 (Figure 1c) – three-dimensional (3D) element of a volume stress-strain state with twenty nodes. The element has a quadratic representation of the displacements and is able to use an irregular grid shape (for example, based on models imported from various CAD complexes). The nodes have three degrees of freedom each, moving in the directions of the X, Y, and Z axes of the nodal coordinate system. It can have an arbitrary orientation in space, has the properties of plasticity, hyper-elasticity, creep, changes in rigidity when applying loads, large displacements and large deformations.

It is possible to have a mixed formulation for the calculation of almost incompressible elastoplastic materials and completely incompressible hyper-elastic materials. To control the output of data, there are special options. In addition, these elements allow analysis of concentration of stresses.

When performing the calculations of the majority of the supporting bar elements, in our opinion, it is necessary to use the FE of type BEAM. When calculating the load-bearing bar elements with a thin wall, it is necessary to use the FE type BEAM or SHELL. The most accurate values for the calculation of structures with load-bearing bar elements of any complexity can be obtained using SOLID-type finite elements.

STATEMENT OF PROBLEM AND OBJECTS OF THE STUDY

In this paper, the possibility of using more “simple” types of finite elements (FE) is justified, without loss of accuracy of calculation. In this case, the calculation procedure will require less computing resources. This will make it possible to use fairly accurate and least resource-intensive solutions in future studies of large-span structures.

The test objects were considered the simplest bar bearing element as well as conventionally used Ishaped cross section (Figure 2, a) in metallic building structures. The selected dimensions are: h = 200 mm; b_f = 100 mm; t_f = 8 mm; t_s = 6 mm; and ℓ = 3000 mm. Material of the bar is low-alloy steel.

Numerical experiments were performed on solid, beam and shell models. A static analysis (Static Structural) and a calculation for loss of stability by its own value (Eigenvalue Buckling) were performed.

The results of the numerical experiment are compared with the values obtained by engineering calculation in Construction Regulation Standards Building Code (CRSBC) and Technical Code of Common Practice EN (TCP EN) (CRSBC II-23-81, 1990, 96; CRSBC 2.01-07-85, 1986, 36).

The boundary conditions were taken as follows: for a beam working on transverse bending, in accordance with Figure 2b; to calculate the bar for longitudinal bending (calculation for stability) – in accordance with Figure 2c. This approach made it possible to assess the advantages of using certain types of FE depending on the loading of the bar.

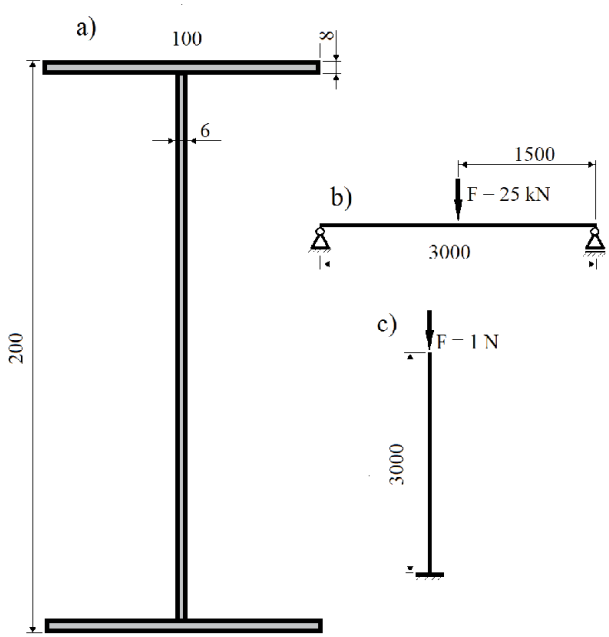

Figure 2. (a) Objects of research: cross-section of investigated models; (b, c) setting boundary conditions.

The sizes of the final elements are chosen as follows: for BEAM – 1 mm; for SHELL – 6 mm; for SOLID – 2 mm. In the study of the loss of stability, the dimensions of the final element were assumed to be equal: for shell FE (SHELL) – 4 mm and for volumetric FE (SOLID) 6 mm.

When using the SOLID type of FE, the normal stresses and deflections were determined in the lower (stretched) layer in the section where the force is applied. As parameters determining the load-carrying capacity of the bar in transverse bending, normal stresses and deflections are chosen. In the longitudinal bending of the bar (central compression), the critical forces and the values of the stability factors were determined.

THE ENGINEERING CALCULATIONS USING THE BUILDING CODE II-23-81*[14]

Strength Calculations: These calculations are based on the Construction Regulation Standards Building Code II-23-81*(CRSBC II-23-81, 1990, 96). According to the standard, when evaluating strength, the following condition must be met:

$$\frac{M}{W_{n,min}} \leq R_y \cdot \gamma_c,$$

where M is the calculated value of the bending moment corresponding to the material reaching the yield point at a critical section of the bar;

$W_{n,\,min}$ is the moment of resistance of the section (see Figure 2a). When this cross-section is used in the elastic stage, we take $W_{n,\,min} = W_{pl} = 1.78689 \cdot 10^{-4}$ m^3;

R_y is the yield strength for steel (we take this as 250 MPa);

γ_c is coefficient of conditions of the design. It is assumed to be 1.1 (see Table 6 [14]).

The values of the calculated and acting moments in the middle of the span (see figure 2b) and the maximum normal stresses are shown in Table 1.

Calculation of Deflections: To ensure the deflections do not exceed the requirements, the following conditions must be met:

$$f \leq f_y,$$

where f is the calculated maximum deflection of the beam; and f_y is the standard deflection of the beam. The ultimate deflection according to CRSBC 2.01.07-85 * (1986, 36) for the loading scheme (see Figure 2b) should not exceed L / 150. The Young's modulus for steel is assumed 206,000 MPa.

The results of calculating the bearing capacity for deflections are also presented in Table 1.

CALCULATION USING EUROCODE EN 1993-1-1-2009, P. 6.2.5 (EN 1993-1-1-2009, 2010, 85):

Strength calculations. The design value of the bending moment M_{Ed} in each cross-section must satisfy the condition:

$$\frac{M_{Ed}}{M_{c,Rd}} \leq 1,0,$$

where $M_{c,\ Rd}$ is the effective value of the bending moment. It is based on the plastic stage of operation $M_{pl,\ Rd}$, and also the partial safety factor γ_{Mo}. In accordance with 6.1 (1) B and Table NP.4 [15], γ_{Mo} = 1.025 / 1.1 = 0.932.

By calculation, the specified values of the moments and normal stresses correspond to the values obtained by the method of CRSBC II-23-81 * (see Table 1).

Deflection limit state. The ultimate deflection in this case should not exceed L / 300. Load deflection (adopted earlier in the CRSBC) f = δ = 0.00382 m. Limit deflection according to the norm δ_{limit} = 3/300 = 0.01 m. Thus, the deflection from the action of force does not exceed the normative one.

Calculation of the bar for loss of stability.

The calculation was carried out using traditional methods of material mechanics. Critical Strength (F_{cr}) is a load exceeding which causes the loss of stability of the original form (position) of the body. From the moment of the onset of the critical state to the moment of failure, the systems develops deflections extremely rapidly. In this way, when calculated for stability, the critical load is similar to the breaking load when calculated for strength. The stability condition is written in the following form:

$$F_{max} \leq F_{cr.}$$

The flexibility of the I-beam cross-section (see Figures 2a,c) λ = 270.3, and the ultimate flexibility of steel λ_u = 100.8. For $\lambda > \lambda_u$, the critical force was determined by Euler's formula: F_{cr} = 75.35 kN.

Table 1. Results of the calculation of the bar for transverse bending according to the methods of CRSBC II-23-81 * (clause 1) and TCP EN 1993-1-1-2009 (clause 2).

№	The design moment **M**, [N·m]	Actual moment M_d, [N·m]	Maximum normal stress **σ**, [MPa]	Normative deflection f_y, [m]	Limiting deflection **f**, [m]
1	49139.48	18750	104.93	0.00382	0.02
2	54822.96	18750	104.93	0.00382	0.01

CALCULATION OF THE BEAM USING THE ANSYS WORK BENCH PROGRAM

Figure 3 shows the finite element mesh partitioning and boundary conditions for the solution of the problem, using 3D (finite element type SOLID).

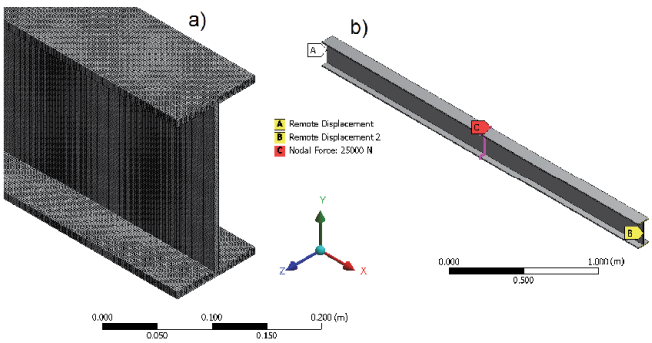

Figure 3. To the calculation of the bar for bending: the fragment of the partitioning of the I-beam into finite elements (a); boundary conditions (b).

For models in which other types of finite elements were used, the boundary conditions were set similarly. The initial load (see Figure 3b, Marker C) was set with the condition that the resulting stresses do not exceed the tensile-compressive yield strength of steel, which is assumed to be 250 MPa for the basic calculation in ANSYS WB. The ultimate tensile strength is 460 MPa.

Support of the bar (see Figure 3b, Markers A and B) was made at the point of the geometric centre of gravity of the cross-section for all models, while for the model with a finite element of the SHELL type three sections of the section (corresponding to two flanges and the I-beam web) were fixed; for FE type

SOLID, the fastening was made behind the end of the beam on the surface, and for the FE type of BEAM, at the extreme points of the element. The results of the calculations are presented in Table 2 and in Figure 4.

Table 2. Results of the numerical study of the work of the bar on bending with the use of FE of different types.

	Finite element type			**Engineering calculation**
	BEAM 188	**SHELL 181**	**SOLID 186**	
Deflection, [mm]	4.1506	4.2209	4.1605	3.82
Normal stresses, [MPa]	104.93	102.40	104.48	104.93
Δ in deflection, %	7.98	10.49	8.91	
Δ on the basis of stresses, %	0	2.41	0.43	

Note: the Δ symbol in Tables 2 and 3 indicates the percentage discrepancies between the results of FEM calculations and engineering calculations for CRSBC and TCP EN.

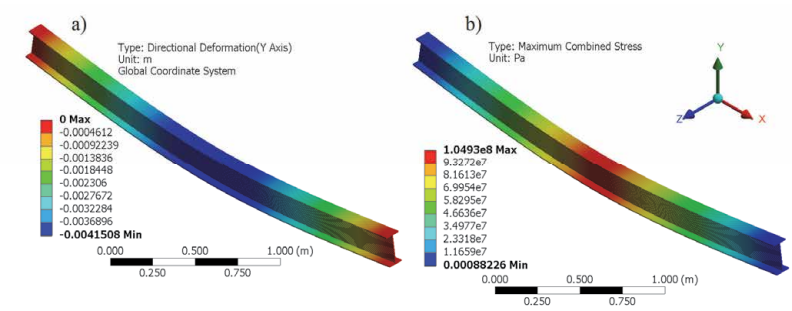

Figure 4. Results of the calculation of the bar for bending (FE of the BEAM type): deflection a); normal stresses b).

BAR FOR LOSS OF SUSTAINABILITY IN THE SOFTWARE COMPLETE ANSYS WB

We consider the finite element mesh partitioning and boundary conditions of the problem, using the volumetric (SOLID) type of finite elements (Figure 5). The support of the bar (see Figure 5b, Marker A) was set at the point of the geometric centre of gravity of the cross section for all models. In this case, for the model with the FE-type SHELL, three faces of the section were fixed (corresponding to the two flanges and the web), for the SOLID type of model, the boundary was set along the surface of the support section, and for FE of BEAM type, at the end point of the element. The results of the calculations are given in Table 3.

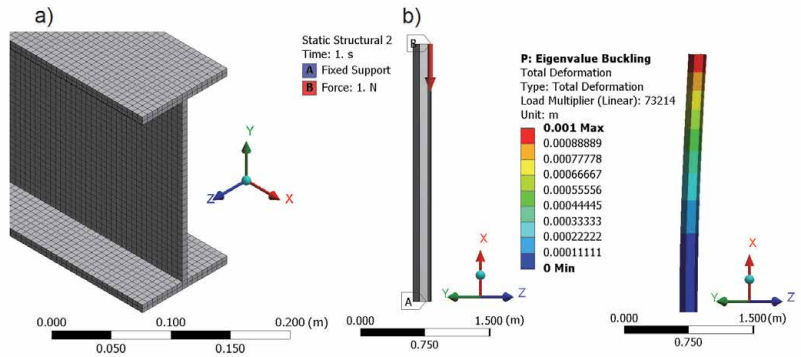

Figure 5. The results for the bar for longitudinal bending, (type of SOLID): a fragment of the mesh of the I-beam into finite elements (a); boundary conditions (b); and loss of stability (c).

Table 3. Results of a numerical study of the operation of the beam on the loss of stability with the use of FE of different types.

	Finite element type			Engineering calculation
	BEAM 188	SHELL 181	SOLID 186	
Critical force, [N]	73312	73200	73214	75350.7
△ by the critical force, %	2.71	2.85	2.84	

RESOURCE REQUIRED FOR THE CALCULATIONS DEPENDING ON THE TYPE OF FE

The resource intensity of the calculation is determined by the time required to complete the calculation, the amount of information the computer operates (the amount of computational RAM, the disk space for calculating and storing equations, the size of the file with the results of the research), and also by the productivity (the computational frequency of the solver of the equations). The calculations were performed on a computer with the following characteristics:

- Intel (R) Core (TM) processor i7-4790K CPU @ 4.00GHz;
- Ansys version 17.1
- Calculation modes: a) Static Structural; B) Eigenvalue Buckling

Table 4 shows the results of a comparative analysis of the computational parameters required to calculate the beam for bending.

Table 4. The resource intensity of the calculation, depending on the type of the final element.

Analysis parameter	Finite element type		
	BEAM 188	**SHELL 181**	**SOLID 186**
Number of cells FE	3000	18424	328000
Number of nodes FE	6001	18852	1718506
The required amount of RAM, [MB]	2112	2112	6421
Required disk space for calculation, [MB]	57	329	6420.99
The size of the results file, [MB]	7,9375	21.75	490.63
The computing frequency of the equation solver, [MFlops]	1670	18480	13034.4
Total processor time, [s]	2	2.8	451

As can be seen from the table, the use of finite elements of the BEAM type has more advantages, with respect to other types (in this case we will make a reservation, with one size considerably exceeding others), both in comparison with engineering calculation and in comparison with saving the PC resource.

CONCLUSION

1. The use of modern software systems based on CAE / CAD systems, and sufficiently powerful personal computers, allows optimizing the calculation of building structures.

2. Comparison of calculation results in the Ansys WB software package and engineering calculation (Table 2) that the closest values of the normal stresses and deflections of the I-beam were obtained using finite elements such as BEAM and SOLID. The finite SHELL element has a greater percentage of discrepancy, and is not recommended for use.

3. When studying the operation of the bar for stability, it is possible to use the FE of all the types considered, although there is some advantage in the FE type of BEAM (Table 3).

4. The use of FE type BEAM significantly facilitates the work of a personal computer, without loss of accuracy of the calculation itself, especially when calculating large-span structures with a large number of elements of constant cross-section, without requiring large computational resources (Table 4).

5. When calculating the FEM based on CAE / CAD systems of bar elements, one of the dimensions of which considerably exceeds the cross-sectional dimensions, the optimal type of FE is BEAM.

REFERENCES

Basov, K. A. (2002). *ANSYS in examples and problems*. Moscow: Computer-Press (In Russian).

Basov, K. A. (2005). *ANSYS: user's guide*. Moscow: DMK Press (In Russian).

Bogdanov, S. V. (2011). Features of the design of fast-erecting welded walls of vertical cylindrical tanks of composite bearing elements. Mogilev: *Vestn. Belarusian-Russian University,* 3, 6-16. (In Russian).

Bogdanov, S. V. (2013). Experimental verification of the accuracy of numerical models in the study of deformation fields in fast-erecting objects from composite bearing elements. In Kuzmenko, I. M., Kuzmenko, D. O. & Cikunova, T. V. (eds.) *New materials, equipment and technologies in industry: materials of the Intern. Scientific-techn. Conf. Young scientists*. Mogilev: Belarusian-Russian Univ., 119. (In Russian).

CRSBC II-23-81 (1990). Steel structures / Gosstroy USSR. M.: TsITP Gosstroy USSR (In Russian).

CRSBC 2.01-07-85 (1986). Loads and effects / Gosstroy USSR. M.: TsITP State Building of the USSR (In Russian).

EN 1993-1-1-2009 (2010). Eurocode 3. Design of Steel Constructions. Part 1-1. General rules and rules for buildings: TCP (In Russian).

Fridkin, V. M. (2011). *Formation of building structures*. Moscow: MGSU (In Russian).

Fridkin, V. M., Chesnokov, S. A. & Kokosadze, A. E. (2015). *Engineering facilities of underground power engineering*. M.: ASV (In Russian).

Kuzmenko, I. M. (2003). Application of welded load-bearing elements in new composite building structures. In Kuzmenko, I. M., Pavlyuk, S. K. & Fridkin, V. M. (eds.) *Welding* 9, 47–50. (In Russian).

Kuzmenko, I. M. (2006). Aspects of designing a composite bearing element using CAD. In Fridkin, V. M., Podimako, M. E., & Leonenko, O. V., Medvedev, V. N. (eds.) Mogilev: *Vestn. Belarusian-Russian University* 4, 198-202. (In Russian).

Kuzmenko, I. M. (2014). Experience of application in the Republic of Belarus of new constructive solutions of span structures of road bridges. In Fridkin, V. M., Sisa, N. S. & Markov, S. N. Naukovedenie 5(24). Retrieved 18 Jan 2018 from https://naukovedenie.ru/PDF/21KO514.pdf. (In Russian).

Kuzmenko, I. M., Fridkin, V.M., & Markov, S. N. (2015). Belarusian-Russian innovation: creation of engineering structures of the XXI century. *Proceedings of the METNET Seminar 2015 in Budapest. Häme University of Applied Sciences*, 40-51.

Kuzmenko, I. M. & Fridkin, V. M. (2017). *Prospects for the development of building structures of engineering structures*: monograph. Mogilev: Belarusian-Russian Univ. (In Russian).

Lagerev, I. A. (2014). Influence of the size of the finite element on the accuracy of the static calculation of the load-bearing metal structure of the overhead crane. *Journal of Science and Modernity* 32(2), 36–40 (In Russian).

Shimanovsky, A. O. (2008). Application of the finite element method in solving problems of applied mechanics: the teaching method. In Shimanovsky, A. O. & Putyato, A. V. (eds.) *Manual for students of technical specialties*. Ministry of Education of the Republic of. Belarus, Byelorussia. State. Un-t trans. Gomel: BelGUT. (In Russian).

European Union
European Social Fund

ruukki
LIVING. WORKING. MOVING.

b-tu Brandenburg University of Technology Cottbus - Senftenberg

HAMK
HÄMEEN AMMATTIKORKEAKOULU
HÄME UNIVERSITY OF APPLIED SCIENCES

The METNET network aims to enhance the development potential and the research and innovation capacities of regional innovation systems and wider communities of Europe. METNET provides an international innovation environment for its members and the possibility to expand their regional innovation networks internationally.

METNET seminars and workshops deal with technical aspects of metal construction as well as issues of concern to industry on management, planning and sustainability of projects.

This book covers papers presented and submitted for the twelfth annual METNET seminar in October 2017 held at Brandenburgische Technische Universität Cottbus-Senftenberg (BTU), Cottbus, Germany.

The seminar continued the METNET tradition of presenting scientific and development papers of high calibre. The publication process of the METNET Proceedings book utilises peer review to assess the validity, quality and the originality of articles for publication.

PRINTED
ISBN 978-951-784-794-0
ISSN 1795-4231
HAMKin julkaisuja 1/2018

ELECTRONIC
ISBN 978-951-784-793-3 (PDF)
ISSN 1795-424X
HAMKin e-julkaisuja 2/2018

HAMK
HÄMEEN AMMATTIKORKEAKOULU
HÄME UNIVERSITY OF APPLIED SCIENCES